Álefe Freire de Almeida

General relativity and modified gravity in galaxies and the Solar System

Brasil

13 de setembro, 2019

Álefe Freire de Almeida

General relativity and modified gravity in galaxies and the Solar System

Tese apresentada ao Programa de Pós-Graduação em Física da Universidade Federal do Espírito Santo, como requisito para obtenção do grau de doutor em Física.

Universidade Federal do Espírito Santo –UFES

Centro de Ciências Exatas – CCE

Programa de Pós-Graduação em Física – PPGFis

Supervisor: Davi Cabral Rodrigues

Co-supervisor: Luca Amendola

Brasil

13 de setembro, 2019

Ficha catalográfica disponibilizada pelo Sistema Integrado de Bibliotecas - SIBI/UFES e elaborada pelo autor

---

Almeida, Álefe de Oliveira Freire de, 1989-
A447g General relativity and modified gravity in galaxies and the solar system. / Álefe de Oliveira Freire de Almeida. - 2019.
123 f. : il.

Orientador: Davi Cabral Rodrigues.
Coorientador: Luca Amendola.
Tese (Doutorado em Física) - Universidade Federal do Espírito Santo, Centro de Ciências Exatas.

1. Curvas de rotação. 2. Galáxias. 3. Gravidade modificada. 4. Relatividade geral. 5. Matéria escura.. I. Rodrigues, Davi Cabral. II. Amendola, Luca. III. Universidade Federal do Espírito Santo. Centro de Ciências Exatas. IV. Título.

CDU: 53

UNIVERSIDADE FEDERAL DO ESPÍRITO SANTO

CENTRO DE CIÊNCIAS EXATAS

PROGRAMA DE PÓS-GRADUAÇÃO EM FÍSICA

"General relativity and modified gravity in galaxies and the Solar System"

Álefe Freire de Almeida

Tese submetida ao Programa de Pós-Graduação em Física da Universidade Federal do Espírito Santo como requisito parcial para a obtenção do título de Doutor em Física.

Aprovada por:

Prof. Dr. Laerte Sodré Júnior
(IAG/USP) Participante remoto

Prof. Dr. Davi Cabral Rodrigues
(Orientador - PPGFis/UFES)

Prof. Dr. Martín Makler
(CBPF/RJ)

Prof. Dr. Humberto Belich Junior
(PPGFis/UFES)

Prof. Dr. Valerio Marra
(PPGFis/UFES)

Prof. Dr. Wiliam S. Hipolito Ricaldi
(PPGFis/UFES)

Vitória-ES, 22 de maio de 2019

Dedicado a Ediane e Alice.

AGRADECIMENTOS

- Agradeço ao Prof. Davi Rodrigues pela orientação, paciência e dedicação durante meu doutoramento. Grande parte de minha formação como físico se deve a ele.
- Agradeço ao Prof. Luca Amendola por sua hospitalidade e coorientação durante o doutorado sanduíche na Universidade de Heidelberg.
- Agradeço ao Prof. Oliver Piattella, ao Dr. Júnior Toniato, ao Dr. Sebastião Mauro, a Dra. Viviana Niro e ao Msc. Nicolas Bertini pelas colaborações científicas aos meus trabalhos publicados.
- Agradeço a minha esposa Ediane que esteve presente em todos os momentos difícies de meu doutorado me dando o suporte sentimental e me inspirando a continuar em frente.
- Agradeço aos meu colegas de mestrado e doutorado do PPGFis e PPGCosmo: Eddy, Felipe, Sara, Isaac, Ingrid, Pedro, Natália, Guilherme, David, Carlinhos, Érico, Ricardo, Olesya, Tays, Denis e Yago. Agradeço pelos momentos de descontração em nossos cafés no PPGFis.
- Agradeço ao José Carlos, secretário do PPGFis, pelo suporte em todas as questões burocráticas pertinentes ao programa e também pelos divertidos assuntos.
- Agradeço, acima de tudo, a Deus pelo sustento ao longo desse anos de doutorado.
- O presente trabalho foi realizado com apoio da Cordenação de Aperfeiçoamento de Pessoal de Nível Superior- Brasil (CAPES).

"A persistência é o menor caminho do êxito". (Charles Chaplin).

ABSTRACT

General relativity has a great success in describing the dynamics of the Solar System and also in the description of gravitational waves. However, its limits are evident in the study of large scales and quantum levels. In this latter scenario it is known that general relativity is not perturbatively renormalizable, hence proposed approaches as functional renormalization have been applied in order to solve this problem. However, the use of such mechanisms gives rise to extensions of general relativity that can generate signatures of the quantum medium at larger scales. In this thesis we study a particular extension of general relativity from renormalization group and we test if such signatures are present at scales at the level of the Solar System. In addition, there is a reasonable understanding that general relativity does not explain the behavior of rotation curves without the hypothesis of a dark matter. The fact that galaxies have very low rotation velocities in relation to the speed of light and a weak gravitational field and that, in this regime, general relativity is simply Newtonian gravity, it suggests that general relativity corrections are inefficient for dark matter effects. We study in this thesis alternatives to the interpretation described above and we propose a model that tests them in their own way. In addition, we study the feasibility of a scenario of coexistence between dark matter and modified gravity assuming that the fifth force from the gravity modification is coupled differently to baryons and dark matter. We investigate the possibility that the galaxy rotation curves can be explained in the framework of modified gravity models that introduce a Yukawa term in the gravitational potential. We aim at constraining the modified gravity parameters β and λ, that is, the strength and the range of the Yukawa fifth force. We include baryonic gas, disk and bulge components, along with a Navarro-Frenk and White (NFW) halo of dark matter. Each galaxy rotation curve is modeled with three free parameters, beside the two global Yukawa parameter. The preference of the observational data in favor or against this new parameterization is studied through Bayesian inference. The Bayesian evidence in favor of a NFW profile plus Yukawa term is higher than 8σ with respect to the standard gravity parametrization.

Keywords: dark matter, galaxies, general relativity, rotation curves, modified gravity.

RESUMO

A relatividade geral tem um grande sucesso na descrição da dinâmica do Sistema Solar e também na descrição das ondas gravitacionais. Porém, seus limites são evidentes no estudo de grandes escalas e em níveis quânticos. Neste último cenário sabe-se que a relatividade geral não é perturbativamente renormalizável, assim propostas como renormalização funcional têm sido aplicadas a fim de solucionar este problema. Porém, o uso de tais mecanismos dão origem a extensões de relatividade geral que podem gerar assinaturas do meio quântico em escalas maiores. Nessa tese estudamos uma particular extensão de relatividade geral oriunda da aplicação de grupos de renormalização funcional e testamos se tais assinaturas estão presentes em escalas a nível do Sistema Solar. Além disso, têm-se um razoável entendimento de que relatividade geral não explica o comportamento das curvas de rotação sem a hipótese de uma matéria escura. O fato de que galáxias possuem velocidades de rotação muito baixas em relação a velocidade da luz e um campo gravitacional fraco e que nesse limites relatividade geral é simplesmente gravitação Newtoniana, sugerem que correções de relatividade geral são ineficientes para efeitos de matéria escura. Estudamos nesta tese alternativas a interpretação descrita acima e propusemos um modelo que as teste de maneira própria. Além disso, estudamos a viabilidade de um cenário de coexistência entre matéria escura e gravidade modificada assumindo que a quinta força advinda da modificação da gravidade se acopla diferentemente aos bárions e à matéria escura. Nós investigamos a possibilidade de que curvas de rotação de galáxia podem ser explicadas no contexto de gravidade modificada que introduzem um termo de Yukawa no potencial gravitacional.Nosso obketivo é restringir os parêmateros de gravidade modificada β e λ, que são, respectivamente, a força e o alcance da quinta força de Yukawa. Incluímos em nossa análise o gás, disco estelar, bojo juntamente com um halo de matéria escura do tipo Navarro-Frenk e White (NFW). Cada curva de rotação é modelada com três parâmetros livres além dos de Yukawa que são globais. A preferência dos dados observacionais em favor ou contra essa nova parametrização é estudada via inferência Bayesiana. A evidência Bayesiana em favor de um perfil de NFW mais Yukawa é maior do que 8σ com respeito à parametrização de galáxias tradicional.

Palavras-chave: curvas de rotação, galáxias, gravidade modificada, relatividade geral, matéria escura.

LIST OF FIGURES

Figure 1 – The Newtonian potential generated by the Sun $\phi_\odot$ across the Solar System, and the value of the Newtonian potentials generated by the Galaxy at the Solar System ($\phi_{\rm MW}|_\odot$). The letters "P" and "A" after Mercury refers to its perihelion and aphelion. 46

Figure 2 – The RC curve analysis of ESO 116-G12 with the CT approach with three free model parameters (p_i). The fit of the total Newtonian circular velocity $V_{\rm N}$ to the effective Newtonian RC is not satisfactory ($\chi^2{}_{\rm red} \gg 10$). 76

Figure 3 – Rotation curves of the galaxies DDO 154, ESO 116-G12, ESO 287-G13 and NGC 2403 2D. The plots use the same conventions of Figure 2, with the addition that the dashed dark red curve, when present, refers to the bulge circular velocity ($V_{\rm bulge}$). 80

Figure 4 – The autocorrelation time analysis (blue solid line) for each set of galaxies respectively containing 10 objects each. When τ reaches the dotted line the convergence of the chains is achieved, see [1]. 88

Figure 5 – The marginalized distribution of the (β, λ) and the one-dimensional posterior distribution according the set of 10 galaxies each and the combined analysis. 90

Figure 6 – The ratio μ_{200} (black dots) and the respective error bars. The cyan dotted line is the average value of μ_{200}. 91

Figure 7 – The rotation curves and their components: gas (dashed yellow line), disk (dashed green line), bulge (dashed red line) and dark matter with Yukawa-like corrections (dashed blue line). The black solid line is the overall best-fit (see equation 7.31) and the values for the parameters are displayed on Tables 10 and 9, the orange solid line is the dark matter component for $\beta = 0$. The red dots with error bars are the observational data taken from SPARC catalogue and the grey ones are the residual of the fit. We have plotted the results for the set A. 95

Figure 8 – continued 96

Figure 9 – Same as Figure 7, but for set B. 97

Figure 10 – continued. 98

Figure 11 – Same as Figure 7, but for set C. 99

Figure 12 – continued. 100

Figure 13 – Same as Figure 7, but for set D. 101

Figure 14 – continued. 102

Figure 15 – The relation between $|\delta G| = |G - 1| \approx 2\nu \ln \mu$ (from equation 2.31) and $|\Phi|$ (from equation A.6) for four different values of ν. 117

Figure 16 – The relation between α and Φ for different values of ν. It shows that the noncovariant approximation, where α is a constant, can be a good approximation for many systems, since large changes of Φ lead to much smaller changes on α. 119
Figure 17 – The relative errors (B.3) introduced by the use of the approximation (2.37), in the context of Mercury's orbit with the external potential of the Galaxy. The range of Φ in this plot spans the variation of the Newtonian potential through the planet orbit added by 10^{-6}. Dividing or multiplying the latter value by 5, does not change the value of $\log_{10}\varepsilon$ significantly. The plot indicates that the noncovariant scale setting works as a good approximation for the covariant one, in the context of Mercury's orbit. 120

LIST OF TABLES

Table 1 – PPN parameters and their interpretation. Adapted from [2]. 44

Table 2 – Limits on the PPN parameters, considering only the strongest limits for each parameter [2]. The ζ_4 does not have a direct measurement. These limits apply to the absolute value of each parameter. 44

Table 3 – Strongest constraints on ν_1 and ν_2 from all the observational constraints on the PPN parameters. 52

Table 4 – Results of the CT approach with three model parameters p_i applied to the galaxy ESO 116-G12 (see Figure 2). This fit considers the full evaluation of the effective Newtonian data with error bars. This table also includes a comparison to the corresponding results when the same galaxy is modelled with baryonic matter and a NFW dark matter halo [3]. 76

Table 5 – The values of the p_i parameters and its errors (δp_i) for both the CT and BG approaches. 78

Table 6 – Results on χ^2 and related quantities of the CT and BG approaches. The corresponding plots are in Figure 3 [3]. 78

Table 7 – Results on the stellar mass-to-light ratios of the CT and BG approaches shown in comparison with the NFW profile results and the expected values from stellar population considerations. Expected values on Υ_* and NFW results are from [4, 5, 3]. 79

Table 8 – Table for the galaxy UGCA442 emphasizing each baryonic component (there is no bulge in this galaxy). $\Sigma_{\rm disk}$ is the surface density for the disk. 86

Table 9 – The acceptance fraction a_f, the maximum likelihood estimation for (β, λ), the total goodness of fit $\chi^2_{\rm red,tot}$ and the one calculated fixing $\beta = 0$, for each set of 10 galaxies and for the combination of the data sets. $k_{\rm Y}$ ($k_{\rm sg}$) is the number of free parameters for the Yukawa model (for standard gravity), while N is the number of data points. We also report the values for the ΔBIC, for $2\log B_{12}$, and the confidence level (CL), see text for more details. 88

Table 10 – The maximum likelihood estimation for the $\Upsilon_{*\rm D}$,$\Upsilon_{*\rm B}$ and M_{200} parameters, and the goodness of fit $\chi^2_{\rm red}$ for each galaxy, for the Yukawa model. 93

Table 11 – The maximum likelihood estimation for the $\Upsilon_{*\rm D}$,$\Upsilon_{*\rm B}$ and M_{200} parameters,and the goodness of fit $\chi^2_{\rm red}|_{\beta=0}$ for each galaxy in the case of $\beta = 0$. 94

LIST OF ABBREVIATIONS AND ACRONYMS

BG	Balasin-Grumiller
CT	Cooperstock-Tieu
ETGs	Extended Theories of Gravity
FLRW	Friedmann-Lemaître-Robertson-Walker
GR	General Relativity
HI	region in the interstellar medium composed by neutral hydrogen
HII	region in the interstellar medium composed by ionized hydrogen
HSB	High Surfece Brightness
IR	Infrared
LCDM	The standard cosmological model, with cosmological constant (L) and cold dark matter (CDM)
LSB	Low Surface Brightness
MCMC	Markov Chain Monte Carlo
MH	Metropolis-Hastings
ML	Maximum Likelihood
MOG	Moffat's Modified Gravity
MOND	Modified Newtonian Dynamics
NFW	Navarro-Frenk-White
NIR	Near-InfraRed
PPN	Parameterized Post-Newtonian
PDF	Probability Density Function
QCD	Quantum ChromoDynamics
QFT	Quantum Field Theory

QED	Quantum EletroDynamics
RG	Renormalization Group
RGGR	Renormalization Group extended General Relativity
SB	Surface Brightness
SINGS	Spitzer Infrared Nearby Galaxy Survey
SPS	Stellar Population Synthesis
THINGS	The HI Nearby Galaxy Survey
UV	Ultraviolet

CONTENTS

	INTRODUCTION	15
1	GENERAL RELATIVITY	18
2	MODIFIED GRAVITY	22
2.1	$f(R)$ theories	22
2.2	Scalar-tensor theories	24
2.3	Renormalization group extended general relativity (RGGR)	26
2.3.1	The noncovariant scale setting	29
2.3.2	The external potential effect	29
2.3.3	GR and RG perturbations	31
2.3.4	Point particle solution of RGGR	32
2.4	Scalar-tensor-vector-gravity	33
3	THE PARAMETRIZED POST-NEWTONIAN FORMALISM	38
4	THE SOLAR SYSTEM ANALYSIS OF RGGR	45
4.1	The Eddington-Robertson-Schiff expansion for RGGR	45
4.2	The Will-Nordtvedt formalism applied to RGGR	48
4.2.1	Λ term and violation of asymptotic flatness	53
4.2.2	Covariant scale setting and new post-Newtonian potentials	55
5	SPIRAL GALAXIES	57
5.1	Rotation curves	58
5.2	Observational data for rotation curves	60
6	STATISTICAL METHODS	64
6.1	Sampling methods	65
6.2	Convergence diagnostics	67
7	TESTING GRAVITY WITH GALAXY ROTATION CURVES	69
7.1	Models based on general relativity	69
7.1.1	The Cooperstock-Tieu approach	69
7.1.2	The Balasin-Grummiler approach	71
7.1.3	The effective Newtonian rotation curve method	72
7.1.4	The fit procedure step by step	73
7.1.5	Application to the Cooperstock-Tieu approach	75

7.1.6 Application to the Balasin-Grumiller approach 77
7.1.7 Results 77
7.2 Models based on Modified gravity 79
7.2.1 A species-dependent coupling 83
7.2.2 The Yukawa correction 84
7.2.3 Analysis with SPARC dataset 85
7.2.4 Fitting the rotation curves 86
7.2.5 Analysis and results 87

8 CONCLUSIONS 103

BIBLIOGRAPHY 105

APPENDIX A – A SPECIFIC COVARIANT SCALE SETTING 115

APPENDIX B – THE NONCOVARIANT SCALE SETTING AS AN APPROXIMATION TO THE COVARIANT ONE 118

INTRODUCTION

The dynamics of the standard cosmological model(LCDM) after cosmic inflation derives from three pillars: gravity, dark matter and dark energy. Naturally, the baryons are present too, but their contribution to the universe, mainly in later times, is negligible. The standard model is a concordance model, i.e. it explains the accelerated expansion and the structure formation. The first phenomenon is attributed to dark energy while the second one is to dark matter.

The gravity behind the standard model is General Relativity, the most accepted modern theory of gravity. Besides its elegant description, based on differential geometry, GR explains successfully the motion of planets around the Sun, e.g. Mercury's precession orbit. But GR finds its own limits in the "dark universe" scenario, i.e. dark matter and dark energy are inserted as extra ingredients to the energy content of the universe. Moreover, there are diverse motivations for extending gravity beyond General Relativity [6, 7, 8], including: quantum gravity, avoidance of singularities, understanding inflation, theoretical and observational improvements on dark matter, alleviating coincidence issues related to dark energy, and others.

In this thesis we investigate the possibility of a GR extension based on the Renormalization Group (RG) framework applied to gravity. Specially, here we will focus on the realization that was named RGGR [9, 10]. There are some procedures for testing gravity beyond Newtonian gravity, and the most used one is the Parametrized Post Newtonian (PPN) formalism. Here we consider two versions of the PPN formalism: the Eddington-Robertson-Schiff parametrization and the Will-Nordtvedt to a class of RG extensions of GR that includes RGGR as a particular case, but considering in this study the presence of the external potential effect which is an effect inherent to RGGR and works as a (partial) screening mechanism.

The possibility of an existence of dark matter appeared for the first time, in literature, when Zwicky [11] perceived the "missing mass" on dynamics of galaxy clusters which was not consistent with only luminous matter. But, the evidences of a dark matter became more relevant forty years later, when Vera Rubin [12] inferred the necessity of an extra matter for explaining the rotation curve of Andromeda. Notwithstanding the indirect evidences that support its existence, dark matter remains a mystery and there is no current sign of a direct detection [13, 14]. Despite the success of the LCDM in the description of the observed universe, certain features are not covered by standard model, for example, at galactic scales there is the Tully-Fisher [15, 16, 17] relation which is an empirical relation between the mass (or luminosity) of a galaxy and its asymptotic rotation

velocity. The latter inconvenience of standard model in galaxies motivated the emergence of a modified gravity known as Modified Newtonian Dynamics [18, 19, 20] (MOND) which assumes a fundamental acceleration scale, namely a_0, such that for accelerations smaller than a_0 the gravitational force decays with distance slower than Newtonian one. In a recent work [21], analyzing 193 disk galaxies and using Bayesian inference, the authors show that the existence of such fundamental acceleration in galaxies is zero and MOND can not be seen as a fundamental theory but rather as a phenomenological one.

In the context of galaxies, we investigate two possibilities, one that galaxies rotation curves could be explained in the framework of GR without dark matter by using certain peculiar geometries, and the other possibility considers dark matter but the existence of an interaction between dark matter and baryons described by a fifth force. The latter one is predicted considering the weak field limit of relativity of several modified gravity theories. To exemplify the first possibility, two relativistic approaches are selected. For some galaxies, the rotation curve fits of these approaches seem satisfactory, but these publications, namely [22, 23, 24, 25, 26, 27], lack a detailed investigation with respect to the baryonic matter data inferred from observations. The main feature of those approaches is to use the observational rotation curve as an imput for deriving the total matter density of galaxies. Models that use this inverse route have not been yet properly tested and confronted with results from other approaches. To address this issue we propose [28] the effective Newtonian rotation curve method.

For the second possibility, the coexistence of dark matter and modified gravity is considered, in particular those that predicts Yukawa-like corrections to the Newtonian potential when the weak field limit of relativity is performed (e.g. $f(R)$, Scalar-tensor-vector-gravity, Nonlocal gravity, Scalar-tensor). We tested this scenario with rotation curves from the newest catalogue SPARC. We found a strong evidence in favor of this scenario, dark matter plus modified gravity, compared to the standard one. Finally, the main content of this thesis was published in [28, 29, 30, 31].

This thesis is organized as follows: In the first chapter we review the basis of general relativity; in Chapter 2 we present the modified gravity theories, in particular, the ones that predict Yukawa-like corrections at weak field regime and a particular extension of general relativity considering renormalization group effects. In Chapter 3 it is reviewed the basis of parametrized post-Newtonian formalism followed by Chapter 4 where we analyze the renormalization group effects at Solar System. In Chapter 5 we review important aspects of spiral galaxies which are important for developing subsequent chapters. In Chapter 6 we review the main tools for statistical analysis of the gravity models discussed in this thesis. In Chapter 7 we present the approaches for galaxies rotation curves description based in general relativity and modified gravity as well their comparison with observational data. In Chapter 8 we present the main conclusions of this thesis as well the perspectives for future

works. In the end, one has two appendices, namely Appendix A and B, where aspects about renormalization group effects in large scales are more detailed.

1 GENERAL RELATIVITY

This chapter is dedicated to briefly review the fundamentals of GR. More detailed reviews, with a similar approach to the one used here, can be found in [32, 33].

General relativity, is the most favored theory for describing gravity. Besides its simplicity suggesting that the gravity is a manifestation of spacetime curvature induced by the presence of matter or energy, GR passes through accurated observational tests, for example the Solar System dynamics [34] and gravitational waves emission [35]. The field equations of GR, or simply Einstein equations, which describes quantitatively how much the spacetime curvature is deformed due the matter are a set of second-order differential equations whose solution is the rank-2 tensor $g_{\mu\nu}$, namely the metric tensor, which is the fundamental quantity in Einstein gravity. In the most general case, $g_{\mu\nu}$ has ten components.

In order to construct the Einstein equations one needs to find a proper way to describe the source term, i.e. the matter or energy. In other words, one must relate the matter (energy) with a tensor, in order to describe covariantly the matter distribution. Besides its covariant behaviour, the tensor which will describe matter in Einstein equations, that is, the energy-momentum tensor $T^{\mu\nu}$, needs to have components that identify properties of fluids. Namely, T^{00} describes the total energy density which is equal to ρc^2 (c is the speed of light), in any coordinate system; T^{0i}, with $i = 1, 2, 3$ is the heat conduction term; T^{ij} is the stress tensor. The standard procedure for obtaining the energy-momentum tensor is via Noether's theorem. However, the latter leads, in general, to a non-symmetric energy-momentum tensor. But, in the context of general relativity, the matter fields couple to matter, hence a symmetric energy-momentum tensor is needed [36]. The conservation of energy-momentum tensor in any coordinate system is given by

$$\nabla_\mu T^{\mu\nu} = \partial_\mu T^{\mu\nu} + \Gamma^\mu_{\mu\rho} T^{\rho\nu} + \Gamma^\nu_{\mu\rho} T^{\mu\rho} = 0, \tag{1.1}$$

where ∇_μ is the covariant derivative and the coefficients $\Gamma^\mu_{\alpha\beta}$ are the Christoffel symbols which relates with the metric tensor via

$$\Gamma^\mu_{\alpha\beta} = \frac{1}{2} g^{\mu\rho} (g_{\rho\alpha,\beta} + g_{\rho\beta,\alpha} - g_{\alpha\beta,\rho}) \,, \tag{1.2}$$

where the commas represent the partial derivative with respect to spacetime coordinates. The equation above can be obtained if one considers $\nabla_\mu g^{\mu\nu} = 0$.

Now, after identify the source term for Einstein equations one needs to link its effects with gravity in the same equations. Since gravity is described as a curvature of spacetime geometry, it is intuitive to connect the metric tensor with the curvature tensor. Hence, a first candidate is the Riemann tensor, namely $R^\alpha_{\beta\gamma\delta}$, which is composed by second

derivatives of the metric tensor. But, $R^{\alpha}_{\beta\gamma\delta}$ is a rank-4 tensor while the energy-momentum tensor is a rank-2 tensor hence it is difficult to connect geometry with matter in a simple equation. Another candidate containing second-order derivatives of the metric tensor that is also a rank-2 tensor is the Ricci tensor $R_{\mu\nu} \equiv R^{\alpha}_{\mu\alpha\nu}$. Hence, a good suggestion for Einstein equations could be $R^{\mu\nu} = \kappa T^{\mu\nu}$, but the latter equation is not compatible with equation (1.1) due $\nabla_\mu R^{\mu\nu} \neq 0$, in general. However, if one looks at the Bianchi identities, namely

$$R^{\alpha}_{\beta\gamma\delta;\epsilon} + R^{\alpha}_{\beta\delta\epsilon;\gamma} + R^{\alpha}_{\beta\epsilon\gamma;\delta} = 0 \,, \tag{1.3}$$

where ";" means the covariant derivative and contracting the above equation with $\delta^{\alpha}_{\gamma} g^{\beta\delta}$, one finds

$$G^{\alpha\beta}_{;\beta} = 0 \,, \tag{1.4}$$

where

$$G^{\alpha\beta} \equiv R^{\alpha\beta} - \frac{1}{2} g^{\alpha\beta} R \tag{1.5}$$

which is called Einstein tensor and is a better candidate for the left-hand side of Einstein equations which becomes now

$$R^{\alpha\beta} - \frac{1}{2} g^{\alpha\beta} R = \kappa T^{\alpha\beta} \,, \tag{1.6}$$

with $\kappa = \frac{8\pi G}{c^4}$ where G is the Newton's gravitational constant. Now, using that $\nabla_\mu g^{\mu\nu} = 0$ the equation (1.6) can be trivially extended

$$R^{\alpha\beta} - \frac{1}{2} g^{\alpha\beta} R + \Lambda g^{\alpha\beta} = \kappa T^{\alpha\beta} \,, \tag{1.7}$$

where Λ is the cosmological constant.

However, many theories both at the classical and quantum level are expressed using the variational principle and the main element of this approach is an action, which is a scalar. Writing a physical theory using an action one enables to see straightforwardly, for example, the symmetries of interest or conserved quantities. Furthermore, by demanding that an action of a given physical theory is invariant under symmetry, one ensures that the field equations of such theory is also invariant under that symmetry. The derivation of Einstein equations using the variational principle was performed by Hilbert and the action that generates the field equations (1.7) is known as Einstein-Hilbert action, namely

$$S_{EH} = \frac{1}{2\kappa} \int (R - 2\Lambda) \sqrt{-g} \; d^4x + S_m \,, \tag{1.8}$$

where R is the Ricci scalar, g is the determinant of $g_{\mu\nu}$ and S_m is matter action. Following [37], let us derive the Einstein equations via variational principle. Varying the action S_{EH} with respect to the metric field $g_{\mu\nu}$ one has

$$\delta S_{EH} = \frac{1}{2\kappa} \int \left[\delta(\sqrt{-g})(g^{\mu\nu} R_{\mu\nu} - 2\Lambda) + \sqrt{-g} \delta g^{\mu\nu} R_{\mu\nu} + \sqrt{-g} g^{\mu\nu} \delta R_{\mu\nu} \right] d^4x + \delta S_m \,. \tag{1.9}$$

Now, using that $g^{\mu\nu}R_{\mu\nu} = \nabla_\alpha \left(g^{\mu\nu}\delta\Gamma^\alpha_{\mu\nu} - g^{\mu\alpha}\delta\Gamma^\nu_{\mu\nu}\right) \equiv \nabla_\alpha V^\alpha$ one finds

$$\int g^{\mu\nu}\delta R_{\mu\nu}\sqrt{-g}\; d^4x = \int \nabla_\alpha V^\alpha \sqrt{-g}\; d^4x \; = 0 \; , \tag{1.10}$$

where we used the Gauss's theorem. Now, using the relation $\delta(\sqrt{-g} = -(1/2)\sqrt{-g}g_{\mu\nu}\delta g^{\mu\nu}$ the equation (1.9) becomes

$$\delta S_{EH} = \frac{1}{2\kappa}\int (R_{\mu\nu} - \frac{1}{2}g_{\mu\nu}R + \Lambda g_{\mu\nu})\delta g^{\mu\nu} + \delta S_m \; . \tag{1.11}$$

Defining the energy-momentum tensor of matter as follows

$$T_{\mu\nu} \equiv -\frac{2}{\sqrt{-g}}\frac{\delta S_m}{\delta g^{\mu\nu}} \; , \tag{1.12}$$

one has

$$\delta S_{EH} = \frac{1}{2\kappa}\int (R_{\mu\nu} - \frac{1}{2}g_{\mu\nu}R + \Lambda g_{\mu\nu} - \kappa T_{\mu\nu})\delta g^{\mu\nu}\sqrt{-g}\; d^4x \; . \tag{1.13}$$

Hence, the Einstein equations (1.7) are obtained demanding that $\delta S_{EH} = 0$. Einstein gravity shows how the spacetime curves due the presence of matter. Hence, it is possible to deduce the motion of test particles in this curved spacetime. Due the influence of gravity only, i.e. the curvature of spacetime, the test particles will move along geodesics. The geodesic equation is the one that describes the motion of these particles and can be obtained starting from the energy-momentum conservation (1.1) and writing it, in a convenient way, as

$$\nabla_\mu T^{\mu\nu} = \frac{1}{\sqrt{-g}}\partial_\mu(\sqrt{-g}T^{\mu\nu}) + \Gamma^\nu_{\sigma\mu}T^{\mu\sigma} = 0 \; , \tag{1.14}$$

where it was used

$$\Gamma^\mu_{\sigma\mu} = \partial_\sigma \ln\sqrt{-g} = \frac{1}{\sqrt{-g}}\partial_\sigma\sqrt{-g}. \tag{1.15}$$

The energy-momentum tensor of a test particle with rest mass m can be written as follows [32]

$$T^{\mu\nu}(x) = \frac{m}{\sqrt{-g}}\int \dot{z}^\mu \dot{z}^\nu \delta^4(x - z(\tau))d\tau \; , \tag{1.16}$$

where the dots means the derivation with respect to proper time τ. Hence, inserting the equation above into equation (1.14) one finds

$$\int \dot{z}^\mu \dot{z}^\nu \frac{\partial}{\partial x^\mu}\delta^4(x - z(\tau))d\tau + \Gamma^\mu_{\sigma\mu}\int \dot{z}^\mu \dot{z}^\sigma \delta^4(x - z(\tau))d\tau = 0 \; . \tag{1.17}$$

Now, observing that Dirac's delta depends only on the difference $x^\mu - z^\mu$, then one can replace $\partial/\partial x^\mu$ by $-\partial/\partial z^\mu$ and noting that

$$\dot{z}^\mu \frac{\partial}{\partial z^\mu}\delta(x - z(\tau)) = \frac{d}{d\tau}\delta^4(x - z(\tau)) \; , \tag{1.18}$$

one can use the relation above in equation (1.17), integrate by parts and collect the terms together, in order to find

$$\int (\ddot{z}^{\nu} + \Gamma^{\nu}_{\sigma\mu}\dot{z}^{\mu}\dot{z}^{\sigma})\delta^4(x - z(\tau))d\tau = 0 \, . \tag{1.19}$$

It is clear that for this integral to vanish, one requires that the expression in the integrand to equal zero, hence one recovers directly the standard geodesic equation.

Einstein gravity is a generalization of Newton's gravity, hence in some limit one can recover, starting from Einstein equations, the Newtonian equations for gravity, i.e. $\nabla^2\Phi = 4\pi G\rho$. This approach is know as the weak-field limit of Einstein equations and consists in to consider the spacetime slightly curved, which means in terms of the metric tensor, $g_{\mu\nu} = \eta_{\mu\nu} + h_{\mu\nu}$, with $|h_{\mu\nu}| \ll 1$ and stationary, i.e. $\partial_t g_{\mu\nu} = 0$. In order to apply the weak-field limit it is convenient to express the Einstein equations as follows

$$R_{\mu\nu} = \kappa \left(T_{\mu\nu} - \frac{1}{2} g_{\mu\nu} T \right) \, , \tag{1.20}$$

where $T = g^{\mu\nu}T_{\mu\nu}$. The only component of the equation above that one needs to consider is the (00), hence

$$R_{00} = \kappa \left(T_{00} - \frac{1}{2} g_{00} T \right) \, . \tag{1.21}$$

From the definition of the Riemann curvature tensor one can obtain the (00) component of the Ricci tensor which is given by

$$R^{\mu}_{0\mu 0} = R_{00} = \partial_0 \Gamma^{\mu}_{0\mu} - \partial_\mu \Gamma^{\mu}_{00} + \Gamma^{\nu}_{0\mu}\Gamma^{\mu}_{\nu 0} - \Gamma^{\nu}_{00}\Gamma^{\mu}_{\nu\mu} \, , \tag{1.22}$$

where the Γ's are the Levi-Civita connection given by equation (1.2). Thus, considering only the linear part of equation (1.20) and assuming the fact that the metric $g_{\mu\nu}$ is stationary one finds

$$R_{00} \approx -\partial_i \Gamma^{i}_{00} \approx -\frac{1}{2}\delta^{ij}\partial_i\partial_j h_{00} \, . \tag{1.23}$$

Assuming that the source of the gravitational field is a perfect fluid and moreover the pressure is negligible compared with the energy density, i.e. $p/c^2 \ll \rho$, one has that the energy-momentum tensor to be that of dust $T_{\mu\nu} = \rho U_\mu U_\nu$ which yields $T = -\rho$, where we used $U^\mu U_\mu = -1$. Hence, the right-hand side of the equation (1.21) now reads as

$$\kappa \left(T_{00} - \frac{1}{2} g_{00} T \right) \approx \frac{1}{2}\rho c^2 \, , \tag{1.24}$$

where we used $U_0 \approx c$. Therefore, using the result above and the equation (1.23), the equation (1.20) reduces to

$$\frac{1}{2}\delta^{ij}\partial_i\partial_j h_{00} \approx -\frac{1}{2}\kappa\rho c^2 \, . \tag{1.25}$$

Now, considering that $h_{00} = -2\Phi_N/c^2$ and remembering that $\kappa = 8\pi G/c^4$, one finally obtains

$$\nabla^2\Phi_N = 4\pi G\rho \, , \tag{1.26}$$

which is the Poisson's equation for Newtonian gravity.

2 MODIFIED GRAVITY

If general relativity is the correct description of gravity hence, according the LCDM, around 96% of all content in Universe is composed by matter and energy that do not interact eletromagnetically. Gravity being described by GR in galaxies and cluster of galaxies, some amount of dark matter is required to explain the observations. As well, more recently, dark energy is necessary to explain the accelerated expansion of the Universe. Such necessity favors the possibility that GR is not the correct theory in largest scales. However, Lovelock's theorem [38, 39] ensures that the only field equations which contains second derivatives of metric tensor, in a four dimensional space from a scalar density Lagrangian of the form $\mathcal{L} = \mathcal{L}(g_{\mu\nu})$, are the Einstein equations (1.7). Hence, whether one wants to describe a theory of gravity that produce field different from GR, one has to add more propagating degrees of freedom, that is, either scalars, vectors or tensors. Is equivalent to consider the presence of higher derivatives of the metric tensor in the field equations.

Also, modifications to gravity can emerge from attempts of a definitive quantum gravity theory. The well known *Extended theories of gravity* (ETGs) [7] are approaches based on adding higher-order curvature invariants (e.g. R^2, $R_{\mu\nu}R^{\mu\nu}$, $R_{\mu\nu\alpha\beta}R^{\mu\nu\alpha\beta}$) and non-minimally coupled scalar fields to geometry (such as $\phi^2 R$). The latter terms can be seen as corrections or enlargements of GR.

In this chapter, we review modified gravity models and their elements present in literature which are relevant for next chapters where we analyzed such theories against observations of the Solar System dynamics and internal dynamics of galaxies, e.g. rotation curves. The review on modified gravity models are mainly based on [37, 8].

2.1 $f(R)$ theories

A simple generalisation of Einstein-Hilbert action is to consider instead of the Ricci scalar a function of it, namely $f(R)$

$$S = \frac{1}{2\kappa}\int f(R)\sqrt{-g}\; dx^4 + S_m(g_{\mu\nu}, \Psi_m)\;, \tag{2.1}$$

where Ψ_m are the matter fields. Note that the general covariance and Lorentz invariance which are within Einstein gravity are preserved in this modification. On the another hand, the field equations obtained from the action above depends on the variational principle adopted. Namely, if one assumes that the action is a functional of the metric only and hence the connection is the Levi-Civita one (1.2), this is known as metric formalism. The Palatini formalism considers the action (2.1) as a functional of metric and connection and

hence they are independent fields in the theory. In this section, we will focus in the metric formalism, hence variating the action (2.1) with respect to the metric $g_{\mu\nu}$ one finds

$$F(R)R_{\mu\nu} - \frac{1}{2}f(R)g_{\mu\nu} - \nabla_\mu\nabla_\nu F(R) + g_{\mu\nu}\Box F(R) = \kappa T_{\mu\nu} \ , \tag{2.2}$$

where $F(R) \equiv \partial f/\partial R$ and the differential operator $\Box \equiv g^{\mu\nu}\nabla_\mu\nabla_\nu$. The trace of equation above gives

$$3\Box F(R) + F(R)R - 2f(R) = \kappa T \ , \tag{2.3}$$

where T is the trace of energy-momentum tensor, i.e. $T = g_{\mu\nu}T^{\mu\nu}$.

If one expands the equation above using the decomposition of the following quantities: $\varphi \equiv F(R)$, $g_{\mu\nu}$ and $T_{\mu\nu}$ into background plus perturbations, namely: $\varphi = \varphi_0(1+\delta\varphi)$, $g_{\mu\nu} = \eta_{\mu\nu} + h_{\mu\nu}$ and $T_{\mu\nu} = \overset{(0)}{T}_{\mu\nu} + \delta T_{\mu\nu}$, the equation (2.3) now reads [40, 41]

$$\left(\frac{\partial^2}{\partial t^2} - \nabla^2\right)\delta\varphi + m_\varphi^2\delta\varphi = \frac{\kappa}{3\varphi_0}\delta T \ , \tag{2.4}$$

where we used $\delta T \equiv \eta^{\mu\nu}\delta T_{\mu\nu}$ and

$$m_\varphi^2 \equiv \frac{1}{3}\left[\frac{f_{,R}(R_0)}{f_{,RR}(R_0)} - R_0\right] \ , \tag{2.5}$$

where $f_{,R}$ and $f_{,RR}$ are the respective first derivative and second derivative with respect to the Ricci scalar and R_0 means the Ricci scalar at the cosmic background.

Let us consider now a body with spherical symmetry and mass M, constant density ρ inside a radius r_c and vanishing density outside the sphere, i.e. $r > r_c$. In this case, the equation above becomes (inside the sphere)

$$\frac{d^2}{dr^2}\delta\varphi + \frac{2}{r}\frac{d}{dr}\delta\varphi - m_\varphi^2\delta\varphi = -\frac{\kappa}{3\varphi_0}\rho \ , \tag{2.6}$$

where $\rho \equiv \delta T$. Hence, the solution of the equation above is

$$\delta\varphi = C_1\frac{e^{-m_\varphi r}}{r} + C_2\frac{e^{m_\varphi r}}{r} \ , \quad \text{for } r > r_c \tag{2.7}$$

$$\delta\varphi = C_3\frac{e^{-m_\varphi r}}{r} + C_4\frac{e^{m_\varphi r}}{r} + \frac{8\pi G\rho}{3\varphi_0} \ , \quad \text{for } r < r_c \tag{2.8}$$

where C_1, C_2, C_3, C_4 are integration constants and we used $c = 1$. Requiring that φ tends to φ_0 implies in $\delta\varphi \to 0$ for $r \to \infty$, when $r > r_c$, which sets $C_2 = 0$. Now, demanding that $\delta\varphi$ must to be finite at $r = 0$ one needs $C_4 = -C_3$ and, finally ordering the equality of $\delta\varphi$ at the boundary $r = r_c$. Considering the latter requirements and according [41], if $m_\varphi r_c \ll 1$ one obtains the following solutions

$$\delta\varphi \approx \frac{2GM}{3\varphi_0 r}e^{-m_\varphi r} \ , \quad \text{for } r > r_c \tag{2.9}$$

$$\delta\varphi \approx \frac{4\pi GM}{3\varphi_0}\left(r_c^2 - \frac{r^2}{3}\right) \ , \quad \text{for } r < r_c \ . \tag{2.10}$$

It is convenient to define a new metric variable

$$\hat{g}_{\mu\nu} \equiv \varphi g_{\mu\nu} \ . \tag{2.11}$$

Hence, the field equations (2.2) now reads as [41]

$$\hat{G}_{\mu\nu} - \frac{3}{2\varphi^2}\partial_\mu\varphi\partial_\nu\varphi + \hat{g}_{\mu\nu}\left(\frac{3}{4\varphi^2}\hat{g}^{\alpha\beta}\partial_\alpha\varphi\partial_\beta\varphi + \frac{1}{2\varphi}\left(\mathcal{R}(\varphi) - \frac{f(\mathcal{R}(\varphi))}{\varphi}\right)\right) = 8\pi\frac{G}{\varphi}T_{\mu\nu} \ , \tag{2.12}$$

where $\hat{G}_{\mu\nu}$ is the Einstein tensor considering the metric $\hat{g}_{\mu\nu}$. The linearisation of the equation above one gives the Einstein gravity with a rescaled Newton's constant $\hat{G}^{(1)}_{\mu\nu} = 8\pi(G/\varphi_0)\delta T_{\mu\nu}$, hence the usual result (as already seen in Chapter 1) for the (00) and (ij) components of the metric pertubation tensor are $h_{00} = 2GM/(\varphi_0 r)$ and $h_{ij} = 2GM/(\varphi_0 r)\delta_{ij}$. Thus, the linearized metric $g_{\mu\nu}$ is

$$g_{\mu\nu} = \frac{\hat{g}_{\mu\nu}}{\varphi} \approx \eta_{\mu\nu} + h_{\mu\nu} - \varphi_0\eta_{\mu\nu} \ . \tag{2.13}$$

Now, using equation (2.9) one can show that the metric outside the sphere of mass M and radius r_c is approximately

$$ds^2 = g_{\mu\nu}dx^\mu dx^\nu \approx -\left(1 - \frac{2GM}{\varphi_0 r} - \frac{2GM}{3\varphi_0 r}e^{-m_\varphi r}\right)dt^2 + \left(1 + \frac{2GM}{\varphi_0 r} - \frac{2GM}{3\varphi_0 r}e^{-m_\varphi r}\right)d\mathbf{x}^2 \ . \tag{2.14}$$

Since $g_{00} \approx -1 - 2\Phi_{grav}$ where Φ_{grav} is the gravitational potential which gives the acceleration of test particles. Hence, from the equation above one has for a point mass source

$$\Phi_{grav} = -\frac{GM}{\varphi_0 r}\left(1 + \frac{1}{3}e^{-m_\varphi r}\right) \ . \tag{2.15}$$

Note that the first term in the above is the standard Newtonian potential with a rescaled Newton's constant accompanied of a Yukawa-like term. One can associate the mass m_φ with a lenght-scale λ which identifies where the Yukawa correction becomes important, the mentioned relation is given by $\lambda = 1/m_\varphi$[1].

2.2 Scalar-tensor theories

The insertion of scalar fields as a mediator of gravity in addition to the metric tensor field started with the Brans-Dicke theory [42] which is a simple modification of GR that inserts a scalar field in attempt to incorporate the Mach's principle, which says that the inertia is defined with respect to the entire mass distribution in the Universe,

[1] Here, we are using $c = \hbar = 1$, where $\hbar$ is the Planck's constant divided by 2π

and also to reproduce the Dirac's idea that the Newton's constant G varies in time. The Brans-Dicke gravity is a particular case of scalar-tensor theories whose the action is given by

$$S_{ST} = \int \left[\frac{1}{2}f(R,\phi) - \frac{1}{2}\chi(\phi)g^{\mu\nu}\nabla_\mu\phi\nabla_\nu\phi\right] + S_m(g_{\mu\nu},\Psi_m)\,, \tag{2.16}$$

where we used units such that $\kappa = 1$.

The action above covers a wide range of theories, for example $f(R)$ and Brans-Dicke gravity. Namely, $f(R)$ is achieved just requiring $f(R,\phi) = f(R)$ and $\chi = 0$. The Brans-Dicke case is recovered when $f(R,\phi) = \phi R$ and $\chi = \omega_{BD}/\phi$, where ω_{BD} is the constant Brans-Dicke parameter. A simple generalization of Brans-Dicke theory can be achieved if one adds a potential $V(\phi)$ to the original action, hence $f(R,\phi) = \phi R - V(\phi)$. The action (2.16) is written in Jordan frame or also known as the physical frame where the the energy-momentum is covariantly conserved, i.e. it obeys the standard conservation equation (1.1). A conformal transformation to the metric tensor, i.e. $\hat{g}_{\mu\nu} = \Omega^2 g_{\mu\nu}$, can be applied in order to write the action (2.16) in the Einstein frame where the field equations of the theory assumes the form of Einstein equations plus scalar fields contributing ordinarily. Hence, choosing the conformal transformation as

$$\Omega^2 = F = \frac{\partial f}{\partial R}\,. \tag{2.17}$$

And considering theories such that

$$f(R,\phi) = F(\phi)R - 2V(\phi) \tag{2.18}$$

one obtains the action (2.16) in the Einstein frame as follows (for details, please see [37])

$$S^E_{ST} = \int \left[\frac{\hat{R}}{2} - \frac{1}{2}\hat{g}^{\mu\nu}\hat{\nabla}_\mu\psi\hat{\nabla}_\nu\psi - \mathcal{V}(\psi)\right]\sqrt{-\hat{g}}\;d^4x + S_m(\hat{g}_{\mu\nu}F^{-1},\Psi_m)\,, \tag{2.19}$$

with $\mathcal{V} = V/F^2$ and

$$\psi = \int \sqrt{\frac{3}{2}\left(\frac{F_{,\phi}}{F}\right)^2 + \frac{\chi}{F}}\;d\phi\,. \tag{2.20}$$

Note that the insertion of ψ is for writing the action (2.19) with a canonical kinetic term. In the Einstein frame the scalar field couples to matter uprising a fifth force interaction. The strenght of this coupling, namely Γ, can be computed via

$$\Gamma \equiv -\frac{F_{,\psi}}{2F} = -\frac{F_{,\phi}}{2F}\left[\frac{3}{2}\left(\frac{F_{,\phi}}{F}\right)^2 + \frac{\chi}{F}\right]^{-1/2}\,. \tag{2.21}$$

Focusing on scalar-tensor theories which the coupling Γ is a constant, e.g. $f(R)$ gravity, from equations (2.20) and (2.21) one finds [43]

$$F = e^{-2\Gamma\psi}\,,\quad \chi = (1-6\Gamma^2)F\left(\frac{d\psi}{d\phi}\right)^2\,. \tag{2.22}$$

Hence, using the relations above the action (2.16) in Jordan frame becomes

$$S_{ST} = \int \left[\frac{1}{2}F(\psi)R - \frac{1}{2}(1-6\Gamma^2)F(\psi)g^{\mu\nu}\nabla_\mu\psi\nabla_\nu\psi - V(\psi)\right]\sqrt{-g}\; d^4x + S_m(g_{\mu\nu},\Psi_m)\;. \tag{2.23}$$

Note that when Γ tends to zero the action above is the one for a minimally coupled scalar field ψ with potential $V(\psi)$. Summarizing, the conformal transformation of the metric, $\hat{g}_{\mu\nu} = \Omega^2 g_{\mu\nu}$ with $\Omega^2 = F(\psi)$, transforms the action (2.23) from Jordan to Einstein frame action, equation (2.19), with constant coupling Γ.

If one sets $\varphi \equiv F = e^{-2\Gamma\psi}$ it is straightforward to see that the action above yields the Brans-Dicke action with a potential V, namely

$$S_{ST} = \int \left[\frac{1}{2}\varphi R - \frac{\omega_{BD}}{2\varphi}g^{\mu\nu}\nabla_\mu\varphi\nabla_\nu\varphi - V(\varphi)\right]\sqrt{-g}\; d^4x + S_m(g_{\mu\nu},\Psi_m)\;. \tag{2.24}$$

The actions (2.23) and (2.24) are equivalents if the relation below, between the parameter ω_{BD} and Γ, is satisfied. Namely,

$$3 + 2\omega_{BD} = \frac{1}{2\Gamma^2}\;. \tag{2.25}$$

Now, taking the variation of the action (2.24) with respect to the metric $g_{\mu\nu}$ and the scalar field φ, one finds

$$R_{\mu\nu} - \frac{1}{2}g_{\mu\nu}R = \frac{1}{\varphi}T_{\mu\nu} - \frac{1}{\varphi}g_{\mu\nu}V + \frac{1}{\varphi}(\nabla_\mu\varphi\nabla_\nu\varphi - g_{\mu\nu}\Box\varphi) + \frac{\omega_{BD}}{\varphi^2}\left[\partial_\mu\varphi\partial_\nu\varphi - \frac{1}{2}g_{\mu\nu}g^{\alpha\beta}\nabla_\alpha\varphi\nabla_\beta\varphi\right], \tag{2.26}$$

$$(3+2\omega_{BD})\Box\varphi + 4V - 2\varphi\frac{dV}{d\varphi} = T\;. \tag{2.27}$$

The relation between $f(R)$ gravity and scalar-tensor theories can be found if one considers the relations below

$$\varphi = F(R)\;, \quad V = \frac{1}{2}(RF - f(R))\;. \tag{2.28}$$

Using the relation in the above it is easy to see that $f(R)$ gravity is a Brans-Dicke theory with a potential V and $\omega_{BD} = 0$, i.e. $f(R)$ is a particular case of scalar tensor theories. Moreover, from equation (2.25) and setting $\omega_{BD} = 0$ one finds that the coupling for $f(R)$ gravity, in the metric formalism, is $\Gamma = -1/\sqrt{6}$.

2.3 Renormalization group extended general relativity (RGGR)

In this section we present the fundamentals of an extended gravity based on RG effects. Several works in literature focused on the application of this framework to

gravity[44, 45, 46, 47, 48, 49, 50, 51, 52, 53, 54, 55, 56, 57, 58, 59, 60, 61] in the context of quantum field theory in curved spacetime [47, 62] or in quantum-gravity[57, 63, 64]. In these approaches the gravitational constant G and the cosmological constant Λ obey a running which is given by renormalization group equations. But, before to proceed a brief parentheses about renormalization in quantum field theories in flat-space is deserved.

Quantum field theories, as one knows, offers an excelent framework for describing the fundamental interactions (e.g. QCD or QED). But, some undesired divergences start to appear when those theories are evaluated at very short distances (UV regime). The renormalization procedure is proposed in order to solve this issue, that is, removing those divergences and guaranteeing the entire description of the fundamental interactions. The divergences commonly appear in integrals, which in turn, are associated to the loops in Feyman diagrams, hence a divergence could be avoided if one considers a pragmatic procedure by choosing a large, but finite, cut-off. But, in this case your theory would be dependent of your cut-off and this can not be physical. The procedure mentioned before is called regularization (e.g. the dimensional regularization used in QCD). After this, one needs to remove the cut-off dependence and, at this point, the renormalization becomes important. The addition of appropriated counterterms in the action would be responsible for eliminating the cut-off dependence ensuring the renormazibility of the theory. One choice of this renormalization scheme is to transfer the cut-off dependence to the coupling constants and in this way to see how they behave according the energy scale of interest, this is called renormalization group procedure. Now, the coupling constants are dependent on a scale parameter, namely μ. Hence, the running of coupling constants are given by the solution of the renormalization group equation

$$\beta(g) = \frac{dg}{d\ln\mu}\,, \tag{2.29}$$

where g is the coupling constant and $\beta(g)$ is called $\beta-$function and it gives the renormalization group flow.

Another point concerning RG effects is a very well understood result, in the context of QFT in flat-space, that is the Appelquist-Carazzone decoupling [65] which, in essence, says that the $\beta-$functions are zero at low-energy limit or IR energy scale, i.e, there is no running for coupling constants at IR. There is an effort for generalizing this result to gravity (e.g. in [66]) but it is not possible to guarantee the no running of G and Λ at IR limit. Therefore, large scale variations of these 'constants' can be a sign of these RG effects.

In [10] was proposed an action in order to describe th RG effects in gravity and we will call this realization as RGGR,

$$S = \int \left[\frac{R - 2\Lambda\{\mu\}}{16\pi G(\mu)} + \lambda\left(\mu - f(g,\gamma,\Psi)\right)\right]\sqrt{-g}\,d^4x + S_m, \tag{2.30}$$

where $S = S[g,\gamma,\mu,\lambda,\Psi]$, $S_m = S_m[g,\Psi]$, Ψ stands for any matter fields of any nature, and μ is the RG scale whose relation with other fields is in a constraint-like way throught

the Lagrange multiplier λ. The field $\gamma_{\alpha\beta}$ is a tensor which works as a reference metric and it is important for the energy-momentum conservation and for stating a covariant scale setting. As we mentioned above, the constants G and Λ now are depending on the RG scale μ. According to [10] G is fixed at the action level while, i.e. its form does not depend on the other fields. For instance, if $G = \mu^2$ for Solar System, then $G(\mu)$ has to be the same for galaxies and cosmology. However, $\Lambda\{\mu\}$ is not universal instead is system dependent, i.e. it is not fixed at action level, but it can be derived from field equations.

Now, it is important to specify the function $G(\mu)$ that we will use hereafter (already derived in different approaches [46, 47, 67, 68, 69]):

$$G^{-1}(\mu) = G_0(1 + 2\nu \ln \mu), \tag{2.31}$$

where ν is a small dimensionless constant, and GR is recovered for $\nu = 0$. G_0 is the gravitational constant at some spacetime point.

The action (2.30) in general violates the energy-momentum conservation since it is not possible to split the action as $S = S_g[g, \Phi_G] + S_m[g, \Psi]$, where Φ_G are fields which do not appear in S_m and Ψ are fields that do not appear in S_g. The term which prevents the spliting of the action is λ, hence in general we have $\nabla_\alpha T^{\alpha\beta} \propto \lambda$. But if we consider a particular class of scale settings, i.e. f functions, namely[10]:

$$\mu = f\left(U^\alpha U^\beta h_{\alpha\beta}\right), \tag{2.32}$$

where $h_{\alpha\beta} \equiv g_{\alpha\beta} - \gamma_{\alpha\beta}$ and U^α denotes the four-velocity field, and variating the action (2.30) with respect to $\gamma_{\alpha\beta}$ we obtain

$$\lambda f' U^\alpha U^\beta = 0. \tag{2.33}$$

We have two possible solutions: i) if $f' = 0$ implies that μ is a constant, and we have standard GR. ii) if $\lambda = 0$ at the level of the field equations we have the energy-momentum conservation, i.e. $\nabla_\alpha T^{\alpha\beta} = 0$.

Furthermore, the variation of the action S with respect to the metric $g_{\alpha\beta}$ reads

$$\mathcal{G}_{\alpha\beta} + \Lambda g_{\alpha\beta} = 8\pi G T_{\alpha\beta}, \tag{2.34}$$

where

$$\mathcal{G}_{\alpha\beta} \equiv G_{\alpha\beta} + g_{\alpha\beta} G \Box G^{-1} - G\nabla_\alpha \nabla_\beta G^{-1}, \tag{2.35}$$

$\Box \equiv g^{\alpha\beta}\nabla_\alpha\nabla_\beta$, and ∇_α is the usual covariant derivative. From the energy-momentum conservation it is possible to derive[70, 71, 10]

$$\nabla_\alpha \left(\frac{\Lambda}{G}\right) = \frac{1}{2} R \nabla_\alpha G^{-1}. \tag{2.36}$$

The equation (2.36) can be also derived if we variate the action (2.30) with respect to μ.

2.3.1 The noncovariant scale setting

An issue that must to be clarified by any RG approach to gravity is the physical meaning of scale μ, i.e. what is the relation between the scale μ and the other quantities. In other words, one has to specify the f function. Previous works, e.g.[9], adopted a non covariant scale setting which is introduced in the context of stationary, slow-velocity and weak-field regime

$$\mu = \left(\frac{\Phi}{\Phi_0}\right)^{\alpha}, \tag{2.37}$$

where Φ_0 and α are constants which caracterizes the system and Φ is the Newtonian potential. The scale setting in equation (2.37) is an approximation to the covariant one (2.33), as described in Appendix B.

Some interesting implications for dark matter distribution in galaxy systems has been achieved by using (2.37)[9, 72, 73, 71, 74, 3, 75], including good results which are achievable even without dark matter.

As we said above α is not an universal constant, actually it depends of the system. In the context of galaxy rotation curves (e.g., [9, 3]), α changes from galaxy to galaxy. Considering the scale setting, introduced by equation (2.37), into the equation for G, namely (2.31), one can replace the two constants α and ν by a single system-dependent constant $\bar{\nu} \equiv \nu\alpha$ and all the dynamical tests will depend on it. In particular, for Solar System dynamics it was found in [76] that $|\bar{\nu}_\odot| \lesssim 10^{-17}$ and in [77], using a more precise data for the Solar System, one arrived the condition $|\bar{\nu}_\odot| \lesssim 10^{-21}$.

2.3.2 The external potential effect

As one can notice, according equation (2.37) which stabilishes the relation between μ and Φ, gravity is sensitive to the Newtonian potential value in the sense that the dynamics of a such system may change due a constant shift of the Newtonian potential. In particular, if we consider a static and spherically symmetric system it is possible to show the presence of an additional effective mass term from RGGR, namely δM_{RGGR} , which can be expressed as

$$\begin{aligned} \delta M_{\mathrm{RGGR}}(r) &\equiv (\Phi'_{\mathrm{RGGR}} - \Phi')r^2 \\ &= \bar{\nu}\frac{r}{1 + \frac{4\pi r}{M(r)}\int_r^\infty \rho(a)a\,da}, \end{aligned} \tag{2.38}$$

where Φ_{RGGR} is the effective potential of RGGR. Note that if the mass distribution, in the equation above, is such that of a particle with mass M, the integral in the denominator of the equation above is zero for $r > 0$, hence the effective additional term will increases linearly with r and consequently the additional force, which is the difference between the derivatives of the potentials in equation (2.38), will decreases with r. However, if we

consider a mass distribution for $r > 0$ the integral is not zero anymore and the term $\delta M_{\rm RGGR}$ can be suppressed. Note that the integral in equation (2.38) brings with it external contributions, i.e. contributions from the environment where the system is included and the larger ammount of mass outside a given region, the smaller the non-Newtonian effects in that region. Indeed, the equation (2.38) represents the external potential contribution in terms of an external mass density effect. In conclusion, the external potential acts as a screening mechanism for RGGR reducing the non-Newtonian contributions and this effect is already part of the theory. Now we will extend the results above to generic systems.

Consider S' a subsystem of a system S, much smaller than S. The subsystem is so small that we can consider the average Newtonian potential of S, namely Φ_s, as a constant. Here, the use of the term "average" means that the substructures of the system S are irrelevant and hence not individually considered. Hence the Newtonian potentials of S and S' can be written as,

$$\Phi_s = \phi_s + \phi_e \,, \tag{2.39}$$

$$\begin{aligned} \Phi_{s'} &= \phi_{s'} + \Phi_s|_{s'} \\ &= \phi_{s'} + \phi_s|_{s'} + \phi_e \\ &= \phi_{s'} + \phi_{e'} + \phi_e \,. \end{aligned} \tag{2.40}$$

In the above, ϕ_s stands for the Newtonian potential generated by the system S, and ϕ_e refers to the total external contribution.

Since the subsystem S' is much smaller than the system S the total external contribution to S' can be computed as $\Phi_s|_{s'}$ which is the potential of the system S evaluated at S'. The entire external potential contribution to the subsystem S' is composed by two terms. One is the same of the system S, which is natural since S' is a small part of S, the other is $\phi_{e'} = \phi_s|_{s'}$. The next step is to evaluate the consequences for G in the system and the subsystem. Hence, let us consider the following expression for G at the system S

$$G_s^{-1}(\phi_s) = G_0^{-1}\left(1 + 2\bar{\nu}_s \ln\frac{\phi_s + \phi_e}{\Phi_0}\right). \tag{2.41}$$

As we said before, Φ_0 is a reference potential, it means that we can change it. In particular, let us consider ϕ_e as our reference potential. In this way, the expression for G_s^{-1} becomes

$$G_s^{-1}(\phi_s) = G_e^{-1}\left[1 + 2\bar{\nu}_e \ln\left(1 + \frac{\phi_s}{\phi_e}\right)\right], \tag{2.42}$$

with G_e and $\bar{\nu}_e$ such that

$$G_e^{-1}\bar{\nu}_e = G_0^{-1}\bar{\nu}_s, \tag{2.43}$$

$$G_e^{-1} = G_0^{-1}\left(1 + 2\bar{\nu}_s \ln\frac{\phi_e}{\Phi_0}\right). \tag{2.44}$$

Using the relations above and changing the reference potential it is also possible to express the expression for G at the subsystem S' as

$$\begin{aligned} G_{s'}^{-1}(\phi_{s'}) &= G_{0'}^{-1}\left(1+2\bar{\nu}_{s'}\ln\frac{\phi_{s'}+\phi_{e'}+\phi_e}{\Phi_{0'}}\right) \\ &= G_{e'}^{-1}\left[1+2\bar{\nu}_{e'}\ln\left(1+\frac{\phi_{s'}+\phi_e}{\phi_{e'}}\right)\right]. \end{aligned} \tag{2.45}$$

The constant ϕ_e satisfies $|\phi_e| \ll |\phi_s|$ which means that $|\phi_e| \ll |\phi_{e'}|$, hence again at system S and subsystem S' the expression for G reads

$$G_s^{-1}(\phi_s) \approx G_e^{-1}\left(1+2\bar{\nu}_e\ln\frac{\phi_s}{\phi_e}\right), \tag{2.46}$$

$$\begin{aligned} G_{s'}^{-1}(\phi_{s'}) &\approx G_{e'}^{-1}\left[1+2\bar{\nu}_{e'}\ln\left(1+\frac{\phi_{s'}}{\phi_{e'}}\right)\right] \\ &\approx G_{e'}^{-1}\left[1+2\bar{\nu}_{e'}\left(\frac{\phi_{s'}}{\phi_{e'}}-\frac{1}{2}\frac{\phi_{s'}^2}{\phi_{e'}^2}\right)\right], \end{aligned} \tag{2.47}$$

where we used that $\ln(1+X) = \ln X + O(1/X)$, for $|X| \gg 1$, and $\ln(1+x) = x - x^2/2 + O(x^3)$, for $|x| \ll 1$. In equation (2.47) is assumed $\phi_{s'}/\phi_{e'} < 1$ and this is a useful condition for Solar System test, as we will show later, namely in Chapter 4.

2.3.3 GR and RG perturbations

Here we will describe a perturbation scheme which will be important for a better comprehension of the Chapter 4 and the next Subsection 2.3.4. Hence, consider the following scheme about the metric $\overset{(0)}{g}_{\alpha\beta}$:

$$g_{\alpha\beta} = \overset{(0)}{g}_{\alpha\beta} + \overset{(1,0)}{g}_{\alpha\beta} + \overset{(0,1)}{g}_{\alpha\beta} + ..., \tag{2.48}$$

$$T_{\alpha\beta} = \overset{(0)}{T}_{\alpha\beta} + \overset{(1,0)}{T}_{\alpha\beta} + \overset{(0,1)}{T}_{\alpha\beta} + ..., \tag{2.49}$$

$$G(\mu) \equiv 1+\delta G(\mu) = 1+\overset{(1)}{G}(\mu) + ... \tag{2.50}$$

$$\Lambda(\mu) \equiv \Lambda_0+\delta\Lambda(\mu) = \Lambda_0+\overset{(1)}{\Lambda}(\mu) + ... \tag{2.51}$$

The metric $\overset{(0)}{g}_{\alpha\beta}$ satisfies the Einstein equation with the energy momentum tensor $\overset{(0)}{T}_{\alpha\beta}$, the gravitational constant G_0 (which is set to be 1) and the cosmological constant Λ_0. Now, just claryfing the notation: the terms $\overset{(n,0)}{X}_{\alpha\beta}$ refer to the perturbation within GR, namely, n refers to the order in a post-Newtonian expansion. The terms of the type $\overset{(n,m)}{X}_{\alpha\beta}$ are the RG correction of the mth order to the respective GR perturbation of order n.

The background here is assumed to be Minkowski, i.e,

$$\overset{(0)}{g}_{\alpha\beta} = \eta_{\alpha\beta}, \qquad \Lambda_0 = 0, \qquad \overset{(0)}{T}_{\alpha\beta} = 0. \tag{2.52}$$

Within this context, it was demonstrated in [10] that, up to first order in both of the perturbations, if the solution of the Einstein equation , namely $\tilde{G}^{\beta}_{\alpha} = 8\pi\tilde{T}^{\beta}_{\alpha}$, is $\tilde{g}_{\alpha\beta}$ then the solution for the equation (4.10) is given by the conformal transformation

$$g_{\alpha\beta} = G\,\tilde{g}_{\alpha\beta} + O(2,2), \tag{2.53}$$

where $O(m,n)$ represents the terms of the m-th or higher order on the GR perturbation, and of n-th or higher order on the RG perturbation. In order to familiarize the reader with respect to the notation and review an important result that can be found in [9, 10], consider $\tilde{g}_{\alpha\beta} = \eta_{\alpha\beta} + \tilde{h}_{\alpha\beta}$ and $g_{\alpha\beta} = \eta_{\alpha\beta} + h_{\alpha\beta}$ and also using the equation (2.53),

$$\begin{aligned} h_{\alpha\beta} &= g_{\alpha\beta} - \eta_{\alpha\beta} \\ &= (\eta_{\alpha\beta} + \tilde{h}_{\alpha\beta})G - \eta_{\alpha\beta} + O(2,2). \end{aligned} \tag{2.54}$$

Hence, in particular,

$$\begin{aligned} h_{00} &= -2\Phi - \overset{(1)}{G} + O(2,2) \\ &= -2\Phi + 2\nu\ln\mu + O(2,2). \end{aligned} \tag{2.55}$$

The h_{00} is the effective potential of RGGR, i.e. is the potential which gives the acceleration. The result above shows the relation between this effective potential and the Newtonian one.

2.3.4 Point particle solution of RGGR

An important result which will be useful for the comprehension of next chapters, in particular the Chapter 4, is the point particle solution in RGGR. In this subsection we will present a detailed derivation of the point-particle solution from field equations of RGGR (4.10). There are other derivations of point-particle solutions for RGGR in literature, e.g. [9], but using the conformal transformation, equation (2.53), which holds only up to first-order perturbations in both GR and RG expansions. However, the direct method (using the field equations) enable us to find the point-particle solution up to order $O(\infty,2)$, i.e. arbitrary order in the GR expansion while only second-order in RG parameter $\bar{\nu}$.

Hence, consider a spacetime with a proper symmetry for a point-like solution which in turn can be written, without loss of generality, as

$$ds^2 = g_{00}(r)dt^2 + g_{11}(r)dr^2 + r^2 d\Omega^2, \tag{2.56}$$

with $d\Omega^2 = d\theta^2 + \sin^2(\theta)\, d\phi^2$. Using the latter line element, it is straightforward to shown the identities:

$$\begin{aligned} \mathcal{G}^{\nu}_{\mu} &= 0 \quad \forall \mu \neq \nu, \\ \mathcal{G}^{2}_{2} &= \mathcal{G}^{3}_{3}. \end{aligned} \tag{2.57}$$

For practical reasons, two field equations from equation (4.10) can be used in a such way that Λ does not appear explicitly, in other words

$$\mathcal{G}^{0}_{0} = \mathcal{G}^{1}_{1}\,, \tag{2.58}$$

$$\mathcal{G}^{1}_{1} = \mathcal{G}^{2}_{2}\,. \tag{2.59}$$

From the first equation above it is possible to deduce a relation between the metric components, namely g_{11} and g_{00}, up to first-order in $\bar{\nu}$:

$$g_{11} = -\frac{K}{g_{00}}\left[1 + 2\bar{\nu}\left(r\frac{\mu'}{\mu} - \ln\frac{\mu}{\mu_1}\right)\right] + O(\infty, 2), \tag{2.60}$$

where a prime means derivative with respect to r and K and μ_1 are integration constants. The latter can be absorbed using a time redefinition, namely $t \to t/\sqrt{K(1 + 2\bar{\nu}\ln\mu_1)}$. To see this, just note that

$$\begin{aligned} &K\left(1 + 2\bar{\nu}\left(r\frac{\mu'}{\mu} - \ln\frac{\mu}{\mu_1}\right)\right) \approx \\ &\approx K(1 + 2\bar{\nu}\ln\mu_1)\left(1 + 2\bar{\nu}\left(r\frac{\mu'}{\mu} - \ln\mu\right)\right), \end{aligned} \tag{2.61}$$

up to first order in $\bar{\nu}$.

From equations (2.59) and (2.60), the solution for the g_{00} component of the metric fields is

$$g_{00} = -1 + \frac{C_1}{r} + C_2 r^2 + 2\bar{\nu}\left(1 - \frac{3C_1}{2r}\right)\ln\mu + O(\infty, 2), \tag{2.62}$$

where C_1 and C_2 are integration constants. In the case of GR, i.e. $\bar{\nu} = 0$, the constants are the mass at $r = 0$ and the cosmological constant, respectively. As expected, the solution derived above is an extension of the Schwarszchild-de Sitter solution.

2.4 Scalar-tensor-vector-gravity

In [78] it was proposed a Scalar-Tensor-Vector modification of Einstein-Hilbert action, also know in literature as MOG (MOdified Gravity) theory, in order to capture renormalization group flow effects. In MOG, the gravitational constant G is treated as a scalar field and an additional one is introduced, namely μ, and also a vector field ϕ_μ. Following [79, 78], the action for MOG[2] is given by

$$S_{MOG} = S_g + S_{\phi_\mu} + S_{sf} + S_m\,, \tag{2.63}$$

[2] Using the metric signature $(+,-,-,-)$ and $c = 1$

where

$$S_g = -\frac{1}{16\pi}\int \frac{1}{G}(R+2\Lambda)\sqrt{-g}\; d^4x \tag{2.64}$$

is the Einstein-Hilbert action and Λ is the cosmological constant,

$$S_{\phi_\mu} = -\frac{1}{4\pi}\int \gamma\left[\frac{1}{4}B^{\mu\nu}B_{\mu\nu} + V_{\phi_\mu}(\phi_\mu\phi^\mu)\right]\sqrt{-g}\; d^4x\ , \tag{2.65}$$

is the action for the massive vector field ϕ_μ, where $B_{\mu\nu} = \partial_\mu\phi_\nu - \partial_\nu\phi_\mu$ and γ is the coupling constant between the massive vector field and the matter,

$$S_{sf} = -\int \frac{1}{G}\left[\frac{1}{2}g^{\alpha\beta}\left(\frac{\nabla_\alpha G\nabla_\beta G}{G^2} + \frac{\nabla_\alpha\mu\nabla_\beta\mu}{\mu^2}\right) + \frac{V_G(G)}{G^2} + \frac{V_\mu(\mu)}{\mu^2}\right]\sqrt{-g}\; d^4x\ , \tag{2.66}$$

is the action for the scalar fields μ and G. The terms $V_{\phi_\mu}(\phi_\mu\phi^\mu)$, $V_G(G)$ and $V_\mu(\mu)$ are the potentials of the vector field and scalar fields, respectively. Varying the action S_{MOG} with respect to the metric field $g_{\mu\nu}$ one finds

$$G_{\mu\nu} - \Lambda g_{\mu\nu} + H_{\mu\nu} = -8\pi G T_{\mu\nu}\ , \tag{2.67}$$

where

$$H_{\mu\nu} = G(g_{\mu\nu}\Box G^{-1} - \nabla_\mu\nabla_\nu G^{-1})\ , \tag{2.68}$$

and $T_{\mu\nu}$ is the total energy-momentum tensor, where by using the equation (1.12) one has

$$T_{\mu\nu} = \frac{-2}{\sqrt{-g}}\frac{\delta S_{MOG}}{\delta g^{\mu\nu}} = \frac{-2}{\sqrt{-g}}\frac{\delta(S_m + S_{sf} + S_{\phi_\mu})}{\delta g^{\mu\nu}} = \mathrm{T}_{\mu\nu} + \mathbb{T}_{\mu\nu} + \mathfrak{T}_{\mu\nu} + \mathcal{T}_{\mu\nu}\ , \tag{2.69}$$

where each term after last equality is the energy-momentum tensor for the matter, the scalar fields G, μ and the massive vector field ϕ_μ. Explicitly, for G, μ and ϕ_μ one has

$$\mathbb{T}_{\mu\nu} = -\frac{1}{G^3}\left[\nabla_\mu G\nabla_\nu G - 2\frac{\partial V_G(G)}{\partial g^{\mu\nu}} - g_{\mu\nu}\left(\frac{1}{2}g^{\rho\sigma}\nabla_\rho G\nabla_\sigma G - V_G(G)\right)\right]\ , \tag{2.70}$$

$$\mathfrak{T}_{\mu\nu} = -\frac{1}{\mu^2 G}\left[\nabla_\mu\mu\nabla_\nu\mu - 2\frac{\partial V_\mu(\mu)}{\partial g^{\mu\nu}} - g_{\mu\nu}\left(\frac{1}{2}g^{\rho\sigma}\nabla_\rho\mu\nabla_\sigma - V_\mu(\mu)\right)\right]\ , \tag{2.71}$$

$$\mathcal{T}_{\mu\nu} = \frac{\gamma}{4\pi}\left[B^\sigma_\nu B_{\mu\sigma} - g_{\mu\nu}\left(\frac{1}{4}B^{\rho\sigma}B_{\rho\sigma} + V_{\phi_\mu}(\phi^\mu\phi_\mu) + 2\frac{\partial V_{\phi_\mu}(\phi^\mu\phi_\mu)}{\partial g^{\mu\nu}}\right)\right]\ . \tag{2.72}$$

Therefore, varying the action (2.63) with respect to the scalar fields one obtains, for G and μ [78]

$$\Box G + V_G'(G) + \Theta = -\frac{1}{G^2}\left(T + \frac{\Lambda}{4\pi G}\right)\ , \tag{2.73}$$

where

$$\Theta = -3G^{-1}\left(\frac{1}{2}\nabla_\alpha G\nabla^\alpha G + V_G(G)\right) + \frac{G}{\mu^2}\left(\frac{1}{2}\nabla_\alpha\mu\nabla^\alpha\mu - V_\mu(\mu)\right) + \frac{3G^2}{16\pi}\nabla_\alpha\nabla^\alpha G^{-1}\ , \tag{2.74}$$

and

$$\Box\mu + V_{\mu}^{'}(\mu) + \Xi = 0 \ , \tag{2.75}$$

where

$$\Xi = -\left[G^{-1}\nabla^{\rho}G\nabla_{\rho}\mu + \frac{2}{\mu}\nabla^{\rho}\mu\nabla_{\rho}\mu + \frac{\gamma}{4\pi}\mu^{2}\frac{\partial V_{\phi_{\mu}}(\phi^{\mu}\phi_{\mu})}{\partial\mu}\right] \ , \tag{2.76}$$

where the last term comes from the fact that the potential $V_{\phi_{\mu}}(\phi^{\mu}\phi_{\mu}) = -\frac{1}{2}\mu^{2}\phi^{\mu}\phi_{\mu}$. Moreover, varying the action (2.65) with respect to the massive vector field ϕ_{μ} one has

$$\nabla_{\nu}B^{\mu\nu} - \mu^{2}\phi^{\mu} = -\frac{4\pi}{\gamma}J^{\mu} \ \ , \text{ with } J^{\mu} \equiv -\frac{1}{\sqrt{-g}}\frac{\delta S_{m}}{\delta\phi_{\mu}} \ , \tag{2.77}$$

where J^{μ} is the matter current density.

The purpose of this section is to show that the fifth force mediated by the massive vector field ϕ_{μ} is described by a repulsive Yukawa force, when the weak-field limit is considered. An important equation for obtaining the weak-field limit is the geodesic equation because it gives to us, in the slow motion regime, the effective potential, i.e. the potential that yields the acceleration of the test particle. Hence, the action for a test particle is given by

$$S_{m} = \int(-m - \gamma Q_{5}U^{\mu}\phi_{\mu})\sqrt{-g}\ d\tau \ , \tag{2.78}$$

where m is the rest mass of the test particle and Q_{5} is the fifth force charge. The relation between Q_{5} and m is $Q_{5} = \varkappa m$, where $\varkappa$ is a constant. The equations of motion for the test particle come from $\delta S_{m}/\delta x^{\mu} = 0$. Hence, variating the action (2.78) with respect to δx^{μ} one obtains

$$\frac{dU^{\mu}}{d\tau} + \Gamma^{\mu}_{\alpha\beta}U^{\alpha}U^{\beta} = \gamma\varkappa B^{\mu}_{\alpha}U^{\alpha} \ . \tag{2.79}$$

Clearly, the usual geodesic equation (1.19) is recovered when $\gamma = 0$. The equation above is the standard geodesic equation with an extra repulsive force, arising from the fifth force, which depends on the velocity of the test particle. Now, focusing in the weak-field limit of MOG. Here, we will present the main results obtained by [79, 78] therefore further details about the calculations the reader is invited to see the latter references.

As was pointed before, the weak-field limit of a metric theory is achieved performing a perturbation around a Minkowkski background metric $\eta_{\mu\nu}$, i.e. $g_{\mu\nu} = \eta_{\mu\nu} + h_{\mu\nu}$. But, MOG also present two scalar fields and one additional massive vector field. Thus, the perturbation for these quantities are given by

$$G = G_{0} + \overset{(1)}{G} \ , \tag{2.80}$$

$$\mu = \mu_{0} + \overset{(1)}{\mu} \tag{2.81}$$

and

$$\phi_{\mu} = \overset{(0)}{\phi}_{\mu} + \overset{(1)}{\phi}_{\mu} \ , \tag{2.82}$$

where G_0 is the gravitational constant in Minkowski space, μ_0 is a constant that will be fixed as the mass of the vector field and for convenience let us label simply as μ. It will be assumed that $\overset{(1)}{\mu}$ is negligible. In the background there is no gravity source for the vector field, hence $\overset{(0)}{\phi}_{\mu}$ is zero and for convenience one sets $\overset{(1)}{\phi}_{\mu} \equiv \phi_{\mu}$. Moreover, one perturbs the total energy-momentum tensor about the background, namely

$$T_{\mu\nu} = \overset{(0)}{T}_{\mu\nu} + \overset{(1)}{T}_{\mu\nu} \ . \tag{2.83}$$

Considering the perturbations in the above, the field equation for the scalar field G gives

$$\Box \overset{(1)}{G} = -\frac{G_0}{16\pi} \overset{(1)}{R} \, , \tag{2.84}$$

where $\overset{(1)}{R}$ is the first-order perturbation of the Ricci scalar. In the derivation of equation (2.84), it was used the trace of the total energy-momentum tensor, from equation (2.73), as $T = (1/8\pi G)(R + 4\Lambda - 3G\Box G^{-1})$.

Now, considering the equations (2.80), (2.81) and (2.82) in equation (2.67) one yields

$$\overset{(1)}{R}_{\mu\nu} - \frac{1}{2} \overset{(1)}{R} \, \eta_{\mu\nu} = -8\pi G_0 (\mathrm{T}^{(1)}_{\mu\nu} + \mathcal{T}^{(1)}_{\mu\nu}) \, . \tag{2.85}$$

Taking the trace of the previous equation and considering that $\mathcal{T}^{(1)}_{\mu\nu} \ll \mathrm{T}^{(1)}_{\mu\nu}$ one finds

$$\overset{(1)}{R} = 8\pi G_0 \mathrm{T}^{(1)} \, , \tag{2.86}$$

where for such systems that the pressure is negligible one has $\mathrm{T} = \rho$. Replacing the result above in the equation (2.84), for the stationary case, one gets

$$\nabla^2 \left(\frac{\overset{(1)}{G}}{G_0} \right) = \frac{1}{2} G_0 \rho \, . \tag{2.87}$$

From the equation (2.87) one perceives that $\overset{(1)}{G} /G_0 \sim G_0\rho \sim (v/c)^2$, where v is the internal velocity of the virialized system. Thus, in the case of systems such as Solar System, galaxies or even cluster of galaxies, the deviation from G_0, namely δG, is such that $\delta G \sim \overset{(1)}{G} /G_0 \sim 10^{-7} - 10^{-5}$. Therefore, one can keep only the background value for G.

The (00) component of $R_{\mu\nu}$, in the weak-field limit, is $\overset{(1)}{R}_{00} = \frac{1}{2}\nabla^2 h_{00}$. Hence, one obtains, from equations (2.85) and (2.86),

$$\frac{1}{2}\nabla^2 h_{00} = -4\pi G_0 \rho \tag{2.88}$$

Assuming that the current J^{μ} is conserved, i.e. $\nabla_{\mu} J^{\mu} = 0$ and adopting the gauge condition $\nabla_{\mu}\phi^{\mu} = 0$, for the stationary case, the equation (2.77) becomes

$$\nabla^2 \phi^0 - \mu^2 \phi^0 = -\frac{4\pi}{\gamma} J^0 \, , \tag{2.89}$$

whoose the solution is

$$\phi^0(\mathbf{x}) = \frac{1}{\gamma}\int \frac{e^{-\mu|\mathbf{x}-\mathbf{x}'|}}{|\mathbf{x}-\mathbf{x}'|}J^0(\mathbf{x}')d^3\mathbf{x}' \ . \tag{2.90}$$

In order to find the effective potential let us consider the weak-field limit of the geodesic equation for MOG, equation (2.79). Hence, considering first-order on perturbations and slow motion regime, i.e. $v \ll c$, one finds from the spatial component of the equation (2.79)

$$\nabla\cdot\mathbf{a} - \frac{1}{2}\nabla^2 h_{00} = -\gamma\varkappa\nabla^2\phi^0 \ , \tag{2.91}$$

where $\mathbf{a}$ is the acceleration of the test particle which relates with the effective potential Φ_{eff} via $\mathbf{a} = -\nabla\Phi_{eff}$. Thus, replacing $\frac{1}{2}\nabla^2 h_{00}$ from the equation (2.91) into equation (2.88) one has

$$\nabla^2(\Phi_{eff} - \varkappa\gamma\phi^0) = 4\pi G_0 \ . \tag{2.92}$$

Comparing the equation above and the equation (1.26) is straightforward to identify the Φ_N as

$$\Phi_N = \Phi_{eff} - \varkappa\gamma\phi^0 \ . \tag{2.93}$$

Inserting the solution of equation (2.90) and setting $J^0 = \varkappa\gamma\rho$, the equation (2.93) becomes

$$\Phi_{eff}(\mathbf{x}) = -G_0\int\frac{\rho(\mathbf{x}')}{|\mathbf{x}-\mathbf{x}'|}d^3\mathbf{x}' + \varkappa^2\int\frac{e^{-\mu|\mathbf{x}-\mathbf{x}'|}}{|\mathbf{x}-\mathbf{x}'|}d^3\mathbf{x}' \ . \tag{2.94}$$

Here, it is seen that the first term is the usual attractive gravitational potential while the second one is a repulsive Yukawa force. In order to complete the weak-field limit one has to find the value of $\varkappa$. For simplicity, let us consider a point mass M as the source of the gravitational field, i.e. $\rho(\mathbf{x}') = M\delta^3(\mathbf{x}')$. Hence, the effective potential becomes

$$\Phi_{eff}(x) = -\frac{G_0 M}{x} + \varkappa\frac{Me^{-\mu x}}{x} \ , \tag{2.95}$$

where $x \equiv |\mathbf{x}|$. Considering scales such that $\mu x \ll 1$, the exponential in the second term can be expanded and one can identify the Newtons's constant G_N, as follows

$$\Phi_{eff}(x) = -\frac{(G_0 - \varkappa^2)M}{x} - \mu\varkappa^2 M \ . \tag{2.96}$$

Since the last term does not contributes to the dynamics of the test particle one has $G_N \equiv G_0 - \varkappa^2$. However, if one applies the limit $\mu x \to \infty$ one finds only the first term in equation (2.96). Thus, G_0 is the gravitational constant at infinity.

Finally, replacing $\varkappa^2$ in equation (2.94) one rewrites the effective potential as follows

$$\Phi_{eff}(\mathbf{x}) = -G_0\left[\int\frac{\rho(\mathbf{x}')}{|\mathbf{x}-\mathbf{x}'|}\left(1 - \frac{G_0 - G_N}{G_0}e^{-\mu|\mathbf{x}-\mathbf{x}'|}\right)d^3\mathbf{x}'\right] \ . \tag{2.97}$$

Defining $\delta \equiv \frac{G_0 - G_N}{G_N}$, the effective potential reduces to

$$\Phi_{eff}(\mathbf{x}) = -G_N\left[\int\frac{\rho(\mathbf{x}')}{|\mathbf{x}-\mathbf{x}'|}(1 + \delta - \delta e^{-\mu|\mathbf{x}-\mathbf{x}'|})d^3\mathbf{x}'\right] \ . \tag{2.98}$$

3 THE PARAMETRIZED POST-NEWTONIAN FORMALISM

This chapter is dedicated to present a short review of the PPN formalism and its utility as a tool for testing gravity against Solar System experiments. The chapter was written based mainly on the References [34, 2] and further details about the formalism can be found therein.

The metric theories of gravity can be compared with each other and with experiments in a simple manner when they are taken at the slow-motion and weak-field limit. This regime, known as post-Newtonian limit, is enough to cover all the Solar System tests. Namely, the Solar System is very well described by Newton's gravity until the precision of 10^{-5}, but it can not account for Mercury's additional perihelion shift of $\sim 5 \times 10^{-7}$ radians per orbit. Hence, a "post" Newtonian theory is required.

At the moment, let focus on the regime very well described for Newton's gravity, that is, the Newtonian limit of metric theories of gravity. At this limit the test bodies move according to

$$\mathbf{a} = \nabla U, \tag{3.1}$$

where $\mathbf{a}$ is the body's acceleration and U is the Newtonian gravitational potential which is the solution of Poisson's equation, namely[1]

$$\nabla^2 U = -4\pi\rho, \qquad U(\mathbf{x}, t) = \int \frac{\rho(\mathbf{x}', t)}{|\mathbf{x}' - \mathbf{x}|} d^3x', \tag{3.2}$$

where ρ is rest-mass density and $\nabla^2 \equiv \delta^{ij}\partial_i\partial_j$.

From the prespective of a metric theory of gravity if the latter is weak, the metric is the Minkowski metric plus a small perturbation, namely $h_{\mu\nu}$, as follows

$$g_{\mu\nu} = \eta_{\mu\nu} + h_{\mu\nu}, \tag{3.3}$$

with $|h_{\mu\nu}| \ll 1$. Furthermore, in the Newtonian limit one does not consider time dependence in the metric fields, i.e. $\partial_t g_{\mu\nu} = 0$. The motion of the test particle due the influence of the gravitational field, equation (3.3), is given by the geodesic equation. The time component of the latter just gives to us that the affine parameter, along the geodesic, is the time coordinate, namely t, while the spatial component of the geodesic equation reads

$$\frac{d^2x^i}{dt^2} = -\Gamma^i_{00} = \frac{1}{2}\delta^{ij}h_{00,j}. \tag{3.4}$$

[1] We use geometrized units, i.e. $c = G = 1$

Hence, the equation above can yield the Newtonian gravitation, i.e. equation (3.1), only if

$$h_{00} = 2U. \tag{3.5}$$

Hence, the weak field regime (3.3) becomes

$$g_{00} \simeq -1 + 2U, \quad g_{ij} \simeq \delta_{ij} \ . \tag{3.6}$$

In order to understand better the post-Newtonian limit let establish a "bookkeeping" system in order to have a small parameter to expand in. As it was pointed out before, the Newtonian gravitational potential, namely U, at the Solar System, is $U \sim 10^{-5}$, in geometrized units. Hence, considering that the Solar System is a virialized system, one can relates the velocity of its constituent, i.e. the planets, with its gravitational potential, in other words one has

$$v^2 \lesssim U \ . \tag{3.7}$$

Also, the matter content of the Sun and the planets is under a pressure p, but this pressure is smaller than ρU, which is the matter's gravitational energy density. Thus,

$$\frac{p}{\rho} \lesssim U \ . \tag{3.8}$$

If there are other forms of energy, e.g. thermal energy, they are also small. Usually, is computed the ratio between those forms of energy and the rest-mass density. This ratio is called specific energy density Π and relates with U by

$$\Pi \lesssim U \ . \tag{3.9}$$

The small quantitites stated above can be related between themselves throught the gravitational potential U. Hence, one has an order of smallness:

$$U \sim v^2 \sim \frac{p}{\rho} \sim \Pi \sim O(2) \ , \tag{3.10}$$

where $O(1)$ are single powers of v. Thus, $U^2 \sim O(4)$, $Uv \sim O(3)$ and so on.

Furthermore, if the evolution of the Solar System as a whole is determined by the motions of the planets, one has

$$\frac{\partial}{\partial t} \sim \mathbf{v} \cdot \nabla \quad \Longrightarrow \quad \frac{|\partial/\partial t|}{|\partial/\partial x|} \sim O(1) \ . \tag{3.11}$$

Now, we are able for analyzing the post-Newtonian limit of any metric theory of gravity only requiring the knowledge of

$$\begin{aligned} &g_{00} \ \text{ up to } \ O(4), \\ &g_{0i} \ \text{ up to } \ O(3), \\ &g_{ij} \ \text{ up to } \ O(2) \ . \end{aligned} \tag{3.12}$$

If one considers that the matter content of the Solar System is described by a fluid, one has that the energy momentum tensor is given by

$$T^{\mu\nu} = (\rho + \rho\Pi + p)U^{\mu}U^{\nu} + pg^{\mu\nu} \tag{3.13}$$

which in turn, in order to obtain the post-Newtonian limit, one must to expand

$$\begin{aligned} &T^{00} \text{ up to } O(4), \\ &T^{0i} \text{ up to } O(3), \\ &T^{ij} \text{ up to } O(2)\ . \end{aligned} \tag{3.14}$$

One can imagine that the post-Newtonian system resides in a homogeneous isotropic universe and adopting a coordinate system such that the outer regions are far from the post-Newtonian system and at rest with respect to the frame in which the universe is isotropic, the metric, in these outer regions, looks like

$$ds^2 = -dt^2 + \left[\frac{a(t)}{a_0}\right]^2 \left(1 + \frac{kr^2}{4a_0^2}\right)^{-2} \delta_{ij}dx^i dx^j + h_{\mu\nu}dx^{\mu}dx^{\nu}\ , \tag{3.15}$$

where $a(t)$ is the cosmological scale factor, and $a_0 \equiv a(t_0)$. The constant k whoose values can be $0, \pm 1$ is the curvature parameter. Hence, the first two terms in equation (3.15) are the FLRW line element for a homogeneous isotropic cosmological model and the last term is the local system , i.e. the post-Newtonian one, which can be seen as a perturbation. If one chooses a particular moment t_0 at a given radius r_0, the metric (3.15) can be written as

$$ds^2 = (\eta_{\mu\nu} + h'_{\mu\nu})dx^{\mu'}dx^{\nu'}\ , \tag{3.16}$$

where the following coordinate transformation was used

$$t' = t, \quad x'^i = x^i(1 - kr_0^2/4a_0^2)^{-1}\ . \tag{3.17}$$

Thus, one ignores the variation of the cosmological scale factor $a(t)$ with time and the space-time metric of the post-Newtonian system, e.g. the Solar System, as being asymptotically Minkowski.

As already mentioned, the matter content of the Solar System is idealized as a fluid. Hence, the post-Newtonian limit of any metric theory of gravity can be obtained solving the field equations and expressing the metric expansion, consistent with the post-Newtonian approximation, in terms of the post-Newtonian functionals of the matter variables (e.g. ρ, p or Π)) or simply post-Newtonian potentials. Thus, the most general way for expressing the post-Newtonian metric is simply writing down the all possible post-Newtonian potentials, each multiplied by some coefficient, and adding them to the Minkowski metric in order to obtain (3.15). Naturally, there are endless ways to build these post-Newtonian potentials and in order to obtain a formalism that is manageable, one should to make some assumptions and restrictions which will be listed below:

- The terms included into the post-Newtonian approximation should tend to zero when $|\mathbf{x}-\mathbf{x}'|$ becomes large. Here, $\mathbf{x}$ is the field point and $\mathbf{x}'$ is located inside the matter. This condition ensures asymptotic flatness.
- The metric should be dimensionless hence the coordinates are chosen accordingly.
- The components of the metric corrections h_{00}, h_{0i} and h_{ij} must to transform under spatial rotations as a scalar (e.g. ρ, v^2, $\mathbf{v}'\cdot(\mathbf{x}-\mathbf{x}')$ etc); vector (e.g. v_i, $(x-x')_j$) and tensor, (e.g. $(x-x')_i(x-x')_j$) respectively.
- The post-Newtonian potentials should be generated only by matter variables, e.g. ρ, p, Π or v, and not by their gradients. Clearly, this restriction is just a convenience and, if necessary, it has to be relaxed.
- The post-Newtonian potentials have to be "simple".

Thus, with those restrictions, it is possible to write down the possible post-Newtonian terms which may appear.

According the statements above, g_{ij} should to transform as a three-dimensional tensor with respect to spatial rotations. Thus, the only terms allowed to $O(2)$ are

$$U\delta_{ij}, U_{ij}\ , \tag{3.18}$$

where U_{ij} is given by

$$U_{ij} \equiv \int \frac{\rho(\mathbf{x}',t)(x-x')_i(x-x')_j}{|\mathbf{x}-\mathbf{x}'|^3} d^3x'. \tag{3.19}$$

Conveniently, we can express U_{ij} in terms of an another potential, namely $\chi(\mathbf{x},t)$, given by

$$\begin{aligned} \chi(\mathbf{x},t) &\equiv -\int \rho(\mathbf{x}',t)|\mathbf{x}-\mathbf{x}'|d^3x'\ , \\ \chi_{,ij} &= -\delta_{ij}U + U_{ij}, \qquad \nabla^2\chi = -2U\ . \end{aligned} \tag{3.20}$$

Thus, the terms that one has to consider, in our post-Newtonian expansion, to $O(2)$ are

$$U\delta_{ij}, \chi_{,ij}\ . \tag{3.21}$$

The components of the metric tensor g_{0i} to $O(3)$ must to transform as a vector under spatial rotations. Hence, the terms which are allowed are:

$$V_i, W_i\ , \tag{3.22}$$

where

$$\begin{aligned} V_i &\equiv \int \frac{\rho(\mathbf{x}',t)v_i'}{|\mathbf{x}-\mathbf{x}'|} d^3x'\ , \\ W_i &\equiv \int \frac{\rho(\mathbf{x}',t)\mathbf{v}'\cdot(\mathbf{x}-\mathbf{x}')(x-x)_i}{|\mathbf{x}-\mathbf{x}'|^3} d^3x'\ . \end{aligned} \tag{3.23}$$

The post-Newtonian potentials V_i, W_i are related with the functional χ via

$$\chi_{,0i} = V_i - W_i \ . \tag{3.24}$$

Finally, the components g_{00} to $O(4)$ must to be scalars under rotations. Hence, the terms that must to be considered are:

$$U^2, \Phi_W, \Phi_1, \Phi_2, \Phi_3, \Phi_4, \mathcal{A}, \mathcal{B} \tag{3.25}$$

where

$$\begin{aligned}
\Phi_W &\equiv \int \rho'\rho'' \frac{\mathbf{x}-\mathbf{x}'}{|\mathbf{x}-\mathbf{x}'|^3} \cdot \left(\frac{\mathbf{x}'-\mathbf{x}''}{|\mathbf{x}'-\mathbf{x}''|} - \frac{\mathbf{x}'-\mathbf{x}''}{|\mathbf{x}'-\mathbf{x}''|} \right) d^3x' d^3x'', \\
\Phi_1 &\equiv \int \frac{\rho' v'^2}{|\mathbf{x}-\mathbf{x}'|} d^3x', \qquad \Phi_2 \equiv \int \frac{\rho' U'}{|\mathbf{x}-\mathbf{x}'|} d^3x', \\
\Phi_3 &\equiv \int \frac{\rho' \Pi'}{|\mathbf{x}-\mathbf{x}'|} d^3x', \qquad \Phi_4 \equiv \int \frac{p'}{|\mathbf{x}-\mathbf{x}'|} d^3x', \\
\mathcal{A} &\equiv \int \frac{\rho'[\mathbf{v}'\cdot(\mathbf{x}-\mathbf{x}')]^2}{|\mathbf{x}-\mathbf{x}'|^3} d^3x', \qquad \mathcal{B} \equiv \int \frac{\rho'}{|\mathbf{x}-\mathbf{x}'|} (\mathbf{x}-\mathbf{x}') \cdot \frac{d\mathbf{v}'}{dt} d^3x'.
\end{aligned} \tag{3.26}$$

The last item in the previous list is the most subjective restriction. Hence, if one analyzes a metric theory of gravity and other possible post-Newtonian potentials appear (e.g. $V_iV_jU^{-1}$, $\Phi_1\Phi_3U^{-2}$ or $U_{ij}U_{ij}$) the formalism has to change accordingly.

The post-Newtonian potentials satisfy some useful relationships:

$$\begin{aligned}
\nabla^2 V_i &= -4\pi\rho v_i, & V_{i,i} &= U_{,0}, \\
\nabla^2 \Phi_1 &= -4\pi\rho v^2, & \nabla^2 \Phi_2 &= -4\pi\rho U, \\
\nabla^2 \Phi_3 &= -4\pi\rho\Pi, & \nabla^2 \Phi_4 &= -4\pi p, \\
\nabla^2(\Phi_W + 2U^2 - 3\Phi_2) &= 2\chi_{,ij}U_{,ij}, & & \\
\chi_{,00} &= \mathcal{A} + \mathcal{B} - \Phi_1 \quad . & &
\end{aligned} \tag{3.27}$$

Now, one has the elements to write down a general post-Newtonian metric considering a fluid. The metric theories of gravity will differ from each other, with respect to the post-Newtonian metric, by the coefficients that multiply each term in the metric. Hence, if one replaces the coefficients by parameters one obtains a parametrized metric such that the particular values of those parameters, i.e. the coefficients, are a particular metric theory of gravity. This parametrized metric is the PPN metric, and the parameters are the PPN parameters.

The use of parameters to write down a general form for the post-Newtonian metric is called PPN Formalism. But, a primitive version of this formalism, hence a particular case of PPN metric, was developed and designed by Eddington, Robertson and Schiff. The Eddington-Robertson-Schiff formalism does not consider the Solar System as a fluid instead

it considers the Sun as a point source and the planets as test bodies. The post-Newtonian metric in this formalism is given by [34, 80]

$$\begin{aligned} g_{00} &= -1 + \frac{2M}{r} - 2(\beta - \gamma)\left(\frac{M}{r}\right)^2, \\ g_{0i} &= 0, \\ g_{ij} &= \left(1 + 2\gamma\frac{M}{r}\right)\delta_{ij}\,, \end{aligned} \tag{3.28}$$

where M is mass of the Sun, and β and γ are the PPN parameters.

Schiff in [81] generalized the metric (3.28) in order to incorporate the Lense-Thirring effect that is a relativistic correction to the precession of a gyroscope near a rotating mass, for example the Earth. Baierlein [82] developed a primitive PPN formalism considering a fluid. But, the full PPN formalism was developed pioneerly by Nordtvedt[83] but still considering point masses. In [84, 85] Will generalized the latter formalism in order to incorporate the fluid description. As in Eddington-Schiff-Robertson expansion, equation (3.28), for each term in the post-Newtonian metric one has a PPN parameter (or a combination of them) in front of it. The total number of parameters is ten and they are denoted $\gamma, \beta, \xi, \alpha_1, \alpha_2, \alpha_3, \zeta_1, \zeta_2, \zeta_3$ and ζ_4. Hence, the PPN metric becomes

$$\begin{aligned} g_{00} =& -1 + 2U - 2\beta U^2 + (2\gamma + 2 + \alpha_3 + \zeta_1 - 2\xi)\Phi_1 + \\ &+ 2(3\gamma - 2\beta + 1 + \zeta_2 + \xi)\Phi_2 + 2(1 + \zeta_3)\Phi_3 + \\ &+ 2(3\gamma + 3\zeta_4 - 2\xi)\Phi_4 - (\zeta_1 - 2\xi)\mathcal{A} - 2\xi\Phi_W, \\ g_{0i} =& -\frac{1}{2}(4\gamma + 3 + \alpha_1 - \alpha_2 + \zeta_1 - 2\xi)V_i - \\ &- \frac{1}{2}(1 + \alpha_2 - \zeta_1 + 2\xi)W_i\,, \\ g_{ij} =& (1 + 2\gamma\, U)\,\delta_{ij}\,. \end{aligned} \tag{3.29}$$

In equation (3.29) one perceives that there is a linear combination of PPN parameters. These linear combinations were chosen such that the parameters $\gamma, \beta, \xi, \alpha_1, \alpha_2, \alpha_3, \zeta_1, \zeta_2, \zeta_3$ and ζ_4 have a physical meaning. Below it is shown the Table 1 and Table 2 containing the interpretation of the PPN parameters and their strongest limits, respectively.

The parameters γ and β are the same present in the Eddington-Robertson-Schiff expansion, equation (3.28), and they are associated to the classical tests of gravity. The parameter ξ is different from zero if the respective theory of gravity predict effects such preferred location, e.g. anisotropy in the local gravitational constant due to the external matter distribution, this effect is also called as "Whitehead" effect. The parameters $\alpha_1, \alpha_2, \alpha_3$ measures if there are preferred-frame effects while $\alpha_3, \zeta_1, \zeta_2, \zeta_3, \zeta_4$ measure if a theory predicts violation of conservation laws for total momentum.

Parameter	Interpretation	Value in GR	Value in semiconservative theories	Value in fully conservative theories
γ	space-curvature produced by a point rest mass	1	γ	γ
β	nonlinearity present in the superposition for gravity	1	β	β
ξ	preferred location	0	ξ	ξ
α_1	preferred frame	0	α_1	0
α_2		0	α_2	0
α_3		0	0	0
α_3	violation of energy-momentum conservation	0	0	0
ζ_1		0	0	0
ζ_2		0	0	0
ζ_3		0	0	0
ζ_4		0	0	0

Table 1 – PPN parameters and their interpretation. Adapted from [2].

Parameter	Limit
$\gamma - 1$	2.3×10^{-5}
$\beta - 1$	$8. \times 10^{-5}$
ξ	$4. \times 10^{-9}$
α_1	$4. \times 10^{-5}$
α_2	$2. \times 10^{-9}$
α_3	$4. \times 10^{-20}$
ζ_1	$2. \times 10^{-2}$
ζ_2	$4. \times 10^{-5}$
ζ_3	$1. \times 10^{-8}$
ζ_4	-

Table 2 – Limits on the PPN parameters, considering only the strongest limits for each parameter [2]. The ζ_4 does not have a direct measurement. These limits apply to the absolute value of each parameter.

4 THE SOLAR SYSTEM ANALYSIS OF RGGR

4.1 The Eddington-Robertson-Schiff expansion for RGGR

In [76, 77] were performed the Solar System test of RGGR. The bounds on the dimensionless parameter $\bar{\nu}_\odot \equiv \alpha_\odot \nu$ were found to be respectively $|\bar{\nu}_\odot| \lesssim 10^{-17}$ and $|\bar{\nu}_\odot| \lesssim 10^{-21}$. In [71, 3], it was shown that $\bar{\nu}$ is about $\sim 10^{-9} - 10^{-7}$ and approximately runs linearly with the msystem mass. The later values on $\bar{\nu}$ agree with the first bound[76] while they do not agree with the second one[77]. Also, these previous works that derived constraints to $\bar{\nu}$ have not considered the external potential effect which is inherent to the RGGR approach, as discussed in Subsection 2.3.2, and acts as a screening mechanism. Here, one presents the PPN analysis including the external potential effect.

Although the results presented here are derived using the noncovariant scale setting, equation (2.37), the same results can be also extended to the covariant one as is shown in the Appendices A and B.

In order to apply the PPN formalism, one considers the Solar System as a subsystem of the Galaxy, i.e. the system S will be the Milky Way and the subsystem S' will be the Solar System. The Milky Way it will be refered by the subscript "MW" and the Solar System by "$\odot$". The estimates for the value of $\phi_{\rm MW}|_\odot$, which is the Newtonian potential of the Milky Way evaluated at the Solar System, using [86, 87] is -5×10^{-7} if only the baryonic matter is considered, or -2.1×10^{-6} if either baryonic matter and standard dark matter is taken into account. Since, according previous works, e.g. [9], the RG effects mimic dark matter-like effects, the exact value of $\phi_{\rm MW}|_\odot$ lies between the two cases.

In Figure 1 one can note the Newtonian potential generated by the Sun ($\phi_\odot$) across the Solar System and the values of $\phi_{\rm MW}|_\odot$ either with or without dark matter. The data used to derive the Solar System contribution can be found in [88]. If the Solar System is the subsystem of the Milky Way then the external potential ϕ'_e is $\phi_{\rm MW}$. As one can see in Figure 1, for all the planets one has $\phi_\odot/\phi_{e'} \lesssim 10^{-2}$, which proves that the expansion in equation (2.47) can be used.

Regarding to the PPN approach, as a first step it will be analyzed in the context of Eddington-Robertson-Schiff, equation (3.28), computing the parameters γ and β. After, it will be presented a detailed analysis of RGGR considering the full PPN approach and also with the covariant expression for the scale setting μ. But first, it is important to remember the reader that in PPN formalism one leads with an order of smallness which is $v^2 \sim (M/r) \sim O(2)$, where v is the velocity of test particle.

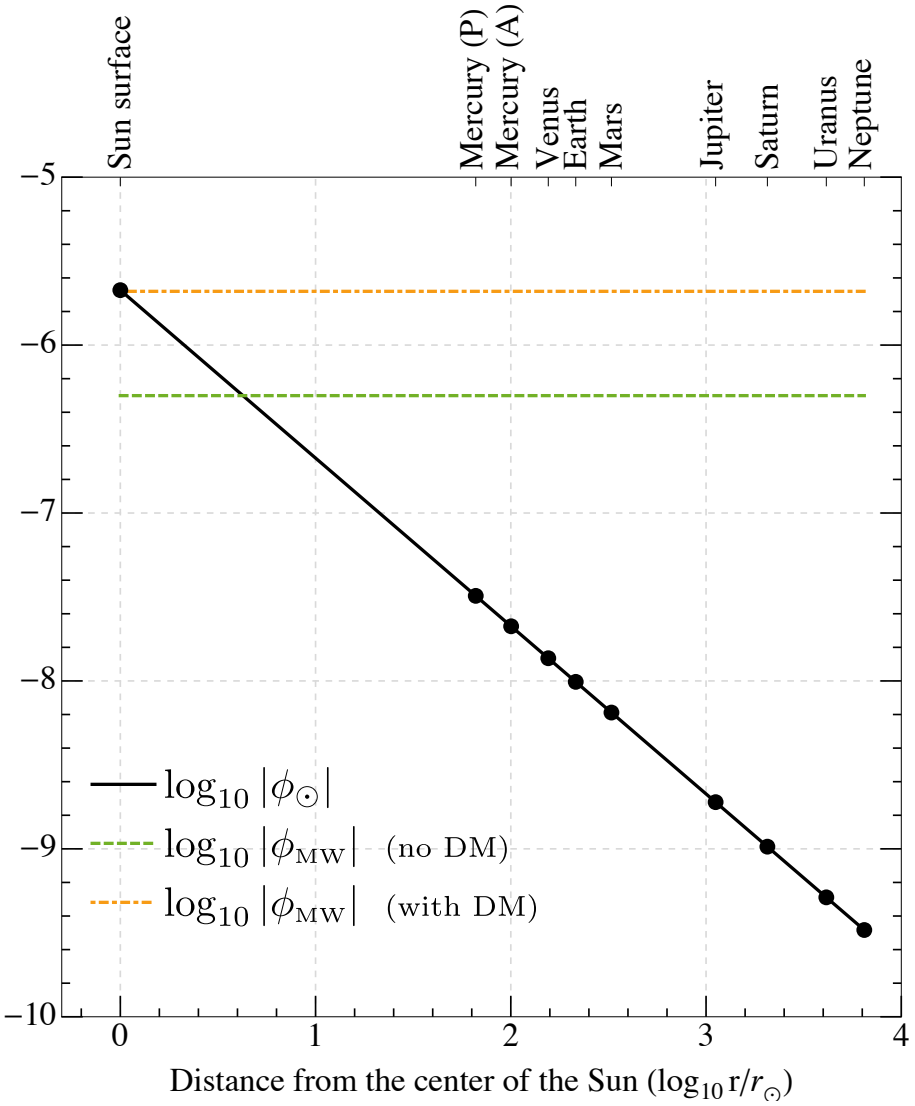

Figure 1 – The Newtonian potential generated by the Sun $\phi_\odot$ across the Solar System, and the value of the Newtonian potentials generated by the Galaxy at the Solar System ($\phi_{\rm MW}|_\odot$). The letters "P" and "A" after Mercury refers to its perihelion and aphelion.

Within the point-like Eddington-Robertson-Schiff post-Newtonian parametrization, in order to obtain γ and β, one must to compare the equations (2.60) and (2.62) with the equation (3.28).

First, one perceives that a minimum requirement for satisfying the parametrization is $|C_2|r^2 \approx 0$ and $C_1/r \sim O(2)$. Considering this, the equations (2.60) and (2.62) becomes

$$\begin{aligned} g_{00} &= -1 + \frac{C_1}{r} + 2\bar{\nu}\left(1 - \frac{3C_1}{2r}\right)\ln\mu + O(\infty, 2)\,, \\ g_{11} &= 1 + \frac{C_1}{r} + 2\bar{\nu}\left[r\frac{\mu'}{\mu} + C_1\left(\frac{\mu'}{\mu} - \frac{\ln\mu}{2r}\right)\right] + O(4, 2)\,, \end{aligned} \tag{4.1}$$

where C_2 is not considered anymore and $O(n, m)$ refers to terms of nth order or higher in C_1, and terms of mth order or higher in $\bar{\nu}$. The $\ln\mu$ can be expanded as in equation

(2.47). For convenience, one writes the dependence on r explicitly, hence one has

$$\frac{\phi_\odot}{\phi_{e'}} \equiv \frac{k}{r}\,. \tag{4.2}$$

Thus, with these considerations,

$$\begin{aligned} g_{00} &= -1 + \frac{C_1}{r} + \frac{k}{r}\bar{\nu}\left(-2 - \frac{k}{r} - \frac{2k^2}{3r^2} + 3\frac{C_1}{r} + \frac{3kC_1}{2r^2} + \frac{k^2C_1}{r^3}\right) + O(\infty, 4, 4), \\ g_{11} &= 1 + \frac{C_1}{r} + 2\frac{k}{r}\bar{\nu}\left(1 + \frac{3C_1}{2r}\right) + O(2, 4, 2), \end{aligned} \tag{4.3}$$

where $O(\infty, 4, 4)$ are the terms of arbitrary order in C_1, of second or higher order in $\bar{\nu}$ and fourth or higher order in k, the same for $O(2, 4, 2)$.

To proceed with the formalism one has to relate the expansions above, i.e. one must to know if, for example, C_1^2/r^2 can be neglected while $k^2\bar{\nu}/r^2$ is preserved. Considering the Mercury planet, one has that the terms of $O(2)$ are the same order of $\phi_\odot(r_\mercury) = -2.7\times10^{-8}$, which is the Newtonian potential generated by the Sun at Mercury's orbit. Hence, this must correspond to $-M/r$. One expects that $\bar{\nu}$ must to be small, namely for galactic internal dynamics, the upper bound for $\bar{\nu}$ was $|\bar{\nu}| \lesssim 10^{-7}$ [9], which will be assumed as a starting point, but a stronger bound will be shown later.

The value for $k/r_\mercury$ can be obtained from equation (4.2), and it corresponds to $O(0.34)$ in the case that one considers only baryonic matter and $O(0.5)$ for the case with standard dark matter.

Considering the above statements, the relation between the expansions is now clarified. Now, one can proceed with the PPN analysis, hence the equations (4.3) and (4.3) are expressed as

$$g_{00} \approx -1 + \frac{C_1}{r} - \frac{k}{r}\bar{\nu}\left(2 + \frac{k}{r}\right), \tag{4.4}$$

$$g_{11} \approx 1 + \frac{C_1}{r} + 2\frac{k}{r}\bar{\nu}\,. \tag{4.5}$$

Comparing the equations (3.28) and (4.4) one obtains the relation between C_1 and M, which is

$$C_1 = 2M + 2\bar{\nu}k\,. \tag{4.6}$$

The parameter γ is found from the coefficient of r^{-1}. Thus,

$$\gamma = 1 + \frac{2\bar{\nu}k}{M} = 1 - \frac{2\bar{\nu}}{\phi_{e'}}\,. \tag{4.7}$$

From Solar System experiments, the parameter γ is constrained to $|\gamma - 1| \lesssim 10^{-5}$[2]. Since $|\phi_{e'}| \sim 10^{-6}$, one derives that $|\bar{\nu}| \lesssim 10^{-11}$.

Now, the parameter β is obtained from the coefficient of r^{-2}, in equation (4.4), the value of γ and the equation (3.28), the parameter β reads as

$$\beta = 1 + \frac{\bar{\nu}k^2}{2M^2} = 1 + \frac{\bar{\nu}}{2\phi_{e'}^2}. \tag{4.8}$$

According the Solar System experiments $|\beta - 1| \lesssim 10^{-4}$ [2], the above implies that

$$|\bar{\nu}_\odot| \lesssim 10^{-16}. \tag{4.9}$$

This result emphasizes that the external potential is essential for the PPN application in the form of the equation (3.28). Also, there is now a concordance with the previous results from galactic internal dynamics.

4.2 The Will-Nordtvedt formalism applied to RGGR

In the previous section we analyzed RGGR using the static and spherically symmetric solution in order to infer the PPN parameters, namely γ and β, comparing the point-like solution with the Eddington-Robertson-Schiff expansion. But, a theory which is compatible with the classical test for gravity, namely the bending of the light and the Mercury's precession, not necessarily is compatible with other experiments. The Will-Nordtvedt version of PPN considers more tests, as one can see in Chapter 3 there are ten parameters being nine of them observationally constrained. Also, the Will-Nordtvedt formalism is based on fluids and not on particles.

Hence, in order to apply the full PPN parametrization, first one has to write down the field equations of RGGR, namely

$$\mathcal{G}_{\alpha\beta} + \Lambda g_{\alpha\beta} = 8\pi G T_{\alpha\beta}, \tag{4.10}$$

where

$$\mathcal{G}_{\alpha\beta} \equiv G_{\alpha\beta} + g_{\alpha\beta} G \Box G^{-1} - G\nabla_\alpha \nabla_\beta G^{-1}, \tag{4.11}$$

$\Box \equiv g^{\alpha\beta}\nabla_\alpha\nabla_\beta$, and ∇_α is the covariant derivative. However, it seems natural to neglect Λ since, according equation (2.51), should be a correction to the cosmological constant Λ_0 that is already neglected in the pure GR case. Thus, it is useful to write the last equation as

$$R_{\alpha\beta} = G\left[8\pi\left(T_{\alpha\beta} - \frac{1}{2}g_{\alpha\beta}\,T\right) + \nabla_\alpha\nabla_\beta\left(G^{-1}\right) + \frac{1}{2}g_{\alpha\beta}\Box\left(G^{-1}\right)\right]. \tag{4.12}$$

In [76, 77, 29] the Λ term was not considered in the Solar System analysis of RGGR. After, it will be shown that the effects of inserting Λ are not in the scope of Will-Nordtvedt formalism because Λ can not be an analytical function and still be compatible with asymptotic flatness.

Initially, it will be considered the noncovariant form for the scale setting μ, as we did in Section 4.1. Further details on the covariant formulation is given later, but antecipating the main result: the covariant version leads to the appearence of post-Newtonian potentials which are not covered by the standard Will-Nordtvedt expansion and a generalization of latter formalism is required in order to include those post-Newtonian potentials, as was already pointed out in Chapter 3. In the Eddington-Robertson-Schiff parametrization, Subsection (4.1), it was used a particular form for the scale setting μ, namely equation (2.37) together with equation (2.31) for the running of G. Here, one generalizes the latter procedure simply demanding that G can be written as a function of U, being the latter given by equation (3.2). Hence, the expression for G now reads as

$$G^{-1}(\mu) = G^{-1}(U) = G_e^{-1} + 2\sum_{n=1}^{\infty} \nu_n U^n. \tag{4.13}$$

Clearly, GR is recoverd when $\nu_n = 0$. In the equation above, G_e is the value of $G(U)$ when $U = 0$ or can be seen as the external value of G. In other words, the Newtonian potential becomes to zero far from the Sun, but the values of G may depend on the environment of the Solar System.

Following the procedures elucidated in Chapter (3), up to the post-Newtonian order, the metric components: g_{00}, g_{0i} and g_{ij} must to be know to order $O(4)$, $O(3)$ and $O(2)$. Thus, up to the desired order, the respective components of the Ricci tensor can be expressed as

$$\begin{aligned} R_{00} = &-\frac{1}{2}\nabla^2 h_{00} - \frac{1}{2}\left(h^k{}_{k,00} - 2\,h^k{}_{0,k0}\right) - \frac{1}{4}\left|\nabla h_{00}\right|^2 + \\ &+ \frac{1}{2}\,h_{00,l}\left(h^{lk}{}_{,k} - \frac{1}{2}\,h^k{}_{k,j}\delta^j_l\right) + \frac{1}{2}\,h^{kl}h_{00,lk}\,, \end{aligned} \tag{4.14}$$

$$R_{0i} = -\frac{1}{2}\left(\nabla^2 h_{0i} - h^k{}_{0,ik} + h^k{}_{k,0i} - h^k{}_{i,k0}\right)\,, \tag{4.15}$$

$$R_{ij} = -\frac{1}{2}\left(\nabla^2 h_{ij} - h_{00,ij} + h^k{}_{k,ij} - h^k{}_{i,kj} - h^k{}_{j,ki}\right), \tag{4.16}$$

where the commas mean simple derivatives. Furthermore, the following quantity up to required order

$$\begin{aligned} \nabla_\alpha\nabla_\beta\left(G^{-1}\right) &= (G^{-1})_{,\alpha\beta} - \Gamma^\lambda_{\alpha\beta}(G^{-1})_{,\lambda}\,, \\ &= 2\nu_1\left(U_{,\alpha\beta} - \Gamma^\lambda_{\alpha\beta}U_{,\lambda}\right) + 4\nu_2\left(U_{,\alpha}\,U_{,\beta} + UU_{,\alpha\beta}\right) + O(6)\,. \end{aligned} \tag{4.17}$$

The initial step is to compute the Newtonian limit, i.e. one must to evaluate the h_{00} to order $O(2)$. Hence, using equations (4.14) and (3.13)up to the required order

$$R_{00} = -\frac{1}{2}\,\nabla^2 h_{00} \quad \text{and} \quad T_{00} = -T = \rho\,. \tag{4.18}$$

Therefore,

$$\nabla^2 h_{00} = -8\pi G_e \rho + 2G_e \nu_1 \nabla^2 U \tag{4.19}$$

and, from equation (3.2)[1],

$$h_{00} = 2\frac{G_e}{G_N}(1 + G_N \nu_1) U \,. \tag{4.20}$$

In order to be in agreement with the Newtonian physics,

$$h_{00} = 2U \,, \tag{4.21}$$

thus we must set

$$G_e(1 + G_N \nu_1) = G_N \,. \tag{4.22}$$

The equation above sets the relation between G_e and G_N. Since this relation is now clear, henceforth we use

$$G_N = 1 \,. \tag{4.23}$$

Thus,

$$G_e = \frac{1}{1 + \nu_1} \,. \tag{4.24}$$

Now, the h_{ij} to order $O(2)$. Hence, imposing the three gauge conditions

$$h^{\mu}{}_{i,\mu} - \frac{1}{2} h^{\mu}{}_{\mu,i} = 2G_e \nu_1 U_{,i} \,, \tag{4.25}$$

the equation (4.16) reduces to

$$\nabla^2 h_{ij} = -8\pi G_e \rho \delta_{ij} - 2G_e \nu_1 \nabla^2 U \delta_{ij} \,. \tag{4.26}$$

The above equation is easily integrated,

$$h_{ij} = 2\left(1 - \frac{2\,\nu_1}{1 + \nu_1}\right) U\, \delta_{ij} \,, \tag{4.27}$$

where one uses the equation (4.24).

The next step is to compute h_{0i} to order $O(3)$. Proceeding with a one more gauge condition

$$h^{\mu}{}_{0,\mu} - \frac{1}{2} h^{\mu}{}_{\mu,0} = -\frac{1}{2} h_{00,0} + 3G_e \nu_1 U_{,0} \tag{4.28}$$

then the equation (4.15) becomes

$$\nabla^2 h_{0i} + G_e U_{,0i} = 16\pi G_e \rho v_i \,. \tag{4.29}$$

In the equation above one used the equation (3.20) also with equation (3.23).Therefore, from equation (4.29) it results

$$h_{0i} = -\frac{7V_i}{2(1 + \nu_1)} - \frac{W_i}{2(1 + \nu_1)} \,. \tag{4.30}$$

[1] Here, we restores G_N

Finally, one must to compute the h_{00} up to $O(4)$. Hence, one has to develop a bit the right-side of the equation (4.12). To this end, some components of the Levi-Civita connection up to the required order are required, namely

$$\Gamma^{i}_{00} = -\,U_{,i}\,, \tag{4.31}$$

$$\Gamma^{k}_{ij} = \left(1 - \frac{2\,\nu_1}{1+\nu_1}\right)\left(U_{,i}\delta^{k}_{j} + U_{,j}\delta^{k}_{i} - U^{,k}\delta_{ij}\right). \tag{4.32}$$

In the same way, for the quantity below, up to $O(4)$, one finds

$$T_{00} - \frac{1}{2}\,g_{00}T = \frac{1}{2}\,\rho\left[1 + 2\left(v^2 - U + \frac{\Pi}{2} + \frac{3p}{2\rho}\right)\right]. \tag{4.33}$$

By considering the gauge fixing conditions, equations (4.25) and (4.28) and using the following relation

$$|\nabla U|^2 = \nabla^2\left(\frac{U^2}{2} - \Phi_2\right), \tag{4.34}$$

the equation (4.14) can be integrated, leading to

$$\begin{aligned} h_{00} = 2U - 2\left[1 + \frac{\nu_1^2 - \nu_2(1+\nu_1)}{(1+\nu_1)^2}\right]U^2 + \frac{4\Phi_1}{1+\nu_1} + \frac{2\Phi_3}{1+\nu_1} + \frac{6\Phi_4}{1+\nu_1} + \\ + \left[\frac{4\,(1-\nu_1+\nu_1^2)}{(1+\nu_1)^2} - \frac{4\nu_1}{1+\nu_1}\right]\Phi_2 + O(6)\,. \end{aligned} \tag{4.35}$$

With the equation above, one concludes the PPN formalism applied to RGGR. Now, one just infers the PPN parameters and one compares them with the observational values, Table 2. Hence, the metric up to post-Newtonian order reads as

$$\begin{aligned} g_{00} =& -1 + 2U - 2\left[1 + \frac{\nu_1^2 - \nu_2(1+\nu_1)}{(1+\nu_1)^2}\right]U^2 + \left(1 - \frac{\nu_1}{1+\nu_1}\right)\left(4\Phi_1 + 2\Phi_3 + 6\Phi_4\right) + \\ &+ 4\left[1 - \frac{4\nu_1 + \nu_1^2}{(1+\nu_1)^2}\right]\Phi_2\,, \end{aligned} \tag{4.36}$$

$$g_{0i} = \left(1 - \frac{\nu_1}{1+\nu_1}\right)\left(-\frac{7V_i}{2} - \frac{W_i}{2}\right),$$

$$g_{ij} = \delta_{ij} + 2\left(1 - \frac{2\nu_1}{1+\nu_1}\right)U\,\delta_{ij}\,.$$

To extract the PPN parameters one must to compare the above equation with equation (3.29). From coeficients of U in g_{ij} and U^2 in g_{00}, one infers that γ and β. According Table 2, one finds

$$|\nu_1| < 1.2 \times 10^{-5}\,, \quad |\nu_2| < 8 \times 10^{-5}\,. \tag{4.37}$$

It is important to remember that the values above are constraints associated only to the parameters γ and β and does not correspond to all observational constraints.

Considering that ν_1 and ν_2 are small and hence neglecting second order contributions on them, the other PPN parameters are given by

$$\begin{aligned}
\gamma &= 1 - 2\nu_1 \,, \\
\beta &= 1 - \nu_2 \,, \\
\alpha_2 &= -\nu_1 \,, \\
\zeta_2 &= -2(\nu_1 + \nu_2) \,, \\
\zeta_3 &= -\zeta_4 = -\nu_1 \,, \\
\alpha_1 &= \alpha_3 = \xi = \zeta_1 = 0 \,.
\end{aligned} \tag{4.38}$$

Now, using the results above and the observational constraints of all PPN parameters, listed in Table 2, one can put strongest constraints on the parameters ν_1 and ν_2 which are displayed in Table 3. One perceives that they do not come from γ and β, but from α_2 and ζ_2.

Table 3 – Strongest constraints on ν_1 and ν_2 from all the observational constraints on the PPN parameters.

Constraint	Origin
$\lvert\nu_1\rvert < 2 \times 10^{-9}$	α_2 constraint
$\lvert\nu_2\rvert < 2 \times 10^{-5}$	ζ_2 constraint

With the result above, the PPN analysis is showing that RGGR presents effects associated to preferred location, due the nonzero α_1 and α_2, and violation of the total energy-momentum conservation law, due the nonzero values for ζ_2, ζ_3 and ζ_4. The appearance of the latter parameters, in principle, one could indicates that RGGR has fundamental problems. Actually, the PPN results are showing that we are not using a full covariant action and some approximation is being used. Interestingly, as it is shown in Appendix A and B, for Eddington-Robertson-Schiff approximation there is no difference between the covariant and noncovariant approach, or the method itself does not see the difference. But, here it is being used a more general approach, namely the Will-Nordtvedt formalism, and the limitations of using the noncovariant approach start to appear. Hence, the formalism itself suggest to proceed with the full covariant action and this is done later, including also the effects from Λ.

However, in the previous analysis it was not considered the external potential effect. Hence, it is interesting to see what happens now with the bounds on ν parameter if is inserted the external potential effect. In particular, if the upper bound obtained in Section

4.1 remains unchanged, since we are using a more general parameterized post-Newtonian approach, perhaps some changes could to appear. Thus, let us assume the particular expression for $G(U)$, equation (2.31) with the scale setting μ given by equation (2.37). Remembering that in this scenario, with an external potential, G depends on the matter distribution inside the system under investigation as well the matter distribution outside it. Hence, one writes

$$\begin{aligned} \rho &= \rho_s + \rho_e \,, \\ U &= U_s + U_e \,, \end{aligned} \tag{4.39}$$

where ρ_s refers to the matter density contribution that is inside the system under consideration, while ρ_e refers to the external mass density. The same for U_s and U_e. Thus, with the latter considerations the expression for G becomes

$$\begin{aligned} G^{-1} &= G_e^{-1}\left[1 + 2\bar{\nu}\ln\left(1 + \frac{U_s}{U_e}\right)\right], \\ &= G_e^{-1}\left(1 + 2\bar{\nu}\frac{U_s}{U_e} - \bar{\nu}\frac{U_s^2}{U_e^2}\right) + ... \end{aligned} \tag{4.40}$$

with $G(U_e) = G_e$ (or, equivalently, $G|_{U_s=0} = G_e$) and $U_s < U_e$. The expression above is compatible with equation (4.13) replacing U by U_s. Hence, one has

$$\begin{aligned} \nu_1 &= \frac{\bar{\nu}}{G_e U_e}\,, \\ \nu_2 &= -\frac{\bar{\nu}}{2G_e U_e^2}. \end{aligned} \tag{4.41}$$

The structure responsible for generating the external potential effect, subsequent to the Solar System structure, is the Milky Way whose Newtonian potential at the Solar System position is about $U_e \sim 10^{-6}$ (for details plea,se see Figure 1), thus

$$|\bar{\nu}| \lesssim 10^{-17} \text{ for } U_e \sim 10^{-6}. \tag{4.42}$$

The bound above is slightly stronger than the bound obtained in Section 4.1 for the same value of the external potential. The disagreement comes from the fact that it is being used the Will-Nordtvedt formalism and the strongest bound does not come from β but from ζ_2.

4.2.1 Λ term and violation of asymptotic flatness

Here, this Section is dedicated to show possible effects of inserting the Λ into the Will-Nordtvedt PPN approach. One of the possible effects that could arise is the restoring of energy-momentum conservation, for example if the insertion of Λ would generate $\zeta_2 = 0$. But, it will be shown that the insertion of Λ is useless if one wants to preserve asymptotic flatness.

The Λ term includes the Λ_0 constant, which is the cosmological constant when $\nu = 0$, and RG corrections on powers of ν (as is already shown in Section 2.3.3). In GR it is already know that the impact of cosmological constant in Solar System dynamics is negligible [89]. Thus, as a starting point in our analysis, one will consider

$$\Lambda_0 = 0\,. \tag{4.43}$$

However, in [10] it is shown that in vacuum, i.e. $T_{\mu\nu} = 0$, writing $\Lambda = \Lambda_0 + O(\nu)$ and $G = G_0 + O(\nu)$ one has

$$\Lambda = \Lambda_0 G_0 G^{-1} + O(\nu^2)\,. \tag{4.44}$$

Hence, using that $\Lambda_0 = 0$ one finds $\Lambda = 0 + O(\nu^2)$. The result above shows that within the approximation in which the Solar System is composed by point particles (the Sun and planets), Λ does not play a role up to one post-Newtonian order. On the other hand, when the Solar System is treated as a fluid the use of the Will-Nordtvedt PPN picture may lead a different answers, for example a difference on β parameter[34].

As pointed out in Section 2.3, the expression for Λ as a function of the scale setting μ is derived from field equations and hence it is not universal, i.e. the dependence on μ changes from system to system. Thus, for the Solar System dynamics Λ should be a function of μ and analogously what was done for G in equation (4.13), one reads

$$\Lambda = \Lambda_0 + \sum_{n=1}^{\infty} \Lambda_n U^n\,. \tag{4.45}$$

The field equations (4.12) with Λ become

$$R_{\mu\nu} = G\left[8\pi\left(T_{\mu\nu} - \frac{1}{2}g_{\mu\nu}\,T\right) + \nabla_\mu\nabla_\nu\left(G^{-1}\right) + \frac{1}{2}g_{\mu\nu}\Box\left(G^{-1}\right)\right] + \Lambda g_{\mu\nu}\,. \tag{4.46}$$

Now, proceeding analogously to what was done in Section 4.2, one has to find the metric solution up to order $O(4)$. Initially, one has to compute the zeroth order on ν contribution of equation (4.46) which results on equation (4.43), as expected. Next, the Newtonian limit which means to compute h_{00} up to $O(2)$, Thus,

$$h_{00} = 2U - \Lambda_1\chi\,, \tag{4.47}$$

where we are assuming $G_N = 1$. Note that the above expression is a extension of equation (4.21), the potential χ is the one defined by equation (3.20).

As already reported in Chapter 3, in PPN formalism the post-Newtonian potentials should tend to zero at large distances and χ is a potential that diverges at infinity. Therefore,

$$\Lambda_1 = 0\,. \tag{4.48}$$

With this result the remaining chance of appearing some contribution from Λ is at $O(4)$. Since the Λ contribution does not include derivatives, its contribution can be easily calculated from previous computations, namely equation (4.35). Hence, the h_{00} up to $O(4)$ now reads as

$$h_{00} = 2U - 2\left[1 + \frac{\nu_1^2 - \nu_2(1+\nu_1)}{(1+\nu_1)^2}\right]U^2 + \frac{4\Phi_1}{1+\nu_1} + \frac{2\Phi_3}{1+\nu_1} + \frac{6\Phi_4}{1+\nu_1} + \\ + \left[\frac{4\,(1-\nu_1+\nu_1^2)}{(1+\nu_1)^2} - \frac{4\nu_1}{1+\nu_1}\right]\Phi_2 + 2\Lambda_2\aleph\,, \tag{4.49}$$

where $\aleph$ is a new post-Newtonian potential defined as

$$\aleph = -\frac{1}{4\pi}\int \frac{U'^2}{|\mathbf{x}-\mathbf{x}'|}d^3x'\,. \tag{4.50}$$

The other metric components are the same as in equation (4.36).

Considering large distances, the new post-Newtonian potential $\aleph$ defined above diverges logarithmically since U decays linearly with distance. Hence, in order to preserve asymptotic flatness one has

$$\Lambda_2 = 0. \tag{4.51}$$

With the above, the contributions of inserting Λ is completely eliminated up to post-Newtonian order. It is clear, with the above result, that if one desires to measure some dynamical effects of inserting Λ (for instance if inserting it one may obtain the restoring of the energy-momentum conservation at post-Newtonian order) it is necessary to extend the Will-Nordtvedt formalism.

4.2.2 Covariant scale setting and new post-Newtonian potentials

In this subsection, it is investigated the effects of a full covariant version for the scale setting μ in the Will-Nordtvedt version of PPN formalism. As pointed out before, some non zero values for PPN parameters specially associated to the special frame effects and non conservation of energy and momentum are the main motivation that a covariant version for μ needs to be taken into account in the PPN analysis.

Here, the covariant extension used is the one proposed by [10, 29], and its form is

$$\mu = f(\Psi), \tag{4.52}$$

with

$$\Psi \equiv h_{\alpha\beta}u^\alpha u^\beta\,, \tag{4.53}$$

where, u^α is the fluid four-velocity, $h_{\alpha\beta} \equiv g_{\alpha\beta} - \gamma_{\alpha\beta}$, and $\gamma_{\alpha\beta}$ is the reference metric, which one uses the Minkowski metric.

Expanding G^{-1} as the same manner than in equation (4.13), but now in a power series of Ψ, one has

$$G^{-1} = G_f^{-1} + \sum_{n=1}^{\infty} \sigma_n \Psi^n \,, \tag{4.54}$$

where, G_f is the value of G when $\Psi = 0$. Hence, the field equations (4.12) up to the required order for PPN analysis become

$$R_{\alpha\beta} = G_f(1 - G_f\sigma_1\Psi)\left[8\pi\left(T_{\alpha\beta} - \frac{T}{2}g_{\alpha\beta}\right) + \sigma_1\nabla_\alpha\nabla_\beta\Psi + \sigma_2\nabla_\alpha\nabla_\beta\Psi^2 + \right.$$
$$\left. + \frac{1}{2}g_{\alpha\beta}\sigma_1\Box\Psi + \frac{1}{2}g_{\alpha\beta}\sigma_2\Box\Psi^2\right] . \tag{4.55}$$

From condition $u_\mu u^\mu = -1$ one finds

$$u^0 = \sqrt{\frac{1+v^2}{1-h_{00}}} \,. \tag{4.56}$$

Hence, Ψ is expanded as follows

$$\Psi = h_{00} + h_{00}^2 + h_{00}v^2 + 2h_{0i}v^i + h_{ij}v^iv^j + O(6) \,. \tag{4.57}$$

At the Newtonian order, it is possible to find the relation between G_f and G_N as follows

$$G_f = \frac{G_N}{1 + \sigma_1 G_N} \,. \tag{4.58}$$

Hereafter, we set $G_N = 1$. Note that the equation above is similar to the relation shown in equation (4.22). Now, solving the field equations (4.55) for h_{00} and h_{ij} up to $O(2)$, after h_{0i} up to $O(3)$ one has

$$h_{00} = 2U + O(v^4) \,, \tag{4.59}$$

$$h_{ij} = 2\left(1 - \frac{2\sigma_1}{1+\sigma_1}\right)U\delta_{ij} + O(v^4) \,, \tag{4.60}$$

$$h_{0i} = -\frac{1}{1+\sigma_1}\left(\frac{7}{2}V_i + \frac{1}{2}W_i\right) + O(v^5) \,. \tag{4.61}$$

Finally, one proceeds to obtain h_{00} up to $O(4)$ and the resulting expression is

$$h_{00} = 2U - 2\left[1 - \frac{\sigma_1 + 2\sigma_2(1+\sigma_1)}{1+\sigma_1}\right]U^2 + 4\Phi_1 + 4\left(1 - \frac{3\sigma_1}{1+\sigma_1}\right)\Phi_2 + 2\Phi_3 + 6\Phi_4 +$$
$$+ 2\sigma_1 U v^2 - 7\sigma_1 V_i v^i - \sigma_1 W_i v^i + O(v^6) \,. \tag{4.62}$$

Note that the three last terms in the above are not covered by the standard Will-Nordtvedt PPN formalism, i.e. new potentials appear. Theories which predicts extra potentials in PPN formalism are not rare in literature[90, 91]. Therefore, if one desires the PPN analysis of RGGR on its covariant extension one needs to extend the Will-Nordtvedt formalism in order to include those extra potentials.

5 SPIRAL GALAXIES

In this chapter we present a review about spiral galaxies based on [92, 93]. The main purpose of this chapter is to show the components of such systems, some important observational aspects of them and how to use them to test gravity. Spiral or disk galaxies are systems which are composed, roughly, by a thick, rotationally supported disk plus a bulge component plus a dark matter halo. In face-on systems it is possible to see the spiral structure in details like: the young stars, HII regions, dust and molecular gas.

The observations of disk galaxies, in their majority, has shown that, for some radial interval, the surface brightness per unit of area of the disk can be modelled by an exponential profile:

$$I(R) = I_0 \exp(-R/R_{\rm D}) \ , \tag{5.1}$$

where I_0 is the central luminosity surface density, R_D is the exponential scale length and R is the cylindrical radius. In edge-on galaxies, some vertical distribution of stars is perceived and well fitted by an exponential profile as well. Namely,

$$I(z) \propto \exp\left(-|z|/z_0\right) \ , \tag{5.2}$$

where z_0 is the scale of height above the plane $z = 0$. Hence, this shows that the disk galaxies are not an ideal infinitesimal disk. Sometimes, it is common to consider an "isothermal" disk for the vertical distribution such that the velocity dispersion is independent of the height z_0. In this case, the vertical distribution $h(z)$:

$$h(z) = h_0 \ \mathrm{sech}^2\left(\frac{z}{2z_0}\right) \quad \text{where} \quad z_0 = \left(\frac{\langle v_z^2\rangle}{8\pi G h_0}\right) \ . \tag{5.3}$$

Note that the vertical distribution is close to the exponential one except near to the plane.

In order to evaluate the kinematics of disk galaxies it is necessary to compute the gravitational potential, which in turn, needs the mass density distribution. It is reasonable, in principle, to consider that the mass is distributed as the light, hence, it is defined the mass-to-light ratio, $\Upsilon_\star \equiv M_\star/L$, which converts light into mass. But this conversion is far from to straightforward. If we analyze a single star one can see that its luminosity depends on several parameters (e.g. metallicity, initial mass and color index). Galaxies, however, are not a simple stellar population rather they are a sum of several ones, hence, the determination of a density mass of a galaxy requires a model that specifies which stellar populations are generating its luminosity. These models are the stellar population synthesis models (SPS)(for further details, please see [94]). With SPS it is possible to infer the mass-to-light ratio and obtain the mass density, which in cases that the luminosity is separable in radial times the vertical distribution, it has a quite general profile

$$\rho(R,z) = \Upsilon_\star(R,z) I(R) f(z) \ , \tag{5.4}$$

where $f(z)$ represents the vertical distribution which can be the equation (5.2), equation (5.3) or even an intermediate case, i.e., between the exponential and isothermal case: $f(z) \propto \mathrm{sech}(z)$. The spatial dependence in $\Upsilon_\star$ exists because each stellar population can have different spatial distribution. This is in agreement with observations since the central regions of a galaxy are dominated by redder (oldest) stars while the external regions are dominated by bluer (youngest) ones.

As the luminosity, the $\Upsilon_\star$ is defined according to the band in which the measurements are performed. At optical band the determination of $\Upsilon_\star$ is very affected by dust, initial mass function, age and chemical composition (metalicity). For surface photometry, the near-infrared (NIR) is the most indicated band to see the stellar structure since the absorption of the radiation by dust is lower compared, for example, the optical case. Moreover, at NIR the SPS models suggest that the dependence between $\Upsilon_\star$ and star formation history is weak and $\Upsilon_\star$ can be considered as constant[95]. Hence, hereafter in our analysis $\Upsilon_\star$ will be considered as a free parameter.

As mentioned above, spiral galaxies have not only a disk structure but a stellar bulge as well. Typically, the bulge-disk decomposition is obtained by fitting the surface brightness considering a sum of an exponential for the disk and a spherical bulge [96], and the latter it is usually modeled with the Sèrsic profile [97] which is given by

$$I_{\mathrm{bulge}}(R) = I_e \exp\left(-\beta_n \left[\left(\frac{R}{R_e}\right)^{1/n} - 1\right]\right), \tag{5.5}$$

where R_e is the radius which contains the half of total surface brightness of the bulge and I_e is the surface brightness at r_e. Actually, the Sèrsic profile is mostly used to model surface brightness of elliptical galaxies, however some studies (e.g. Ref.[98, 96]) have shown that bulges contains similarities with elliptical galaxies. In Some galaxies cataloques, e.g. [99], the bulge is considered as an exponential disk but with a scale length R_{B} smaller than an usual disk since the bulge structure is more compact. Bulges which are modeled as disk are called pseudo-bulges. Analogously to the disk case, we can compute a mass density distribution for the bulge just multiplying the surface brightness by a mass-to-light ratio which will be considered as a free parameter as well.

5.1 Rotation curves

The observed rotation curve of a spiral galaxy is the circular velocity $V_c(R)$ and it is measured using the 21-cm line radio emission of the neutral hydrogen (HI). This radiation arises from the spin-flip transitions of the HI when both electron and proton have the spins aligned, the latter corresponds a higher energy configuration hence the electron spin flips to anti parallel configuration in order to minimize the energy. This transition, known as hyperfine transition, is extremely rare so that the spontaneous occurrence of this transition

takes around 10 million years. But, due the fact that the HI is the most abundant element in the Universe and since this radiation is not absorbed by the interstellar medium, in practice it is possible to measure this radiation using radio interferometers. At innermost regions of a galaxy the use of HI data for rotation curve can be problematic since the observations of HI have low angular resolution. Hence, for innermost regions in a galaxy, the radiation emitted by the ionized hydrogen (HII) is a better option. Such radiation is called Hα and arises when hydrogen electron falls from state $n = 3$ to $n = 2$. The HII regions are the ones which there are star formation and where the neutral hydrogen is excited by the youngest stars. Containing a wavelength of 628.281 nm, the Hα radiation is in the visible spectra (at the red part) and offers a higher resolution than HI data. Thus, it is frequent to find in literature hybrid rotation curves or HI/Hα rotation curves, that is, the observational data is composed by Hα at the innermost region and HI at the outer region of a galaxy.

After corrections (e.g. inclination effects) it is assumed that the observed rotation curve data corresponds to circular velocity of a disk, or in some cases a sum of a disk and a spherical bulge. Beyond that, the flat behaviour observed in rotation curves (for a majority spiral galaxies at large radii) suggests that matter dominant is a darker halo. Hence, galaxy rotation curves, in principle, can be used to infer the distribution of this halo. The circular velocity can be computed considering that the centripetal force is the sum of central forces due to the disk (gas and stars), stellar bulge and dark matter halo at the plane $z = 0$. However, we know that the resulting force is $\boldsymbol{F} = -\boldsymbol{\nabla}\Phi_N$, where Φ_N is the total Newtonian gravitational potential. Hence, we can relate the centripetal acceleration with the Newtonian potential and obtain the circular velocity as follows

$$V_c^2(R) = R\,\frac{\partial \Phi_N}{\partial R}\,. \tag{5.6}$$

The Newtonian potential, on the other hand, can be obtained solving the Poisson's equation, $\nabla^2\Phi_N = 4\pi G\rho$, which in turn has the following general solution

$$\Phi_N(\mathbf{x}) = -G\int \frac{\rho(\mathbf{x}')}{|\mathbf{x}-\mathbf{x}'|}d^3\mathbf{x}'\,. \tag{5.7}$$

The luminous matter distribution can be obtained using the surface brightness profiles mentioned previously for the disk (stars and gas) and bulge times a mass-to-light ratio ($\Upsilon_\star$). The surface density distribution of the gaseous component is accurately obtained by observations and it is not necessary any assumptions about it. The dark halo contribution to the circular velocity is straightforward computed given its distribution. AT the end of the day, we have the following formula for the circular velocity

$$V_c^2(R) = V_{\rm gas}^2(R) + \Upsilon_{\star \rm D}V_{\rm stars}^2(R) + \Upsilon_{\star \rm B}V_{\rm bulge}^2(R) + V_{\rm DM}^2(R)\,. \tag{5.8}$$

Clearly, under the same reasons mentioned above we can compute the circular velocity for each component just using equation (5.6). In the case of a generic disk, for

convenience setting $\Upsilon_\star = 1$, it is possible to reach an expression for the circular velocity using the equations (5.7), (5.6), (5.1) and (5.4)

$$V^2_{\rm disk}(R) = \frac{G}{\sqrt{R}}\int_0^\infty\int_{-\infty}^{+\infty}\Big[\mathcal{K}(y) - \frac{1}{4}\Big(\frac{y^2}{1-y^2}\Big)\Big(\frac{R'}{R} - \frac{R}{R'} + \frac{z'^2}{RR'}\Big)\mathcal{E}(y)\Big]y\sqrt{R'}\rho(R',z')dR'dz' \ , \tag{5.9}$$

where

$$y^2 = \frac{4RR'}{(R+R')^2 + z'^2} \tag{5.10}$$

and $\mathcal{K}(y)$ and $\mathcal{E}(y)$ are the complete elliptical integrals of first and second kind respectively which are defined as follows

$$\mathcal{K}(y) \equiv F(\pi/2, y) = \int_0^{\pi/2}\frac{d\phi}{\sqrt{1-y^2\sin^2\phi}}, \quad \mathcal{E}(y) \equiv E(\pi/2, y) = \int_0^{\pi/2}\sqrt{1-y^2\sin^2\phi}\, d\phi \ . \tag{5.11}$$

Notwithstanding infinitesimally thin disks are not realistic, the exponential thin disk is frequently used for modelling rotation curves and disk formation. Hence, in this case we just have $\rho(R,z) = \Sigma(R)\delta(z)$ and the surface matter density is given by

$$\Sigma(R) = \Sigma_0\exp(-R/R_D) \ , \tag{5.12}$$

where $M_D = 2\pi\Sigma_0 R_D^2$ is total mass of the disk. But, we can write the total mass in terms of the stellar mass-to-light times the total luminosity. Thus, the surface mass density reads

$$\Sigma(R) = \Upsilon_{\star D}\frac{L}{2\pi R_D^2}\exp(-R/R_D) \ . \tag{5.13}$$

One of the main evidences of dark matter is obtained by observations of galaxy rotation curves. As we already pointed out earlier, the light of the stellar and gaseous parts are converted into mass densities, from the latter one derives the respective Newtonian potentials and hence their individual contribution to the rotation curve, equation (5.8). Considering this, these contributions can not reproduce the observed rotation curve and this difference is commonly atributed to dark matter. The usual procedure for computing the dark matter contribution to rotation curves is to assume a dark matter profile depending on some free parameters which can be fitted to the observed data.

5.2 Observational data for rotation curves

Here, we describe the datasets used in this thesis, specially the ones that were used in [100, 31]. The first sample of rotation curves that we will discuss is the one derived from THINGS [101]. The THINGS project is a survey that measured the HI emission of 34 nearby galaxies. The high-resolution, about few parsecs[1], of the radio-interferometer NRAO

[1] 1 parsec≈ 3.26 light-years.

Very Large Array, allied to the proximity of galaxies, enabled to obtain high quality HI data. Using these HI data from THINGS in [99] the rotation curves of 19 galaxies were selected according the following requirements: i) the inclination angle i (e.g. for face-on systems $i = 0°$ while in edge-on $i = 90°$) such that $40° \leq i \leq 80°$. At lower inclinations the rotation starts to be measured within a two-dimensional disk and the projected rotation velocity, i.e. the velocity along the line-of-sight, decreases its amplitude, hence the dispersion velocity from the gaseous and stellar component becomes a contaminant. At higher inclinations, close to edge-on configuration, it is difficult to determine the rotation velocity because of the crossing between the line-of-sight and the wide range of projected velocities; ii) galaxies which do not present non-circular motion.

As a general result, each rotation curve derived from THINGS presents few hundreds of observed points, at least one order of magnitude higher than previous samples, e.g. [102]. In THINGS [99] it was not used the Hα data were not used for the innermost region; instead the proper HI data (because of the high-resolution in the radio measurements) was used for deriving rotation curves. Moreover, using the relation between mass-to-light and colors present in [101], namely

$$\log(\Upsilon_\star^K) = 1.43(J - K) - 1.38 \,, \tag{5.14}$$

where the observations of J and K bands are obtained from 2MASS Large Galaxy[103], an accurated treatment of the stellar component was performed. Once again, the equation above is dictated by SPS models. Hence, observing the J and K bands immediately the $\Upsilon_\star^K$ is fixed.

Since the photometry of galaxies in Spitzer Infrared Nearby Galaxy Survey (SINGS) are measured at 3.6μm, according [104], it is possible to convert $\Upsilon_\star^K$ to $\Upsilon_\star^{3.6}$ using SPS models, as follows

$$\Upsilon_\star^{3.6} = 0.92\Upsilon_\star^K - 0.05 \,, \tag{5.15}$$

such that the radial variation of the mass-to-light ratio becomes

$$\Upsilon_\star^{3.6}(R) = \Upsilon_\star^{3.6}\mathcal{C}(R) \,, \tag{5.16}$$

where $\mathcal{C}(R)$ means the radial variation of J and K colors and $\Upsilon_\star^{3.6} = M_\star/L_{3.6}$ where $L_{3.6}$ is the luminosity at 3.6μm. Using the magnitude profile $\mathcal{M}_{3.6} \propto -2.5 \log I$, whose units are mag/arcseg^2, obtained from SINGS it is possible to reach the surface brightness profile of the stellar disk as being

$$I_{\rm D}^{3.6}(R) \propto 10^{-0.4[\mathcal{M}_{3.6}(R) - \mathcal{D}_\odot^{3.6}]} \,, \tag{5.17}$$

where $\mathcal{D}_\odot^{3.6} \equiv \mathcal{M}_\odot^{3.6} + 21.56$ [104] and $\mathcal{M}_\odot^{3.6}$ is the absolute solar magnitude at 3.6μm band. Hence, it is straightforward to obtain the surface density of the stellar disk,

$$\Sigma_{\rm D}(R) \propto \Upsilon_\star^{3.6}\mathcal{C}(R)\cos[i(R)]10^{-0.4[\mathcal{M}_{3.6}(R) - \mathcal{M}_\odot^{3.6}]} \,, \tag{5.18}$$

where the factor $\cos i$ is due the deprojection of the surface density. Note that we explicitly show the radial dependence of inclination and the mass-to-light ratio. The radial dependence of inclination is due the model used to derive the rotation curves, namely the tilted ring model (for further details, please see [99]). The radial dependence in the mass-to-light ratio, as we already said, occurs because of the different stellar populations within the galaxy. Finally, the density matter for the stellar disk, assuming that a profile as sech^2 is the one for the vertical distribution, is given by

$$\rho_{\rm D}(R,z) = \Sigma_{\rm D}(R)\frac{1}{2z_{\rm D}}\text{sech}^2\left(\frac{z}{z_{\rm D}}\right) \ , \tag{5.19}$$

where one considers $z_{\rm D} = R_{\rm D}/5$ [99].

The bulge in this sample is modelled as a pseudo-bulge. According [99], in the region where the central component dominates there is no data enough for fitting a $R^{1/n}$ parametrization, equation (5.5). Hence, the stellar part is characterized by an "inner disk", equation (5.18), plus an "outer disk" which is the pseudo-bulge. Finally, for the gaseous component the surface density is obtained directly from observation of HI and one assumes a thin disk. Hence, the matter density is

$$\rho_{\rm gas}(R,z) = \Sigma_{\rm HI}(R)\delta(z) \ , \tag{5.20}$$

where $\delta(z)$ is the Dirac's delta.

The next sample used in this thesis, is the one published in [4]. The sample contains five late-type, HSB and bulgeless galaxies whose rotation curves are hybrids, that is, the innermost region of rotation curve is measured using Hα emission while the outer one is obtained via HI data. The method used to derive the rotation curves, called Warped Modified Envelope Tracing, is an alternative to the tilted ring. The method is indicated for galaxies which the velocity fields, directly associated to the HI measurements, are not well defined and when the galaxies present high inclinations. The error bars of the rotation curves include effects associated to erros of the inclination measurements and asymmetry of the galaxy.

The five galaxies were chosen from a sample of 967 galaxy rotation curves in [105]. The criterias used to this particular choice are: suitable inclination, symmetry and good resolution. The observations of luminous matter at I band reveals that the stellar component distributes as an exponential disk with a disk scale lenght given by [106]. The gaseous component, as the stellar one, is assumed to lie within a thin disk and its surface distribution is obtained via HI measurements. A factor of 1.33 is taken into consideration in order to include the presence of helium in gaseous component.

The last sample that we will comment is the one presented in [107]: the SPARC sample. It consists of 175 nearby galaxies with hybrid (HI/Hα) rotation curves from previous works (e.g. [102, 105, 108]) and a surface photometry based on measurements

at 3.6μm band. The errors of the rotation curves are obtained according to the following equation [109]:

$$\delta_V^2 = \sqrt{\delta_{V_{\rm fit}}^2 + \left(\frac{V_{\rm app} - V_{\rm rec}}{4}\right)^2}\,, \tag{5.21}$$

where $V_{\rm app}$ and $V_{\rm rec}$ are, respectively, the velocities obtained from fits of the approaching and receding sides of the disk. The $\delta_{V_{\rm fit}}^2$ is the error derived from the fit of the disk as a whole. The equation (5.21) includes deviations from circular motions and asymmetries. However, it is not included, in the error bars of the rotation curves, the errors due the assumed inclination.

The mass modelling of the luminous part in SPARC sample proceed as follows: the gaseous component is modelled as a thin disk, equation (5.20), and a factor of 1.33 is considered in order to include helium distribution. Hence, $V_{\rm gas}$ is computed from HI surface measurements, namely $\Sigma_{\rm HI}$, and using the equation (5.9). The modelling of the stellar component is made from the surface brightness at 3.6μm, and for large radii an exponential disk is used. The estimation of the disk scale lenght $R_{\rm D}$ is done by fitting the exponential function at the outer parts of the surface brightness profiles. The vertical distribution of the disk is modelled as an exponential with scale height $z_{\rm D=0.196}R_{\rm D}$ [110]. The bulge-disk decomposition in SPARC sample is performed as follows: first one identifies the radius such that the central component dominates, this radius is labelled as $R_{\rm B}$. After, one subtracts an exponential fit of the stellar disk at $R < R_{\rm B}$ and the remnant luminosity (assuming spherical symmetry) is used to compute the $V_{\rm bulge}$.

6 STATISTICAL METHODS

In this chapter we clarify some elements of statistics that will be used in this thesis (e.g. maximum likelihood estimation, Bayes's theorem, probability density functions), for a detailed review on these elements the reader is invited to consult [111, 112, 37].

In a statistical inference, an important quantity is the *random variable* which is a quantity that can assume random values in a measurement operation or in a serie of experiments. The mathematical description of the behavior of random variables is assured by a *probability density function* (PDF) which models how often certain value can appear. Let us write the corresponding PDF as $p(x|M(\boldsymbol{\theta}))$ which means the probability of the data given the model, where x is the random variable, $\boldsymbol{\theta}$ is the set of unknown parameters, namely $\boldsymbol{\theta} \equiv \{\theta_1, \theta_2, ..., \theta_m\}$, and M represents the model, that is, our knowledge about the measurements. The "|" is for separating random variables from parameters. If the measurements of each x_i is done in an independent way, the theory of probability ensure us that

$$\mathcal{L}(D|M(\boldsymbol{\theta})) \equiv \prod_i p(x_i|M(\boldsymbol{\theta})), \tag{6.1}$$

where D is the *sample data* which is a part of a *population* (collection of all possible samples or an infinity number of measurements) and the quantity $\mathcal{L}$ is called likelihood.

The likelihood is a function of data and parameters, hence if the dataset is fixed one can variate the parameters in order to maximize $\mathcal{L}$. This process is known as *maximum likelihood estimation* (ML) and, in practice, it consists by solving the following system of equations

$$\frac{\partial \mathcal{L}}{\partial \theta_i} = 0, \quad i = 1, ..., m \ . \tag{6.2}$$

Note that now one can write the parameters $\boldsymbol{\theta}$ in terms of the random variables, that is, the data. In other words, if we can solve the equation (6.2) we can write the parameters $\boldsymbol{\theta}$ in terms of real numbers (values), hence we can obtain the *best values* for $\boldsymbol{\theta}$ which maximizes the likelihood $\mathcal{L}$. Let us denote those best values for the parameters as $\hat{\boldsymbol{\theta}}$. The approach of calculating the parameter distribution in terms of data is known as *frequentist statistics*. Hence, repeating the experiment several times, under the same conditions, at the end of the day one can assign the distribution of $\hat{\boldsymbol{\theta}}$. However, the frequentist approach does not consider the previous knowledge about the parameters, that is, the *prior* information about them acquired by previous experiments. If we are interested in to insert properly the previous knowledge in our inference we have to switch to the *Bayesian statistics*. Hence, one can estimate the probability distribution of parameters given the data, namely $\mathcal{P}(M(\boldsymbol{\theta})|D)$. The function $\mathcal{P}$ is called *posterior* and in order to address it we can use the

Bayes's theorem, given by

$$P(M|D) = \frac{P(D|M)P(M)}{P(D)} \,, \tag{6.3}$$

where $P(M|D)$ is the probability of having theory given data, $P(D|M)$ is the probability of having data given theory, lastly $P(D)$ and $P(M)$ are the probabilities of having data and theory. In terms of our notation, the equation (6.3) becomes

$$\mathcal{P}(M(\boldsymbol{\theta})|D) = \frac{\mathcal{L}(D|M(\boldsymbol{\theta}))\pi(\boldsymbol{\theta})}{\mathcal{E}(D)} \,, \tag{6.4}$$

where $\mathcal{E}$ is called *evidence* and it is given by

$$\mathcal{E} = \int \mathcal{L}(D|M(\boldsymbol{\theta}))\pi(\boldsymbol{\theta}) d^n\boldsymbol{\theta} \,. \tag{6.5}$$

Its non-dependence on the parameters $\boldsymbol{\theta}$ makes the evidence only a normalization constant.

6.1 Sampling methods

In the situation when the vector of parameters $\boldsymbol{\theta}$ is large, the pursuit for the ML estimators $\hat{\boldsymbol{\theta}}$ and the posterior $\mathcal{P}$ may be costly. For example, if we consider a grid approach for sampling a m-dimensional posterior considering $m = 10$ and 10 values per dimension, we need to perform 10^{10} computations. Although the implementation of grid approach is simple, manageable and its parallelization is easily feasible, in higher dimensional problems the time for sampling the entire posterior becomes huge. An alternative to the grid approach is the random sampling, the most popular at present days is the MCMC. The reason for the preference for random sampling than grid one is due the fact that the grid loses time sampling regions with small probability, i.e. the PDF tails.

As the name suggest, MCMC is composed by two elements: the Markov process and the Monte Carlo method. The latter one, developed in [113], has an interesting usage in Bayesian analysis and we will discuss a bit about it in next paragraph.

An advantage of Bayesian inference is that one can marginalize over nuisance parameters which can be understood as parameters whose the interest in them is lower with respect to others. A PDF that is result of a marginalization, namely $\mathcal{P}(\boldsymbol{\Theta}|D)$ (here we have omitted the model M for simplicity), is mathematically described by

$$\mathcal{P}(\boldsymbol{\Theta}|D) = \int \mathcal{P}(\boldsymbol{\Theta}, \alpha|D) d\alpha \,, \tag{6.6}$$

where $\boldsymbol{\Theta}$ is a subset of $\boldsymbol{\theta}$ such that $\boldsymbol{\theta} = \{\boldsymbol{\Theta}, \alpha\}$. Indeed, sometimes marginalizations could be very discouraging (for example if one wants to compute the evidence, equation (6.5), one needs to marginalize over all parameters), specially on high dimensional situations. At this point that Monte Carlo is interesting and the application of it for such inconvenient is

called *Monte Carlo integration*. It consists into replacing a complicated integration of some function f over some domain $\mathcal{V}$ by checking if N random points, $x_1, x_2, ..., x_N$, over $\mathcal{V}'$ (a superset of $\mathcal{V}$) are within $\mathcal{V}$, hence estimating the area (here in a heuristic sense) of $\mathcal{V}$ as the area of $\mathcal{V}'$ times the fraction of points inside $\mathcal{V}$. Hence, translating it exactly, one has

$$\int f d\mathcal{V} \approx \mathcal{V}\langle f\rangle \pm \sqrt{\frac{\langle f^2\rangle - \langle f\rangle^2}{N}} \,, \tag{6.7}$$

where

$$\langle f\rangle \equiv \frac{1}{N}\sum_{i=1}^{N} f(x_i), \quad \langle f^2\rangle \equiv \frac{1}{N}\sum_{i=1}^{N} f^2(x_i) \,. \tag{6.8}$$

The Markov process or *Markov chain* is a set of random variables which the present value of a given variable depends only on the preceding value of it. The process can be summarized as follows

$$\text{Prob}(\theta_{i+1}|\{\theta_i\}) = \text{Prob}(\theta_{i+1}|\theta_i) \,. \tag{6.9}$$

When the Markov process reaches the equilibrium, it is said that the chain has a stationary distribution, i.e. the distribution looks the same if one runs forward or backward in time. In terms of the joint probability, one has

$$\text{Prob}(\theta_{i+1}|\theta_i) = \text{Prob}(\theta_i|\theta_{i+1}) \,, \tag{6.10}$$

in other words, it is symmetric. The relation in the above is called *balance* or *reversibility condition*. After the convergence, the final chains are used in the Markov integration, equation (6.7), i.e. one has the MCMC.

An important quantity in MCMC algorithms is the *transition probability* which, in a continuum space, is given by

$$K(x, y) = \text{Prob}(x_{i+1} = y|x_i = x) \,. \tag{6.11}$$

In the case of discrete space, the transition probability is a matrix K_{xy}. What differs MCMC algorithms from each other is the choice of the transition probability. There are many MCMC algorithms in literature, e.g. Metropolis-Hastings, Gibbs sampling, Nested sampling. One of the most traditional is the Metropolis-Hastings [114] and it consists of a transition probability given by $K(x, y) = q(y|x)\alpha(x, y)$ where q is an arbitrary function called *proposal distribution* and α is called *acceptance ratio*. In MH, the acceptance ratio is given by $\alpha(x, y) = \min\left[1, \frac{f(y)q(x|y)}{f(x)q(y|x)}\right]$, where the f function is the desired distribution or *target distribution*, e.g. $\mathcal{P}(M(\boldsymbol{\theta})|D)$.

The effectiveness of MH algorithms depends on the choice of the proposal distribution where effectiveness here means how correlated the samples are. In order to guarantee the convergence of the chains the samples needs to be independent. There are suggestions for MH algorithms in literature (e.g. [115], the adaptive MH) which try to optimize the

proposal distribution. An interesting solution for the optimization of proposal distribution was presented by [116]: the ensemble approach. The basic idea is that there are *walkers*, the elements of the ensemble, which interact with each other in order to improve their proposal distributions. In [117], it is presented an elegant way to do this, the procedure is called affine-invariant sampler. Now, we describe briefly how the affine-invariant sampler works [1]: Let us consider an ensemble of K walkers, namely $\mathcal{S} = \{X_k\}$, and its *complementary* set $\mathcal{S}' = \{X_i, \forall i \neq k\}$. The proposal distribution of a walker X_k is based on the real-valued parameter space, i.e. the "positions", of the $k-1$ walkers in $\mathcal{S}'$. In other words, the position of a walker X_k is updated to Y by drawing a walker X_j from $\mathcal{S}'$ according the following relation

$$Y = X_j + Z[X_k(t) - X_j] \,, \tag{6.12}$$

where Z is a random variables provided by the distribution $g(Z = z)$. Note that if g obeys

$$g(z^{-1}) = zg(z) \,, \tag{6.13}$$

the equation (6.12) is symmetric. The acceptance ratio is given by

$$\alpha = \min \left[1, Z^{N-1} \frac{p(Y)}{p(X_k(t))} \right] \,, \tag{6.14}$$

where N is the dimension of the parameter space. The procedure is repeated for each walker in the ensemble. In [117], the following function g is recommended

$$g(z) \propto \begin{cases} \frac{1}{\sqrt{z}} & \text{if } z \in [\frac{1}{a}, a] \\ 0 & \text{otherwise} \end{cases} \tag{6.15}$$

where a is a parameter called "stretch move" and the default value for it is 2. In this thesis we have used a python package which implements this affine-invariant sampler called `emcee`: the MCMC hammer, available in <http://dan.iel.fm/emcee/current/> developed by [1].

6.2 Convergence diagnostics

An important point for every MCMC sampler is the convergence of the chains. There are several proposed ways by diagnosing this convergence in literature (for a detailed review, please see [118]), but there is no a schedule by detecting convergence properly, instead what we can detect is the convergence failure. Hence, convergence diagnostics are not the enough conditions but they are necessary in any MCMC application. The diagnostic convergence chosen in this thesis is the *autocorrelation time* which enable us to estimate the minimum number of interactions (steps) in order to produce independent chains. This minimum quantity is called *burn-in*, a certain number of steps which one needs to discard afterwards. A detailed explanation about autocorrelation diagnostic is

performed in [119]. Here, we will focus only in the essential points of this convergence diagnostic.

An important quantity to define is the autocorrelation function ρ_f,

$$\rho_f(\tau) = \frac{C_f(\tau)}{C_f(0)} \,, \tag{6.16}$$

with

$$C_f(\tau) = \frac{1}{M-\tau} \sum_{t=1}^{M-\tau} \left[f(X(t+\tau)) - \langle f \rangle \right] \left[f(X(t)) - \langle f \rangle \right] \,, \tag{6.17}$$

where $\langle f \rangle = \frac{1}{M} \sum_{t=1}^{M} f(X(t))$, $X(t)$ is the sampled random variable of the parameter space, and M is the total length of the chain. C_f is a function which measures the covariance between samples separated by a time lag τ. The independent samples are obtained at certain value of τ, namely $\hat{\tau}$, such that $C_f(\hat{\tau}) \to 0$. Hence, $\hat{\tau}$ offers a lower bound of minimal posterior samplings that are necessary for producing independent samples. The equation below gives the τ estimation

$$\tau_{\text{est}}(N) = 1 + 2 \sum_{\tau=1}^{N} \rho_f(\tau) \,, \tag{6.18}$$

where N starts at $N \ll M$.

7 TESTING GRAVITY WITH GALAXY ROTATION CURVES

This chapter is dedicated to show the inference of approaches either based on GR or modified gravity with respect to observational rotation curve data that would either indicate a complete elimination or a partial one of dark matter in galaxies. In [28], we tested two specific models based on GR. In order to test them properly, we present a new method and using it we find that neither of two tested models can fit the observational data in a satisfactory way. In [31], we investigated frameworks of modified gravity which introduces a Yukawa correction in gravitational potential, as we already shown in Chapter 2. We assumed that the fifth-force couples to dark matter and to baryons in a different way. By constraining of the parameters β and λ which are, respectively, the strength and the range of the fifth-force, we found that the Yukawa correction improves the fit with respect to the observed rotation curves. Beyond that, we performed a Bayesian analysis and we found an evidence in favor of a dark matter plus Yukawa term higher than 8σ with respect to the standard case.

7.1 Models based on general relativity

Galaxies are stationary systems in which the Newtonian potential is small, about $10^{-6} \sim 10^{-8}$ in units that $c = 1$. Beside this, the typical speeds of these systems are a few hundred kms^{-1} in $c = 1$ units. In other words, these numbers are suggesting that corrections coming from GR to Newtonian dynamics are negligible, smaller than 1 percent hence they are completely covered by the uncertainties of astrophysical data. Thus, if Newtonian gravity is, in practice, the underlying theory for modeling the internal dynamics of the galaxies, it is not possible to reproduce the observed rotation curve without assuming a dark matter profile.

Some authors, namely [22, 25, 26, 27, 120], claim that GR is the correct gravitational theory and these small numbers actually could affect the distribution of dark matter in galaxies and the corrections on rotation curves, arising from GR, could be larger than 10 per cent.

7.1.1 The Cooperstock-Tieu approach

The Cooperstock-Tieu (CT) approach [22, 23, 24, 25, 26] assumes that a galaxy can be modeled as pressureless fluid in a axisymmetric stationary spacetime. Hence, the latter can be written, in $c = 1$ units and using the cylindrical coordinates (r, ϕ, z), as

follows

$$ds^2 = -e^w(dt - N d\phi)^2 + e^{-w} r^2 d\phi^2 + e^{\nu - w}(dr^2 + u\, dz^2), \tag{7.1}$$

where w, N, ν, u are functions that only depend on the coordinates r, z. The line element above is the most general in terms of the desired symmetry [121] although it is not the most convenient to work with galactic dynamics. Since the fluid that fills the spacetime is dust it is possible to reduce the number of functions which the metric (7.1) depends on, just choosing coordinates in a convenient way. Hence, the line element becomes [27]

$$ds^2 = -(dt - N d\phi)^2 + r^2 d\phi^2 + e^{\nu}(dr^2 + dz^2). \tag{7.2}$$

An asymptotic observer at rest with respect to the galaxy centre measures a rotation given by [25, 27]

$$V = \frac{N}{r}\,. \tag{7.3}$$

The N fuction is determined by Einstein field equations, equation (1.6), in particular by the following equation

$$N_{rr} + N_{zz} - \frac{N_r}{r} = 0\,. \tag{7.4}$$

Solving the differential equation for N above is straightforward to deduce V using equation (7.3. Hence, the solution for $z \geqslant 0$ is given by [22]

$$V_{\mathrm{CT}}(r, z \geq 0) = -\sum_n D_n e^{-k_n z} J_1(k_n r)\ , \tag{7.5}$$

where J_α is a Bessel function of the first kind, and k_n and D_n are arbitrary constants. The velocity profile can connected with mass density from the following GR equation

$$\frac{N_r^2 + N_z^2}{r^2} \approx 8\pi G\rho\,. \tag{7.6}$$

Hence, the solution proposed by CT approach shows a non-Newtonian solution for velocity in galaxies. The arbitrary constants D_n can be fixed using the observational rotation curve data. If higher precision is demanded the larger is the number of D_ns to be fitted. The authors claim that 10 coefficients is enough for fitting some sets of galaxies. The k_n constants corresponds to nth root of the Bessel function $J_0(k_n\, r_{\max})$, where $r_{\max}$ is the radius of the farthest observed circular velocity data of a given galaxy. Actually, it is not surprising that the velocity formula in equation (7.5) fits the observed rotation curve, because CT solution for velocity is just Fourier-Bessel series at $z = 0$, which can fit any curve in the interval $(0, r_{\max})$. The non-triviality of CT solution is its vertical distribution, i.e. whether CT approach is correct the mass density, inferred by equation (7.6), has to match the observed baryonic density. There is a work, namely [122], that criticizes the CT approach with respect to the dispersion velocity of stars outside the galactic plane, in the specific case of [122] the galaxy analyzed was the Milky Way. The criticism is valid

but too restrict for invalidating the model. The CT approach received also criticisms from the theoretical side (please see [123, 27], for further details), for example the extension of equation (7.5) by using $V(r,z) = V(r,-z)$ is problematic although the authors claimed to have answered in [25].

7.1.2 The Balasin-Grummiler approach

The Balasin-Grummiler (BG) approach considers the same assumptions of the CT one, i.e. the line element, equation (7.1), the same energy-momentum tensor, i.e. that of a presureless fluid. But, the BG solution includes the symmetry about the $z = 0$ plane, what does not occur in the case of equation (7.5).

The GR field equations for (7.2) and considering the energy-momentum tensor as $T^{\nu}_{\mu} = \rho U_{\mu} U^{\nu}$ read

$$2r\nu_r + N_r^2 - N_z^2 = 0\,, \tag{7.7}$$

$$r\nu_z + N_r N_z = 0\,, \tag{7.8}$$

$$\nu_{rr} + \nu_{zz} + \frac{1}{2r^2}(N_r^2 + N_z^2) = 0\,, \tag{7.9}$$

$$N_{rr} + N_{zz} - \frac{N_r}{r} = 0\,, \tag{7.10}$$

$$\frac{N_r^2 + N_z^2}{r^2} = 8\pi G\rho\, e^{\nu}\,. \tag{7.11}$$

For equation (7.10) BG present the following solution

$$N(r,z) = A_0 + \int_0^{\infty} \cos(\lambda z)(r\lambda)A(\lambda)K_1(\lambda r)d\lambda\,, \tag{7.12}$$

where $A(\lambda)$ is a "sufficiently regular" arbitrary function, A_0 is a constant and K_1 is a modified Bessel function of the second kind. Here, it is possible to see that the selection of $A(\lambda)$, in front of the observed rotation curve, characterizes that the rotation curve is the physical imput. A suitable choice for $A(\lambda)$ leads to the following velocity formula

$$V_{\rm BG}(r,z) = \frac{(R-r_0)V_0}{r} + \frac{V_0}{2r}\sum_{\pm}\left(\sqrt{(z\pm r_0)^2 + r^2} - \sqrt{(z\pm R)^2 + r^2}\right), \tag{7.13}$$

with, $|z| < r_0$. Hence, at $z = 0$,

$$V_{\rm BG}(r,0) = \frac{V_0}{r}\left(R - r_0 + \sqrt{r_0^2 + r^2} - \sqrt{R^2 + r^2}\right). \tag{7.14}$$

Note that the profile above is composed by three stages:i) the linear behavior for $r \lesssim r_0$; ii) the constant velocity for $r_0 \lesssim r \lesssim R$; iii) the $1/r$ behavior for $r \gg R$ (although the R parameter can not be accurately derived since the transition to a decreasing rotation curve cannot be seen up to latest rotation curve data).

At the much lower velocities regime compared with speed of light and assuming that $r < r_0$, the BG approach should to coincide with Newtonian gravity. At this regime, [27] shows that ν is close to a constant. Moreover, the authors of [27] claim that the corrections arisen from GR could reduce the necessity of dark matter in 30 per cent.

In our work [28], we proposed (as we will show in next subsection) the *effective Newtonian rotation curve method* in order to test these two approaches properly. We also assumed both approaches without dark matter.

7.1.3 The effective Newtonian rotation curve method

The purpose of this method is to evaluate properly models in which the mass density is derived from the rotation curve. It is important to emphasize that this inverse procedure is not possible in Newtonian gravity even assuming that all matter is enclosed in a thin axisymmetric disk [93]. The essential feature of this method is to change the unfamiliarity of matter density error bars by a model dependent transposition of error bars from observed rotation curve to an effective Newtonian rotation curve. The method ends providing an effective rotation curve which can be fitted by traditional Newtonian procedures.

In literature, in a large number of works on rotation curve data, it is common to present only the values of the baryonic density without its corresponding uncertainties. Actually, the relevant uncertainties are encoded in the rotation curves error bars [5, 4], e.g. violation of axial symmetry. Hence, to compare a model which derives the density profile by certain means with the observed baryonic density is not obvious.

The effective Newtonian rotation curve method is based on two minimizations procedures. The first one is to obtain the best fit values of the model parameters with respect to the observational data, i.e. the ML estimators for the parameters. The second minimization is important for deriving the baryonic parameters, e.g. stellar mass-to-light ratio, and even the dark matter parameters. Now, we will describe the method [28]:

- The model circular velocity at $z = 0$, which is designated by $V(r, p_i)$, where p_i represent the model parameters, is fitted to the observed RC. This RC is described by the table whose k-th line reads $(r_k, V_{\mathrm{Obs},k}, \delta V_{\mathrm{Obs},k})$, where r_k is the radius of the galaxy whose corresponding circular velocity is $V_{\mathrm{Obs},k}$ with a 1σ error bar given by $\delta V_{\mathrm{Obs},k}$. The fit determines the best fit parameters $\bar{p}_i$ and the corresponding error bars δp_i.

- From $V(r, \bar{p}_i \pm \delta p_i)$ one can (numerically) determine the corresponding mass density profile as a function of the model parameters, $\rho(r, z, \bar{p}_i \pm \delta p_i)$, for instance from equations (7.3, 7.6).

- From $\rho(r, z, \bar{p}_i \pm \delta p_i)$ one can determine the effective Newtonian circular velocity at $z = 0$. The latter is written as $V_{\rm eN}(r, \bar{p}_i \pm \delta p_i)$ and it is defined as being the circular velocity derived from Newtonian gravity for the matter density $\rho(r, z, \bar{p}_i \pm \delta p_i)$.

- The effective Newtonian RC data with error bars is built from $V_{\rm eN}$. These data can be expressed as a table whose k-th line is given by $(r_k, \bar{V}_{{\rm eN},k}, \delta V_{{\rm eN},k})$, where r_k assumes the same values of the original data on the observational RC, $\bar{V}_{{\rm eN},k} = V_{\rm eN}(r_k, \bar{p}_i)$ and $\delta V_{{\rm eN},k}$ is an approximation for the corresponding 1σ error bar, which is detailed afterwards.

- The astrophysical expectation on the gas and stellar densities, together possibly with a given dark matter profile, are used to derive the Newtonian circular velocity $V_{\rm N}$, which will depend on baryonic parameters (like the mass-to-light ratios) and possibly on dark matter parameters as well.

- If the gravitation theory being considered is compatible with both the observational RC and the matter content assumed for the galaxy, then $V_{\rm eN}$ and $V_{\rm N}$ should be mutually compatible. Hence, one fits $V_{\rm N}$ to the effective Newtonian RC data, thus deriving the baryonic (and dark matter) parameters, and deriving the quantities χ^2 and $\chi^2_{\rm red}$. The latter are the quantities that have physical information on the quality of the fit and that can be compared to other approaches.

7.1.4 The fit procedure step by step

Here we detail the two fitting procedures contained in the effective Newtonian rotation curve method in four steps.

- *The derivation of $\bar{p}_i$ and ρ.* We assume that the observational errors for rotation curves obey a Gaussian distribution. Hence, the likelihood is $\mathcal{L} \propto e^{-\chi^2/2}$. The ML estimation, or the minimization of χ^2, is used to compute the best-fitting parameters for velocity formula $V(r, p_i)$ with respect to data. The quantity χ^2 is given by

$$\chi^2_p = \sum_{k=1}^{N} \left(\frac{V(r_k, p_i) - V_{{\rm Obs},k}}{\delta V_{{\rm Obs},k}} \right)^2 . \tag{7.15}$$

  The meaning of subscript p is only for emphasizing that the aim of χ^2 is for finding the ML estimators. The latter are denoted by $\bar{p}_i$, and N is the total number of observational data points of the circular velocity $V_{\rm Obs}$. By knowing $V(r, \bar{p}_i)$ it is straightforward to evaluate the matter density $\rho(r, z, \bar{p}_i)$. Moreover, one can compute ρ for all values of p_i within the range established by the error bars δp_i, therefore one can obtain $\rho(r, z, \bar{p}_i \pm \delta p_i)$.

- *The derivation of V_{eN}.* By solving the Poisson equation, namely $\nabla^2\Phi(r,z,\bar{p}_i) = 4\pi G\rho(r,z,\bar{p}_i)$, and using the already known relation between circular velocity and gravitational velocity, $V^2_{\rm eN}(r,\bar{p}_i) = r\partial_r\Phi(r,\bar{p}_i)$, it is possible to derive $V_{\rm eN}$ directly using equation (5.9). Moreover, using equation (5.9) it is possible to derive $V_{\rm eN}$ for all values of p_i allowed by the 1σ uncertainties, i.e. one can find the $V_{\rm eN}(r,\bar{p}_i \pm \delta p_i)$.

- *The effective Newtonian rotation curve.* The aim of this step is to generate data, including its error bars, that can be used for the next fitting procedure. The effective Newtonian rotation curve data are given by $(r_k, \bar{V}_{{\rm eN},k}, \delta V_{{\rm eN},k})$, where k goes from 1 to N. The quantity $\bar{V}_{{\rm eN},k}$ is simply $V_{\rm eN}(r_k,\bar{p}_i)$ and $\delta V_{{\rm eN},k}$ is its corresponding 1σ error bar. Here, it was used the same radial values r_k from observational rotation curve. The error bars of effective Newtonian rotation curve data are derived as follows: firstly one finds $V_{{\rm max},k}$ and $V_{{\rm min},k}$, which are respectively the maximum and the minimum of $V_{\rm eN}(r_k,p_i)$, with fixed r_k, such that $\chi^2(p_i) \leq \chi^2_{\rm min} + \Delta\chi^2$, where $\Delta\chi^2$ is the constant associated to a 1σ uncertainty considering the total number of the model parameters (p_i). This guarantees that $V_{{\rm max},k}$ is the maximum value achievable for $V_{{\rm eN},k}$ inside the 1σ confidence region. In other words, it is being considered that the PDF of the parameters p_i is Gaussian which is an approximation valid up to 1σ level. Strictly, one had to compute the proper PDF for the parameters p_i but one understands that a Gaussian distribution for the parameters, or in others words a *Fisher approximation*, is reasonable. In general, the error bars will be exactly symmetric. In this case, one chooses, as the 1σ uncertainty, the maximum between $V_{{\rm max},k} - \bar{V}_{{\rm eN},k}$ and $\bar{V}_{{\rm eN},k} - V_{{\rm min},k}$. Note that the quantity $\Delta\chi^2$ increases with the number of parameters p_i.

- *The derivation of the baryonic and dark matter parameters.* The matter content of all galaxies is composed by baryons and dark matter, hence the total Newtonian circular velocity is given by equation (5.8). Here, in other to test the two approaches, namely CT and BG, the only free parameters will be the baryonic ones, namely $\Upsilon_{*\rm B}$ and $\Upsilon_{*\rm D}$, hence the dark matter contribution will not be considered for now, i.e. $V^2_{\rm DM} = 0$. Finally, the Newtonian circular velocity is $V^2_{\rm N} = V^2_{\rm N}(r,\Upsilon_{*\rm B},\Upsilon_{*\rm D})$. Therefore, if a model predicts the matter density in some way and the latter is compatible with the matter distribution of such galaxy, then then $V_{\rm eN}$ and $V_{\rm N}$ should be mutually compatible. The second and last minimization procedure also assumes that the error follows a Gaussian distribution, thus one performs the minimization of the following quantity

$$\chi^2 = \sum_{k=1}^{N} \left(\frac{V_{\rm N}(r_k,\Upsilon_{*\rm D},\Upsilon_{*\rm B}) - \bar{V}_{{\rm eN},k}}{\delta V_{{\rm eN},k}} \right)^2 . \tag{7.16}$$

From the above quantity, the goodness of fit $\chi^2_{\rm red}$ can be used for comparison between different approaches.

7.1.5 Application to the Cooperstock-Tieu approach

In this section we present the result of applying the effective Newtonian rotation curve method, according the last section, to the CT approach.

- *The derivation of $\bar{p}_i$ and ρ.* In Table 5 is available the results for $\bar{p}_i$ and its corresponding error bars. In the case of CT approach the p_i parameters corresponds to the D_n constants in equation (7.5). For all galaxies that we tested we adopted the 10 parameters recommended by the authors in [22]. One can perceive that the first fit, the CT approach easily fits the observed rotation curve. This can be measured from the values of $\chi^2_{\mathrm{p,red}}$, in Table 6. We also tested, for a few galaxies, that less than five free parameters can provide good fits, i.e. $\chi^2_{\mathrm{p,red}} \sim 1$. Those galaxies have rotation curves that typically increases slowly and smoothly and therefore do not need high frequency terms of the equation (7.5). Although there are some examples in which 10 parameters are not enough, e.g. [26].

  The matter density profile ρ is derived from the circular velocity V after the first fitting procedure, that is, which determines the ML estimators for D_ns. The derivation of ρ comes from the combination of equations (7.3, 7.5, 7.6). As the equation (7.5) states, the circular velocity in CT approach is defined within the interval $(0, r_{\mathrm{max}})$. Hence, if one wants to extend the matter density beyond r_{max} by using the equation (7.5), according [23], requires different values for the constants D_n and k_n in relation with the previous ones already fitted from observational rotation curve. Indeed, from phenomenological point of view, it is expected that the baryonic density of a galaxy drops at larger radii. A viable approximation for the baryonic matter beyond the last observed rotation curve data is

$$\rho(r \geq r_{\mathrm{max}}, z) = e^{(r\mathrm{max}-r)/r_{\mathrm{d}}}\rho(r_{\mathrm{max}}, z), \tag{7.17}$$

  which is an extension based on a Freeman disc [124]. This approximation will end to be a good one in gas rich galaxies, since the gas density decays slower than the stellar one. Notwithstanding, the impact on V_{eN} is negligible, since the approximation is only beyond r_{max}.

- *The derivation of V_{eN}.* Using the latter extension, the matter density is known entirely. Hence, one can derives the V_{eN} via equation (5.9). Due the high number that $V_{\mathrm{eN}}(r, D_n)$ depends on a difficult on next step arises. Nevertheless, the effective Newtonian circular velocity $\bar{V}_{\mathrm{eN}}(r)$ is immediately computed with the best fit D_n.

- *The effective Newtonian RC data.* These are expressed as $(r_k, \bar{V}_{\mathrm{eN,k}}, \delta V_{\mathrm{eN,k}})$ and the main purpose of this step is to compute the error bars $\delta V_{\mathrm{eN,k}}$. In order to have this,

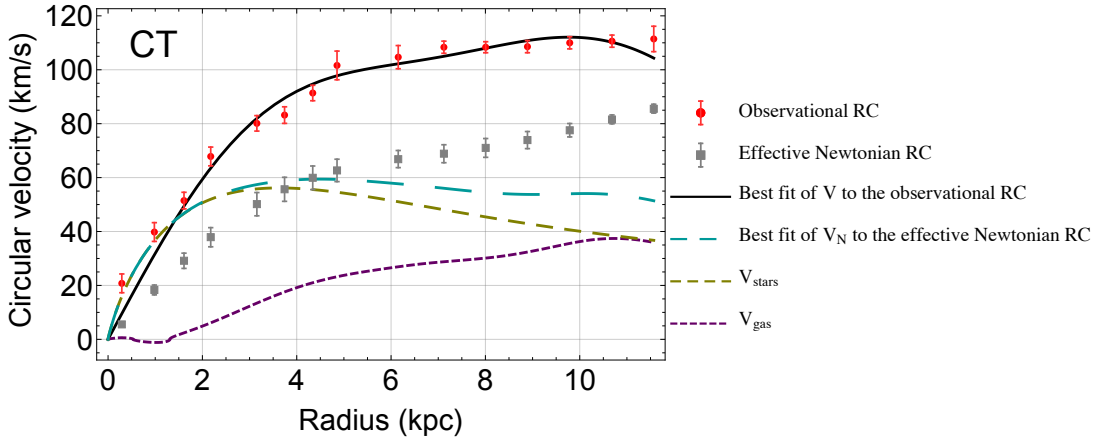

Figure 2 – The RC curve analysis of ESO 116-G12 with the CT approach with three free model parameters (p_i). The fit of the total Newtonian circular velocity $V_{\rm N}$ to the effective Newtonian RC is not satisfactory ($\chi^2_{\rm red} \gg 10$).

Table 4 – Results of the CT approach with three model parameters p_i applied to the galaxy ESO 116-G12 (see Figure 2). This fit considers the full evaluation of the effective Newtonian data with error bars. This table also includes a comparison to the corresponding results when the same galaxy is modelled with baryonic matter and a NFW dark matter halo [3].

Galaxy	CT (3 parameters p_i)				NFW	
	$\chi^2_{\rm p}$	$\chi^2_{\rm p,red}$	χ^2	$\chi^2_{\rm red}$	χ^2	$\chi^2_{\rm red}$
ESO 116-G12	31.60	2.63	1341.35	95.81	31.15	2.60

one should perform a minimization and maximization of $V_{\rm eN}(r, D_n)$ considering the constraint $\chi^2(p_i) \leq \chi^2_{\rm min} + \Delta\chi^2$ at each radius r_k.

In the particular case of CT approach, is not trivial (computationally) to evaluate $\delta V_{\rm eN,k}$ since the approach requires 10 D_n parameters. However, it is not necessary at all to compute $\delta V_{\rm eN,k}$ in order to conclude that the CT approach is incompatible, i.e. the $V_{\rm eN}$ and $V_{\rm N}$ do not agree sistematically. We analyzed the CT approach with fewer than 10 free parameters in order to ilustrate this incompatibility. The galaxy analyzed was the ESO 116-G12 and was considered only three D_n parameters. The results are in Figure 2 and Table 4.The derived values of $\delta V_{\rm eN}$ ranges from 0.6 km/s to 4.5 km/s. With the exception of the first point, all the others have $\delta V_{\rm eN}$ larger than 1 km/s. The mean $\delta V_{\rm eN}$ is about 3 km/s.

- *The derivation of the baryonic paramters.* With the effective Newtonian rotation curve, one fits the $V_{\rm N}$ and derives χ^2, $\chi^2_{\rm red}$, $\Upsilon_{*\rm B}$ and $\Upsilon_{*\rm D}$. The results will be commnented later.

7.1.6 Application to the Balasin-Grumiller approach

The application of the effective Newtonian method it straightforward tothe BG approach and much easier than CT one. The numerical integrals, in particular the equation (5.9), are faster because the model often uses 3 free parameters p_i and the extension for the matter density ρ is already included in the BG approach.

- *The derivation of $\bar{p}_i$ and ρ.* The parameters p_i for BG approach are three, namely R, r_0 and V_0 and the results from the ML estimation method for those parameters are available in Table 5. The fits of the velocity formula in the BG approach, namely equation (7.14), to the observed rotation curve are reasonable as one can see by the values of $\chi^2_{\mathrm{p,red}}$ which are in the range from 0.5 to 1.6.

  The quantity ρ is derived from the combination of the equations (7.3, 7.11, 7.14). The extesion of ρ is already guaranteed in BG approach, pratically it depends on a single parameter R. The values of this parameters vary from some kpc's (for some galaxies) to very large ones, that is, pratically with no maximum for R. This kind of result occurs specially in galaxies whise the rotation curve increases up to r_{max}.

- *The derivation of V_{eN}.* The effective Newtonian circular velocity V_{eN} is directly computed from equation. (5.9).

- *The effective Newtonian RC data.* Here, one computes the error bars $\delta V_{\mathrm{eN,k}}$. Performing the minimization and maximization of $V_{\mathrm{eN}}(r, r_0, V_0, R)$ regarding the constraint $\chi^2(r_0, V_0, R) \leq \chi^2_{\mathrm{min}} + \Delta\chi^2$ at each radius r_k. Hence, one derived constrained minimizations and maximizations with three free paramters, for each observational rotation curve data and for each six galaxies. The error bars derived from the forementioned method were close to symmetric and therefore they were all symmetrized considering the largest value. This was performed for all six galaxies that were applied the BG approach.

- *The derivation of the baryonic parameters.* Fiitng the V_{N} to the effective Newtonian rotation curve the quantities χ^2, χ^2_{red}, $\Upsilon_{*\mathrm{B}}$ and $\Upsilon_{*\mathrm{D}}$ are derived straightforwardly. In the next subsection the results are preented and commented.

7.1.7 Results

Here, we present the results of the fit procedures for CT and BG are in the Tables 5, 6 and 7, and the rotation curve plots are shown in Figure 3.

Table 5 – The values of the p_i parameters and its errors (δp_i) for both the CT and BG approaches.

CT approach						
parameters	DDO 154	ESO 116-G12	ESO 287-G13	NGC 2403 2D	NGC 2841	NGC 3198 1D
D_1 (km/s)	303 ± 10	962 ± 30	3455 ± 87	1864 ± 13	1.155 ± 0.017	4407 ± 54
D_2 (km/s)	$6.3^{+5.7}_{-5.8}$	34 ± 22	200^{+61}_{-69}	111.2 ± 8.3	1303^{+91}_{-90}	415 ± 31
D_3 (km/s)	10.4 ± 4.4	27 ± 13	191^{+47}_{-46}	103.5 ± 6.3	928^{+78}_{-76}	280 ± 23
D_4 (km/s)	-1.1 ± 3.5	-4 ± 14	22 ± 44	26.5 ± 5.5	252 ± 55	55 ± 21
D_5 (km/s)	4.8 ± 3.0	$9.7^{+9.6}_{-9.7}$	60^{+49}_{-43}	13.4 ± 5.0	293 ± 58	21.9 ± 5.9
D_6 (km/s)	-2.1 ± 2.8	1 ± 11	12 ± 23	11.4 ± 4.5	101^{+46}_{-47}	5 ± 16
D_7 (km/s)	$1.4^{+2.7}_{-2.6}$	$2.1^{+8.0}_{-7.9}$	1 ± 43	7.1 ± 4.1	112^{+46}_{-47}	26 ± 14
D_8 (km/s)	$-0.3^{+2.3}_{-2.4}$	-1.4 ± 8.4	3^{+16}_{-15}	7.5 ± 3.8	17^{+40}_{-41}	9 ± 14
D_9 (km/s)	0.7 ± 2.0	0.6 ± 7.5	16^{+29}_{-28}	8.7 ± 3.5	33^{+39}_{-38}	11 ± 13
D_{10} (km/s)	0.2 ± 1.5	1.9 ± 6.5	-3^{+18}_{-16}	7.9 ± 3.2	60^{+28}_{-27}	-0.1 ± 11
BG approach						
parameters	DDO 154	ESO 116-G12	ESO 287-G13	NGC 2403 2D	NGC 2841	NGC 3198 1D
R (kpc)	$2.1^{+\infty}_{-2.1} \times 10^7$	$63^{+\infty}_{-40}$	$6.7^{+\infty}_{-6.7} \times 10^7$	$4.37^{+\infty}_{-0.10} \times 10^7$	109^{+13}_{-11}	$78.9^{+12}_{-9.3}$
r_0 (kpc)	$1.18^{+0.13}_{-0.12}$	$1.79^{+0.56}_{-0.38}$	$1.308^{+0.095}_{-0.090}$	$0.706^{+0.034}_{-0.033}$	$0.31^{+0.14}_{-0.13}$	$2.01^{+0.19}_{-0.18}$
V_0 (km/s)	$58.3^{+5.1}_{-1.8}$	146^{+40}_{-19}	$191.9^{+6.2}_{-2.3}$	$141.14^{+0.77}_{-0.76}$	$345.4^{+7.1}_{-6.8}$	$197.3^{+6.8}_{-6.3}$

Table 6 – Results on χ^2 and related quantities of the CT and BG approaches. The corresponding plots are in Figure 3 [3].

Galaxy	CT (10 parameters p_i)				BG				NFW	
	$\chi^2_{\rm p}$	$\chi^2_{\rm p,red}$	χ^2	$\chi^2_{\rm red}$	$\chi^2_{\rm p}$	$\chi^2_{\rm p,red}$	χ^2	$\chi^2_{\rm red}$	χ^2	$\chi^2_{\rm red}$
DDO 154	5.93	0.12	103.56	1.73	26.46	0.45	53.29	0.89	50.42	0.87
ESO 116-G12	8.84	1.77	200.75	14.34	63.38	1.22	12.36	0.88	31.15	2.60
ESO 287-G13	13.96	0.87	358.70	14.35	37.68	1.63	2278.12	91.12	36.33	1.58
NGC 2403 2D	239.29	0.86	9200.02	32.17	275.66	0.96	17802.40	62.25	155.59	0.55
NGC 2841	58.18	0.44	23468.80	168.84	75.79	0.55	147.06	1.06	26.52	0.19
NGC 3198 1D	22.14	0.26	2918.39	31.38	59.54	0.65	3733.66	40.14	115.67	1.27

The CT approach demands much computational time than the BG ones, about 10^5 times more. Thus, an approximation for $\delta V_{\rm eN}$ was necessary. The error bars on CT approach were taken with thesame value of 4.5 km/s, which is based on the maximum error obtained form the CT approcah with 3 free parameters already presented in Figure 2. Considering that additional parameters only yield more Bessel functions with higher frequency, hence one expects that the error bars derived using ten free parameters did not differ too much from the three parameters case.

The plots in Figure (3), show for the galaxies analyzed within the CT approach, the behaviour of the effective Newtonian rotation curve, namely the grey dots in the plots, does not agree with the Newtonian circular velocity $V_{\rm N}$. One perceives, looking to the six galaxies analyzed, the $V_{\rm N}$ is too high for small radii, and becomes too low at large radii. This is a clear indication that a dark matter insertion would improve the fit. The effective

Table 7 – Results on the stellar mass-to-light ratios of the CT and BG approaches shown in comparison with the NFW profile results and the expected values from stellar population considerations. Expected values on Υ_* and NFW results are from [4, 5, 3].

Galaxy	CT (10 parameters)		BG		NFW		Expected	
	$\Upsilon_{*\mathrm{D}}$	$\Upsilon_{*\mathrm{B}}$	$\Upsilon_{*\mathrm{D}}$	$\Upsilon_{*\mathrm{B}}$	$\Upsilon_{*\mathrm{D}}$	$\Upsilon_{*\mathrm{B}}$	$\langle\Upsilon_{*\mathrm{D}}\rangle$	$\langle\Upsilon_{*\mathrm{B}}\rangle$
DDO 154	4.18	-	3.24	-	1.25	-	0.2-0.6	-
ESO 116-G12	0.80	-	0.55	-	0.05	-	0.5-1.8	-
ESO 287-G13	1.16	-	0.63	-	1.69	-	0.5-1.8	-
NGC 2403 2D	2.39	0.00	0.23	2.17	0.32	0.63	0.2-0.8	0.3-1.2
NGC 2841	1.66	0.00	0.005	0.24	0.72	1.28	0.4-1.5	0.4-1.7
NGC 3198 1D	1.07	-	0.41	-	0.51	-	0.4-1.6	-

Newtonian rotation curve is the same, but the fit of the Newtonian circular velocity V_{N} changes due the addition of a new component, namely the V_{DM}.

For BG approach, there is no systematics. But it is possible to perceive that curve V_{N} is too high at large radii which means that an addition of usual dark matter halos does not yield an improvement of the fit.

Since the CT approach uses more parameters than BG one, it is expected that the values of χ^2_{p} in Table 6 are significantly lower for the CT approach than for the BG one. A good fit with respect to the effective Newtonian rotation curve, measured by the quantity χ^2_{p}, is an indicative that the evaluated model works. It is not the most indicate for comparing models because of the number of free parameters. In this case a better option is the proper χ^2 that is the physically meaningful fit.

Table 7 shows the stellar mass-to-light ratios. The expected ranges for ESO 116-G12 and ESO 287-G13 are the same stated by Gentile [4]. The other galaxies expectations come from THINGS [5]. We considered a factor two of uncertainty to generate the stated ranges in this table [125, 126], hence the lower bound is found by dividing the expected value from [5] by two, and the upper bound by multiplying it by two. The CT approach has a tendency towards higher Υ_* values, while the BG one tends towards low Υ_* values. This indicates that, by adding a dark matter halo to these approaches, the CT one may benefit from it, achieving better agreement with the expected Υ_* values, but the BG approach cannot improve and may worsen the Υ_* concordance if the presence of dark matter is considered.

7.2 Models based on Modified gravity

We already mentioned that rotation curves constitute one of the main evidences for dark matter. This evidence is also based in the assumption that Newtonian gravity, or in other words the weak-field limit of GR, is the gravity which plays a role in the internal dynamics of those objects. Alternatively, there are some proposals which states the the

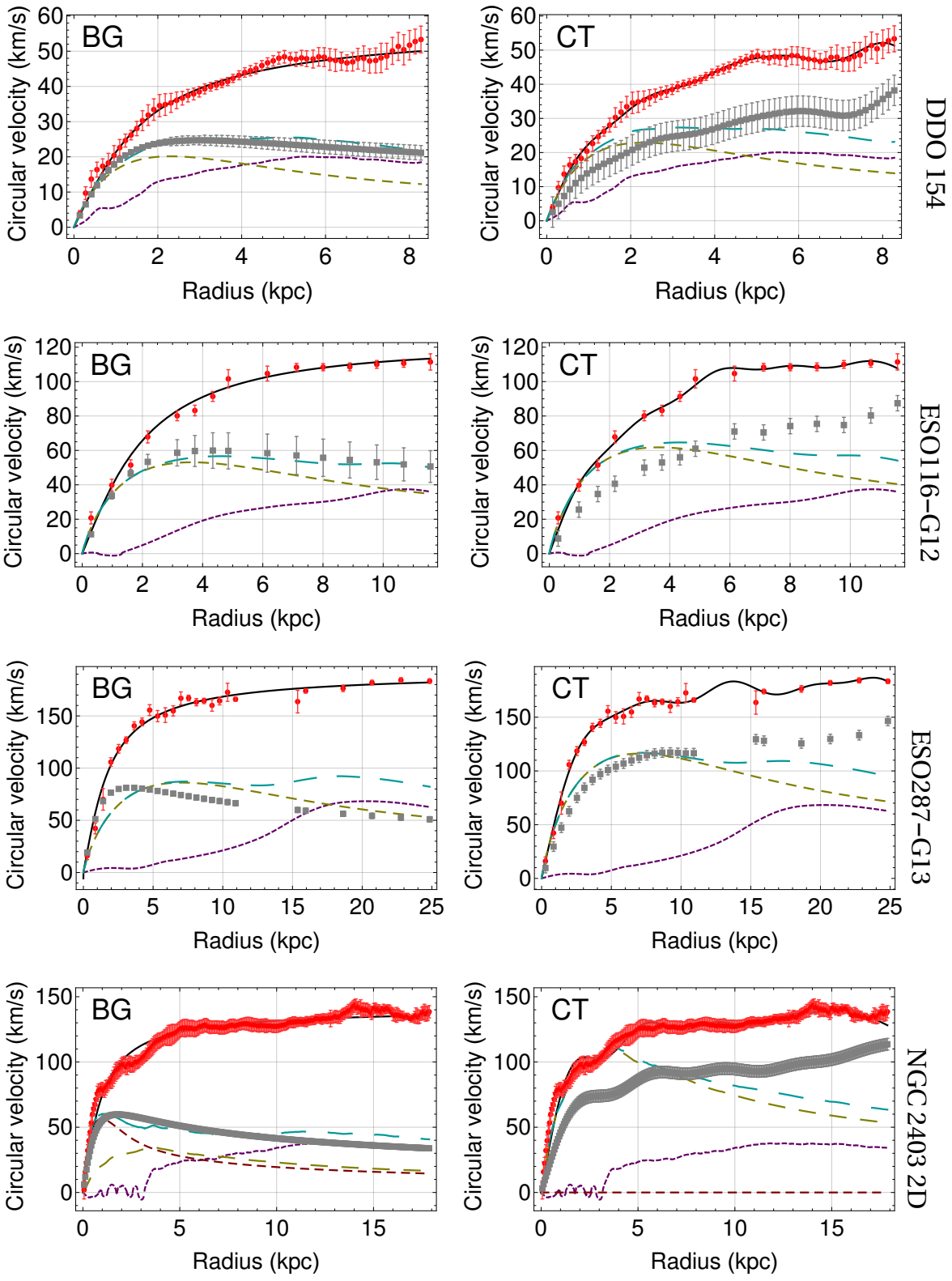

Figure 3 – Rotation curves of the galaxies DDO 154, ESO 116-G12, ESO 287-G13 and NGC 2403 2D. The plots use the same conventions of Figure 2, with the addition that the dashed dark red curve, when present, refers to the bulge circular velocity ($V_{\rm bulge}$).

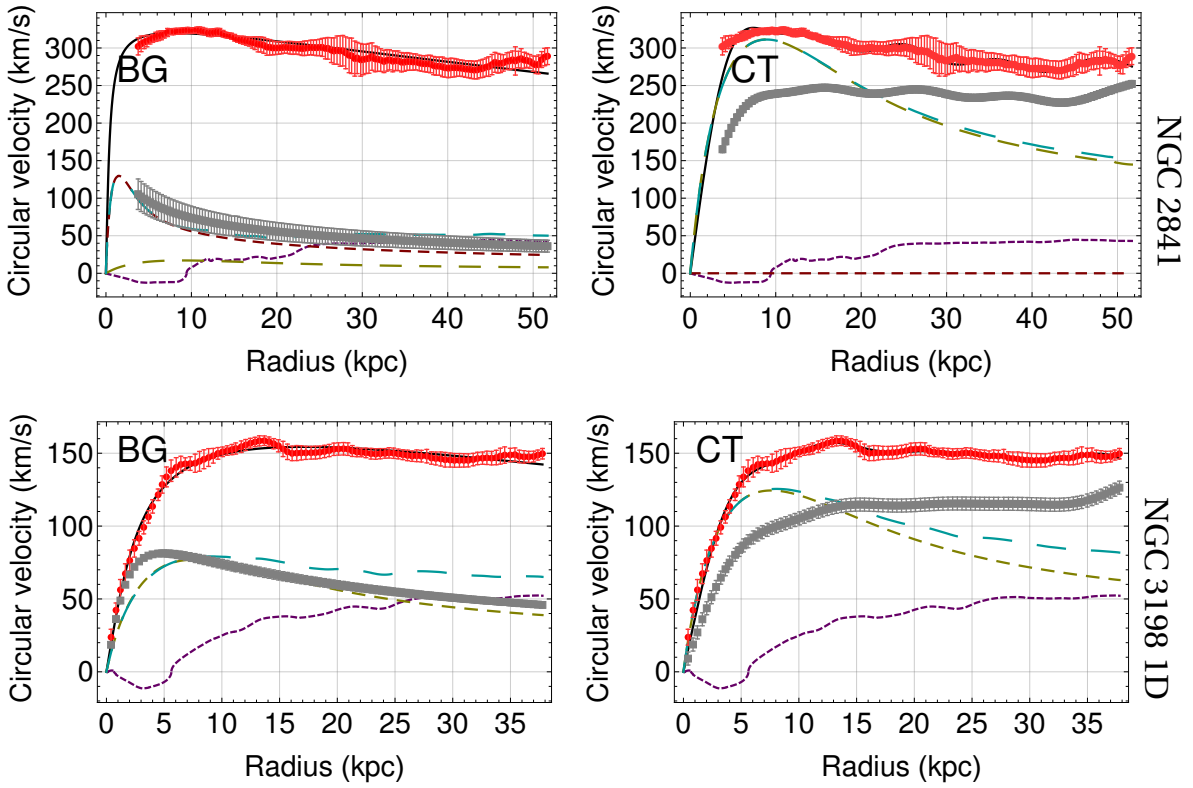

Figure 3 – Rotation curves of the galaxies NGC 2841 and NGC 3198 1D.

underlying gravity at galactic scales may be not Newtonian [127, 128, 129, 130, 20, 131, 132, 133, 134, 135, 136, 137] and instead a new material component a different gravity should be considered. In these models, when one applies the weak-field limit of relativity, the problem reduces to a modification in the Newtonian potential. Here, we worked with ones that predicts Yukawa-like corrections (as we already mentioned in Chapter 2), e.g. $f(R)$ and MOG. Namely, the Yukawa-like correction is given by

$$\Phi(\mathbf{x}) = -G \int \frac{\rho(\mathbf{x}')}{|\mathbf{x}-\mathbf{x}'|} \left(1 + \beta e^{-|\mathbf{x}-\mathbf{x}'|/\lambda}\right) d^3\mathbf{x}' \,. \tag{7.18}$$

where $\rho(x)$ is the matter density distribution. It is also common in literature to refer this extra interaction with matter as "fifth-force". The strength of the latter is measured by the parameter β while λ measures its range. As we briefly detailed in Chapter 2, many modified gravity theories predicts a Yukawa-like correction to the Newtonian potential, see for example [138, 139, 140, 131, 141, 142, 143, 144, 145, 79, 146]. Hence, according to these works this extra interaction could be mediated by scalars [141, 142, 144, 145, 146], massive vectors[138, 139, 131, 79] or even with two rank-2 tensor field[140, 143]. There are several previous works thta we need to review in order to highlight the differences with our work, for some of them the theoretical background was already clarified in Chapter 2. In [145] the sum of a repulsive and an attractive Yukawa obtained from weak-field regime of higher-order gravity model was investigated. Namely, the theory consists in by considering an extension of GR such that the Ricci scalar, in Einstein-Hilbert action, is replaced

by a general function $f(X,Y,Z)$ where $X \equiv R$, $Y \equiv R^{\alpha\beta}R_{\alpha\beta}$ and $Z \equiv R^{\alpha\beta\delta\gamma}R_{\alpha\beta\delta\gamma}$. In [145] the Yukawa parameters are not fitted, rather the authors fixed the parameter to $\lambda_1 = 100$ kpc, $\lambda_2 = 10^{-2}$ kpc, and $\beta_1 = 1/3, \beta_2 = -4/3$, claiming that these values provide a good fit for rotation curve of Milky Way and to NGC 3198. Although, they also conclude that only baryons which obey the effective potential induced by $f(X,Y,Z)$ is not sufficient to reproduce entirely the behaviour of galaxy rotation curves, hence some amount of dark matter is still necessary. Conversely, in [138] (see also [146]) repulsive Yukawa correction could reproduce constant profiles for rotation curves ar large radii without the necessity of dark matter with fifth-force parameters $-0.95 \leq \beta \leq -0.92$ and $\lambda \simeq 25 - 50$ kpc.

In the sense of [138], one has to mention [140, 145] that are works which do not consider dark matter at all but apply the prediction only to two or one galaxy. However, in [79] one finds a full comparison of MOG theory (see Section 2.4) against nine observed rotation curves from THINGS. It was assumed that β and λ could vary galaxy by galaxy and in the end they computed the average values: $\beta = -0.899 \pm 0.003$ and $\lambda = 23.81 \pm 2.27$ kpc. Finally, they used the latter values to fit the THINGS and the Ursa Major catalogue. The THINGS was also used in [147] for an analysis of nonlocal gravity and the values are very similar: $\beta = -0.916 \pm 0.041$ and $\lambda = 16.95 \pm 8.04$ kpc, again without dark matter.

The case of an attractive fifth force, i.e. positive values for β, were analyzed in a few works. In [148], in the context of ST theories, only Low Surface Brightness galaxies were analyzed. Restricting to only positives values for β in the fit, values from 1.83 to 11.67 were found, while the λ values ranged from 0.349 kpc to 75.810 kpc. On the other hand, in the context of $f(R)$ theories [144], the value of β was kept fixed to 1/3 according $f(R)$ predictions. The derived Yukawa correction to the Newtonian potential, equation (2.15), was investigated in comparison with simulated datasets of galaxy rotation curves. It is importante to emphasize that a strength $\beta = 1/3$ has been found to be compatible also with the dynamics of clusters [149], again without dark matter.

Our work also considers the inclusion of dark matter and is closer in spirit to [150]. There, it was found that a repulsive Yukawa between baryons and dark matter provides a good fit for LSB galaxies, namely UGC 4325, β=-1.0 ± 0.25 and λ=1.7 ± 0.6 kpc; NGC 3109, β=-1.1 ± 0.16 and λ=1.2 ± 0.17 kpc; LSBC F571-8, β=-0.9 ± 0.18 and λ=1.1 ± 0.1 kpc; NGC 4605, β=-1.1 ± 0.3 and λ=0.2 ± 0.02 kpc. In [150], due the fact that only LSB were analyzed it was not used the baryonic component, since the LSD typically are dominated by dark matter, and the dark matter halo was taken as a simple power law.

As in [150] we have constrained β and λ against galaxy rotation curve data. However, our analysis in [31] differs itself from most previous works because i) we considered dark matter; ii) we did not impose restrictions on the coupling sign and we assumed that baryons and dark matter couples differently to fifth-force iii) we included the baryons, i.e.

gas, disk and bulge for each galaxy together with a NFW dark matter halo; iv) we did not fit β, λ individually to each galaxy, but rather look for a global fit, and finally, v) we have used a much larger dataset, namely 40 galaxies from SPARC.

7.2.1 A species-dependent coupling

If we are considering that the fifth-force couples differently to dark matter (subscript dm) and baryons (b), one has to introduce two coupling constants, namely α_b and α_{dm}. In order to pedagogial, we will assume for now that the fifth-force is carried by a scalar field with conformal coupling and canonical kinetic term. As it was already seen in Chapter 1 the geodesic equation can be derived via energy-momentum conservation. As already discussed in Chapter 2 the presence of fifth force alters the standard geodesic equation, hence for each component here, that is, dark matter and baryons the geodesic equation is of the form

$$T^{\mu}_{(b)\nu;\mu} = -\alpha_b T_{(b)}\phi_{;\nu} \tag{7.19}$$

$$T^{\mu}_{(dm)\nu;\mu} = -\alpha_{dm} T_{(dm)}\phi_{;\nu} \tag{7.20}$$

where $T^{\mu}_{(x)\nu}$ is the energy-momentum tensor of component x and $T_{(x)}$ its trace. The equation for the scalar field is the Klein-Gordon equation which can be written as follows

$$T^{\mu}_{(\phi)\nu;\mu} = (\alpha_b T_{(b)} + \alpha_{dm} T_{(dm)})\phi_{;\nu} \tag{7.21}$$

Note that the total energy-momentum tensor is clearly conserved.

In the context of quasi-static approximation, that is, when we do not consider the propagation of ϕ-waves, the total potential between two particles of species x, y acquires a a Yukawa term as in equation (7.18) with strenght [151, 152, 150]

$$\beta = \alpha_x \alpha_y \tag{7.22}$$

and a universal range $\lambda = m^{-1}$, where m is the scalar field mass. As we discussed in Chapter (5), in a galaxy the baryons which follows rotation curves feel the sum of the potential determined by the baryons themselves and by dark matter. Consequently, baryons feel a fifht force from baryon-baryon interaction and baryon-dark matter one. The first interaction is chacterized by α_b^2, while while the second one to $\alpha_b \alpha_{dm}$. However, the local tests of gravity show that $|\alpha_b|$ has to be very small, typically less than 10^{-2} [153, 154]. Thus, one can neglect the baryon-baryon interaction, that is, only assume that baryons exert standard gravity on the others baryons. Therefore, this means that the Yukawa strength coupling is $\beta = \alpha_b \alpha_{dm}$ and along with the parameter λ one wishes determine using galaxy rotation curves.

In many previoues works, as we pointed out in the previous section, the dark matter component was not considered. Hence, according the interpretation given above, what

they measured was the baryon-baryon strength, namely $\beta = \alpha_b^2$. The values for the latter parameters, provided by fiiting the rotation curves, were negative. Thus, one has to modify the picture mentioned above by introducing a non-canonical kinectic term (actually, a field with imaginary sound speed, which then suffers of a gradient instability), or a vector boson rather than a scalar one. Anyway, a value a value $|\alpha_b|$ of order unity is in contradiction with local gravity experiments. The only way to circumvent this is to assume that the fifth force is screened on Earth experiments while stars are not.

7.2.2 The Yukawa correction

The general form for Yukawa-like corrections to the Newtonian potential is given by

$$\Phi(\mathbf{x}) = -G \int \frac{\rho(\mathbf{x}')}{|\mathbf{x}-\mathbf{x}'|} \left(1 + \beta e^{-|\mathbf{x}-\mathbf{x}'|/\lambda}\right) d^3\mathbf{x}' \,. \tag{7.23}$$

Note thar we recover Newtonian gravity by setting $\beta = 0$, or at scales much larger than λ. In scales much smaller than λ, gravity could be stronger or weaker than Newtonian, depending on the sign of β, that we considered as a free parameter.

As we mentioned in Section 7.2 we will consider the dark matter component in our analysis. Hence, we have to choose a specific dark matter profile in order to proceed with the analysis. Thus, we will assume a dark matter profile derived from N-body simulations of cold dark matter, the NFW profile

$$\rho_{\rm NFW}(r) = \frac{\rho_s}{\frac{r}{r_s}(1+\frac{r}{r_s})^2} \,, \tag{7.24}$$

where ρ_s is the characteristic density and r_s is the scale radius. The N-body simulations claims that there is a relation between ρ_s and r_s [155, 156]. Usually, this relation is written in terms of the concentration parameter $c \equiv r_{200}/r_s$ and $M_{200} \equiv (4\pi/3)200\rho_{\rm crit} r_{200}^3$, where $\rho_{\rm crit}$ is the critical density. Hence, using the latter parameters it is possible to write the NFW profile depending on a single parameter, namely M_{200}. The relation between $(\rho_s, r_s) \to (c, M_{200})$ is given by [92]

$$\rho_s = \frac{200}{3} \frac{c^3 \rho_{\rm crit}}{\ln(1+c) - \frac{c}{1+c}} \,, \tag{7.25}$$

$$r_s = \frac{1}{c} \left(\frac{3M_{200}}{4\pi 200 \rho_{\rm crit}}\right)^{1/3} \tag{7.26}$$

For the galaxies analyzed in [31], it was assumed a $c - M_{200}$ relation[155]

$$c(M_{200}) = 10^{0.905} \left(\frac{M_{200}}{10^{12} h^{-1} \mathrm{M}_\odot}\right)^{-0.101} \,. \tag{7.27}$$

Hence, the equation (7.26) becomes

$$r_s \approx 28.8 \left(\frac{M_{200}}{10^{12} h^{-1} \mathrm{M}_\odot}\right)^{0.43} \mathrm{kpc} \,, \tag{7.28}$$

where we used $\rho_{\rm crit} = 143.84\ {\rm M}_\odot/{\rm kpc}^3$ and $h = 0.671$[157].

Therefore, inserting the equation (7.24) in equation (7.23) one can split the total gravitational potential as the usual Newtonian potential for NFW profile, namely $\Phi_{\rm NFW}$, plus the contribution coming from modified gravity $\Phi_{\rm mg}$ ($\propto \beta$). The latter can be integrated analytically for NFW [158]

$$\Phi_{\rm mg}(r) = \frac{2\pi G\beta\rho_s r_s^3}{r}\left\{ \exp\left(-\frac{r_s+r}{\lambda}\right)\left[{\rm Ei}\left(\frac{r_s}{\lambda}\right) - {\rm Ei}\left(\frac{r_s+r}{\lambda}\right)\right] + \right.$$
$$\left. - \exp\left(\frac{r_s+r}{\lambda}\right){\rm Ei}\left(-\frac{r_s+r}{\lambda}\right) + \exp\left(\frac{r_s-r}{\lambda}\right){\rm Ei}\left(-\frac{r_s}{\lambda}\right)\right\}, \tag{7.29}$$

where ${\rm Ei}(x)$ is defined as

$${\rm Ei}(x) = -\int_{-x}^{\infty}\frac{e^{-t}}{t}dt\ . \tag{7.30}$$

Hereafter, we will refer the parameterization which consider gas, disk, bulge plus NFW for dark matter profile (using the mass-concentration relation) as the "standard model" and the same parametrization plus a Yukawa term as simply Yukawa model.

7.2.3 Analysis with SPARC dataset

The observed rotation curve used in [31] to evaluate Yukawa-like corrections are taken from SPARC [107]. The details about this catalogue were already reported in subsection 5.2. To evaluate the contribution of Yukawa corrections in kinematics of disk galaxies, we have to use the total circular velocity, equation (5.6), adding now the contribution form modified gravity, hence we have the following formula

$$V_c^2(r) = V_{\rm gas}^2(r) + \Upsilon_{*\rm D}V_{\rm disk}^2(r) + \Upsilon_{*\rm B}V_{\rm bulge}^2(r) + V_{\rm NFW}^2(r) + V_{\rm mg}^2(r)\ , \tag{7.31}$$

The velocities $V_{\rm gas}, V_{\rm disk}$ and $V_{\rm bulge}$ are actually available in astroweb.cwru.edu/SPARC. But as an example we show in Table 8 the details of each baryonic component. The details about how each component was derived is already commented in subsection 5.2 and for further details the reader is invited to read [107]. For practical purposes in the derivation of $V_{\rm disk}$ and $V_{\rm bulge}$, [107] assumed $\Upsilon_{*\rm D} = \Upsilon_{*\rm B} = 1$. This normalization is very useful since we just need to rescale the problem inserting $\Upsilon_{*\rm D}, \Upsilon_{*\rm B}$ as free parameters in our case.

We are considering that baryons obey standadr gravity, thatis, there is no fifth force between baryon-baryon. Thus, the procedure performed by [107] can be adapted to our purpose directly. Therefore, one can capture the functions $V_{\rm gas}(r), V_{\rm disk}(r)$ and $V_{\rm bulge}(r)$ just using a cubic spline interpolation.

The components $V_{\rm NFW}$ and $V_{\rm mg}$ are given by

$$V_{\rm NFW}^2(r) = \frac{4\pi G r_s^3\rho_s}{r}\left[-\frac{r}{r+r_s} + \ln\left(1+\frac{r}{r_s}\right)\right] \tag{7.32}$$

Table 8 – Table for the galaxy UGCA442 emphasizing each baryonic component (there is no bulge in this galaxy). $\Sigma_{\rm disk}$ is the surface density for the disk.

Radius (kpc)	$V_{\rm obs}$ (km s^{-1})	$V_{\rm gas}$ (km s^{-1})	$V_{\rm disk}$ (km s^{-1})	$\Sigma_{\rm disk}$ ($L_\odot$pc^{-2})
0.42	14.2 ± 1.9	4.9	4.8	11.0
1.26	28.6 ± 1.8	13.1	10.8	5.8
2.11	41.0 ± 1.7	19.6	13.6	2.7
2.96	49.0 ± 1.9	22.4	13.3	1.0
3.79	54.8 ± 2.0	22.8	12.6	0.7
4.65	56.4 ± 3.1	21.4	12.3	0.4
5.48	57.8 ± 2.8	18.7	12.0	0.2
6.33	56.5 ± 0.6	16.7	10.6	0.0

and

$$V^2_{\rm mg}(r) = -\frac{2\pi G\beta\rho_s r_s^3}{r}\left\{\frac{2r}{r_s+r} + \exp\left(\frac{r_s+r}{\lambda}\right)\left(\frac{r}{r_s}-1\right)\mathrm{Ei}\left(-\frac{r_s+r}{\lambda}\right) + \exp\left(-\frac{r_s+r}{\lambda}\right) + \right.$$
$$\left. + \exp\left(-\frac{r_s+r}{\lambda}\right)\left(1+\frac{r}{\lambda}\right)\left[\exp\left(\frac{2r_s}{\lambda}\right)\mathrm{Ei}\left(-\frac{r_s}{\lambda}\right) + \mathrm{Ei}\left(\frac{r_s}{\lambda}\right) - \mathrm{Ei}\left(\frac{r+r_s}{\lambda}\right)\right]\right\}. \tag{7.33}$$

7.2.4 Fitting the rotation curves

The procedure that we used in [31] in order to find the best-fit values for the free parameters, namely $\{\Upsilon_{*\rm D}, \Upsilon_{*\rm B}, M_{200}\}$ for each galaxy plus $\{\beta, \lambda\}$, is the ML estimation (already detailed in Chapter 6). It is considered that the errors of the observed rotation curves follows a Gaussian distribution, so that one can build the likelihood for each galaxy according the following expression

$$\mathcal{L}_j(p_j, \beta, \lambda) = (2\pi)^{-N/2}\left\{\prod_{i=1}^{N}\sigma_i^{-1}\right\}\exp\left\{-\frac{1}{2}\sum_{i=1}^{N}\left(\frac{V_{{\rm obs},j}(r_i) - V_c(r_i, p_j, \beta, \lambda)}{\sigma_i}\right)^2\right\} \tag{7.34}$$

where $p_j = \{\Upsilon_{*{\rm D},j}, \Upsilon_{*{\rm B},j}, M_{200,j}\}$,$N$ is the number of observational points for each galaxy, σ_i is the data error, $V_{{\rm obs},j}(r_i)$ is the observed circular where $p_j = \{\Upsilon_{*{\rm D},j}, \Upsilon_{*{\rm B},j}, M_{200,j}\}$,$N$ is the number of observational points for each galaxy, σ_i is the data error, $V_{{\rm obs},j}(r_i)$ is the observed circular velocity of the j-th galaxy at the radius r_i and $V_c(r_i, p_j, \beta, \lambda)$ is the total rotation curve, which was expressed in equation (7.31). The values of $V_{{\rm obs},j}(r_i)$ are provided by SPARC catalogue. AS already commented, we are considering β and λ as global parameters hence in order to constrain them with respect to some set of galaxies one needs to consider an overall likelihood which can be obtained just multiplying the individual galaxy likelihoods. Therefore, the full likelihood is given by

$$\mathcal{L}(\mathbf{p}, \beta, \lambda) = \prod_{j=1}^{N_g}\mathcal{L}_j(p_j, \beta, \lambda)\ , \tag{7.35}$$

where $\mathbf{p} = \{p_1, ..., p_{N_g}\}$ and N_g is the total number of galaxies.

The Bayes theorem, equation (6.4) estabilsh that the posterior distribution is proportional to likelihood time the prior. In [31] we considered flat (uniform) prior for the parameters. That is, the mass-to-light ratios, for bulge and disk, are bounded to $0.3 < \Upsilon_{*\mathrm{D}} < 0.8$ and $0.3 < \Upsilon_{*\mathrm{B}} < 0.8$, which is in agreement with SPS models [159, 160]. For the other parameters, that is, M_{200}, β and λ a wide range is considered: $10^9 < M_{200}/\mathrm{M}_\odot < 10^{14}$, $-2 < \beta < 2$ and $\overline{\lambda}_0 < \lambda/\mathrm{kpc} < 100$, where $\overline{\lambda}_0$ is the mean value among the smallest observable radii when the N_g galaxies are considered. We imposed a lower limit on λ in order to avoid undesired divergences when $\lambda \to 0$.

In order to find the ML estimators for the set of free parameters, we used sampling methods for exploring the parameter space, in particular MCMC methods. We used the affine-invariant ensemble sampler designed by [117], which is implemented by the very well tested and stable open-source Python package `emcee`[1]. This sampling method offers several advantages over traditional samplers, e.g. Metropolis-Hastings [114], among the advantages are: high performance and few hand-tunning in the parameters.

7.2.5 Analysis and results

The SPARC catalogue contains 175 galaxies, therefore a complete analysis would require 384 free parameters, that is, 175 $\Upsilon_{*\mathrm{D}}$ plus 175 M_{200} plus 32 $\Upsilon_{*\mathrm{B}}$(many galaxies do not show a bulge) plus β and λ. Even considering the affine-invariant ensemble sampler, the number of parameters, for the entire SPARC catalogue, is too high and the computation of the likelihood becomes discouraging. Hence, we decided to analyse randomly 4 sets containing 10 galaxies each. Therefore, for two sets, namely B and D, one has 25 free parameters each, while the sets A and B one has 23 free parameters each.

As we have already emphasized early, in Chapter 6, the issue of the convergence is crucial for any MCMC performance. The strategy that we used for convergence of the chains was the autocorrelation time (for details, please see Section 6.2 or in [119]). Remembering the reader that the autocorrelation time ($\hat{\tau}$) is the quantity which defines the minimum number of posterior samplings necessary for producing independent samples.

In Figure 4, we shown autocorrelation time estimations (τ_{est}) versus the number of samples, each blue dot in Figure 4 is a evaluation of equation (6.18) for a certain number of samples N. We started with $N \ll M$ where M is the total length of the chain. We increased the chains until to perceive a plateau, the latter gives to us a number, the autocorrelation time $\hat{\tau}$. After obtaining $\hat{\tau}$ we discard the number of iteractions $N_{\mathrm{disc}} \sim \hat{\tau}$ and we compute the posterior for each free parameter in our galaxy sets considering the remaining chain. The developers of `emcee` suggests that a chain with total length $M = 50\hat{\tau}$ is sufficient for generating independent samples. We tested this hypothesis running again a MCMC routine considering now a shorter chain, namely $M = 70\hat{\tau}$ and $N_{\mathrm{disc}} = \hat{\tau}$, and indeed the results did not change. With respect to the acceptance ratio of `emcee`, in our

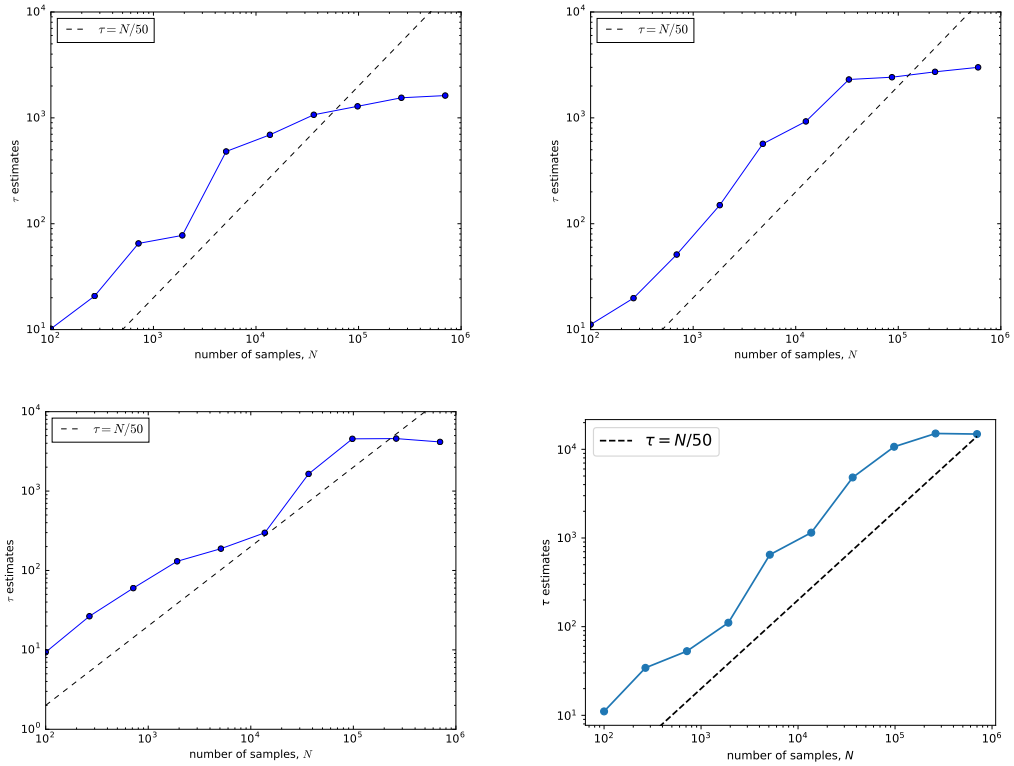

Figure 4 – The autocorrelation time analysis (blue solid line) for each set of galaxies respectively containing 10 objects each. When τ reaches the dotted line the convergence of the chains is achieved, see [1].

Table 9 – The acceptance fraction a_f, the maximum likelihood estimation for (β, λ), the total goodness of fit $\chi^2_{\rm red,tot}$ and the one calculated fixing $\beta = 0$, for each set of 10 galaxies and for the combination of the data sets. $k_{\rm Y}$ ($k_{\rm sg}$) is the number of free parameters for the Yukawa model (for standard gravity), while N is the number of data points. We also report the values for the ΔBIC, for $2\log B_{12}$, and the confidence level (CL), see text for more details.

Set	a_f	Best-fit values		$k_{\rm Y}$	$\chi^2_{\rm red,tot}$	$k_{\rm sg}$	$\chi^2_{\rm red,tot}\vert_{\beta=0}$	N	ΔBIC	$2\log B_{12}$	CL
		β	λ(kpc)								σ
A	0.16	$0.34^{+0.12}_{-0.10}$	$10.27^{+2.89}_{-3.82}$	25	0.88	23	1.11	206	32.18	31.84	5.29
B	0.14	0.30 ± 0.08	$7.42^{+2.94}_{-3.99}$	23	0.80	21	0.96	180	17.12	23.21	4.44
C	0.12	$0.28^{+0.09}_{-0.08}$	$8.18^{+5.39}_{-6.31}$	25	0.83	23	1.04	163	20.52	12.41	3.09
D	0.15	$0.54^{+0.11}_{-0.10}$	$4.15^{+0.81}_{-0.95}$	23	0.78	21	1.02	196	32.92	20.38	4.12
Combined	-	0.34 ± 0.04	5.61 ± 0.91	90	0.82	88	1.03	745	91.61	87.83	8.26

analysis we obtained values between 0.1 and 0.2 as can be seen in Table 9.

Furthermore, the main results are displayed in Table 9. There, we show the ML estimations for the (β, λ) and their 1σ error bars, the acceptance fraction a_f and the overall goodness of fit $\chi^2_{\rm red,tot}$, that is, considering all galaxies of the same set together. Note that there is an inprovement of χ^2 from the standard model to the Yukawa one for each set and also for the combination of all sets. The total data, that is, summing all data points in the case of the combined analysis is 745 while the number of free parameters is 90. Namely, 40 $\Upsilon_{*\rm D}$ plus 40 M_{200} plus 8 $\Upsilon_{*\rm B}$ plus β and λ. Hence, a total of 655 degrees of freedom.

In Table 10 we show the ML estimations for the set of parameters $\{\Upsilon_{*\rm D}, \Upsilon_{*\rm B}, M_{200}\}$ and their respective 1σ error bars and also the goodness of fit $\chi^2_{\rm red}$. In Table 11 we have the same results but for the standard model, that is $\beta = 0$.

In Figure 5 we plotted, for each galaxy set, the marginalized distribution for the parameters (β, λ) and the respective 1σ and 2σ contours and also one-dimensional PDF for β and λ. At last, the rotation curves for each galaxy according equation (7.31), with the ML estimations (best-fit values) displayed in Tables 10 and 9 are plotted in Figures 7,9,11 and 14. In the end, the combined posterior on β and λ is obtained just multiplying the narginalized posteriors of each set, the combined result is also shown in Figure 5. The global best-fit for the parameters β and λ along with 1σ error bars are also displayed on Table 9.

Our results show an attractive Yukawa force, consequently a reduction in the amount of dark matter for reproducing galaxy rotation curves is clearly expected. We quantified this decreasing computing the quantity $\mu_{200} \equiv \frac{M_{200}}{M_{200(\beta=0)}}$ whoose values are plotted in Figure 6. In order to quantify the uncertainty in μ_{200} we propagated errors using the largest value of the asymmetric errors bars. We quantified the ratios for the other parameters $\Upsilon_{*\rm D}$ and $\Upsilon_{*\rm B}$, namely $\gamma_{*\rm D} \equiv \frac{\Upsilon_{*\rm D}}{\Upsilon_{*\rm D}(\beta=0)}$ and $\gamma_{*\rm B} \equiv \frac{\Upsilon_{*\rm B}}{\Upsilon_{*\rm B}(\beta=0)}$. Because of the asymmetry of the error bars of $\Upsilon_{*\rm D}$ and $\Upsilon_{*\rm B}$ we proceed of the same manner than in μ_{200} for finding the uncertainties on the ratios$\gamma_{*\rm D}$ and $\gamma_{*\rm B}$. The average values for the ratios are:$\langle\mu_{200}\rangle = 0.80 \pm 0.02$, corresponding to a 20% of reduction of dark matter due the fifth force. We also obtained the average values $\langle\gamma_{*\rm D}\rangle = 0.96 \pm 0.01$ and $\langle\gamma_{*\rm B}\rangle = 0.96 \pm 0.04$.

It is important to note that the counting of degrees of freedom described above is actually ambiguous. Indeed, data are not compared only to a theoretical model depending on some free parameters, instead, they are compared to the combination of a theoretical model (the NFW profile) plus the observed baryonic component, rescaled by the mass-to-light ratios. Because of this, we have to use the Bayesian approach in order to arises in fact the difference between the models. In particular, we have to compute the *evidence*, equation (6.5), and in this case the only difference which matter is the presence or not of

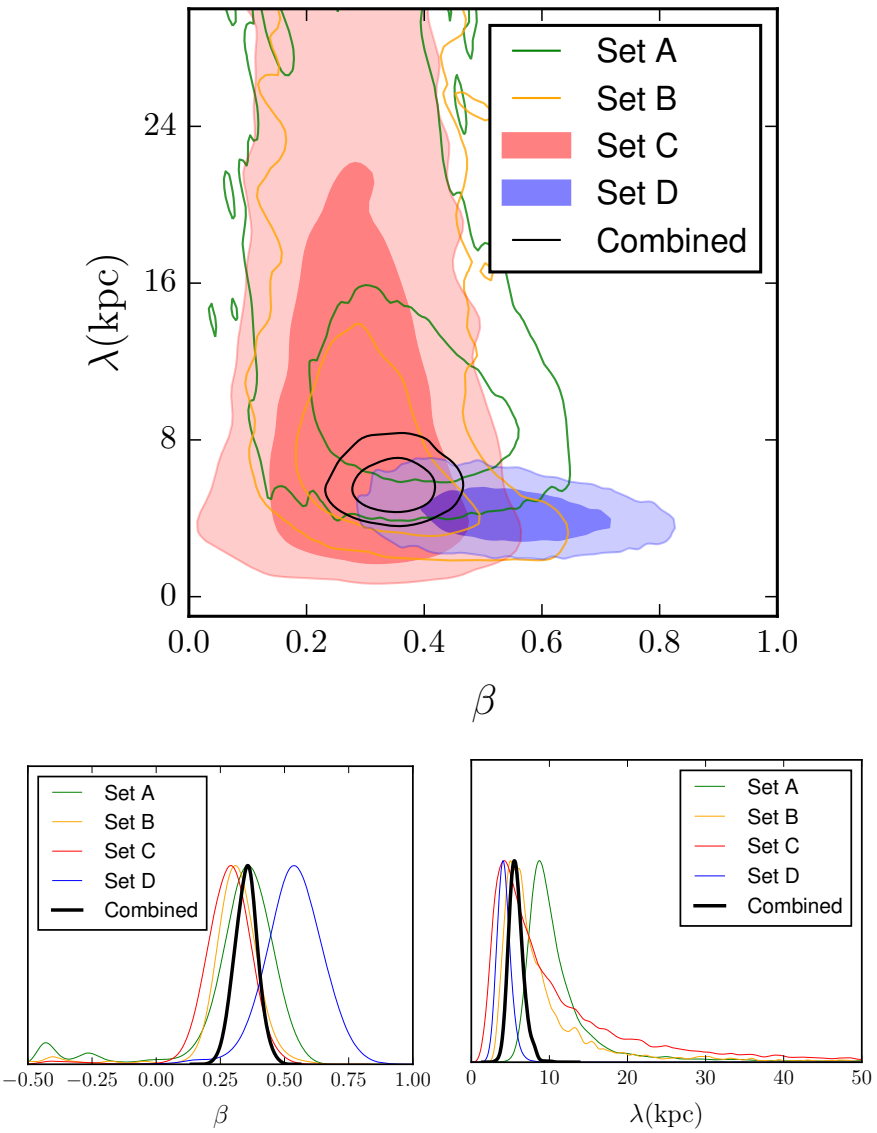

Figure 5 – The marginalized distribution of the (β, λ) and the one-dimensional posterior distribution according the set of 10 galaxies each and the combined analysis.

the Yukawa term. Now, particularizing the equation (6.5) for our case one has

$$E = \int \mathcal{L}(\mathbf{p}, \beta, \lambda)\mathcal{P}(\mathbf{p}, \beta, \lambda) d\beta d\lambda d\mathbf{p} \ , \tag{7.36}$$

where $\mathcal{P}$ is the prior distribution. The Bayes ratio between the model 1 ($\beta \neq 0$) and model 2 ($\beta = 0$) is defined as

$$B_{12} = \frac{\int \mathcal{L}_1(\mathbf{p}, \beta, \lambda)\mathcal{P}_1(\mathbf{p}, \beta, \lambda) d\beta d\lambda d\mathbf{p}}{\int \mathcal{L}_2(\mathbf{p})\mathcal{P}_2(\mathbf{p}) d\mathbf{p}} \ . \tag{7.37}$$

The expression above can be computed analitically is one considers both likelihood and priors as Gaussian *in the parameters*. Considering this, the evidence becomes

$$E = \mathcal{L}_{\max} \sqrt{\frac{\det \mathbf{P}}{\det \mathbf{Q}}} \exp\left[-\frac{1}{2} (\hat{\theta}_\alpha F_{\alpha\beta} \hat{\theta}_\beta + \bar{\theta}_\alpha P_{\alpha\beta} \bar{\theta}_\beta - \tilde{\theta}_\alpha Q_{\alpha\beta} \tilde{\theta}_\beta) \right] \ , \tag{7.38}$$

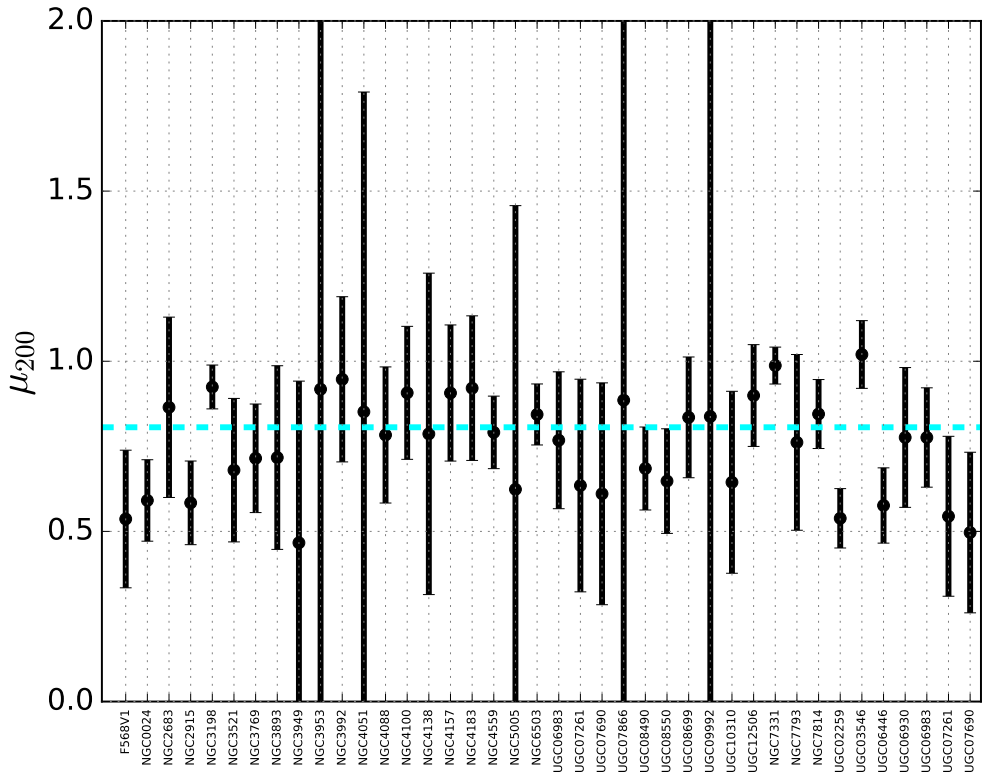

Figure 6 – The ratio μ_{200} (black dots) and the respective error bars. The cyan dotted line is the average value of μ_{200}.

where $-2\ln\mathcal{L}_{\max} = \chi^2_{\min}$, $\theta_\alpha = \{\mathbf{p}, \beta, \lambda\}$ for our general case; $\hat{\theta}_\alpha$ are the best fit values for the parameters and $\bar{\theta}_\alpha$ are the prior means. The matrix $\mathbf{Q}$ is $\mathbf{Q} = \mathbf{F} + \mathbf{P}$ and $\tilde{\theta}_\alpha = (\mathbf{Q}^{-1})_{\alpha\beta}[F_{\beta\sigma}\hat{\theta}_\sigma + P_{\beta\sigma}\bar{\theta}_\sigma]$, where $\mathbf{F}$ is the Fisher matrix and $\mathbf{P}$ is the inverse of the covariance matrix of the prior. In our case, the prior is weak hence the exponetial term in the last equation becomes to unity. Thus, the Bayes ratio becomes

$$B_{12} = e^{-\frac{1}{2}(\chi^2_{\min,1} - \chi^2_{\min,2})}\sqrt{\frac{\det\mathbf{P}_1 \det\mathbf{F}_2}{\det\mathbf{P}_2 \det\mathbf{F}_1}}\ . \tag{7.39}$$

If one assumes that the prior is uncorrelated, that is, the matrix $\mathbf{P}$ is diagonal consequently the determinant is the product of diagonal elements which are the inverse of the squared errors. In our case, the prior is flat hence one considers the variance of an uniform distribution as squared error. The model 1,2 shares most of the parameters hence the ratio $\det\mathbf{P}_1/\det\mathbf{P}_2$ all terms simplify except the β, λ. Hence the equation (7.39) becomes

$$B_{12} = e^{-\frac{1}{2}(\chi^2_{\min,1} - \chi^2_{\min,2})}\frac{1}{p_\beta p_\lambda}\sqrt{\frac{\det\mathbf{F}_2}{\det\mathbf{F}_1}}\ , \tag{7.40}$$

where p_β, p_λ are the square root of the variance of the uniform distribution assumed for β, λ.

In the combined analysis, the total Fisher matrix $\mathbf{F}_{\rm comb}$, i.e. considering the combination of the Fisher matrices of all sets, is just a block diagonal matrix, since there is no

correlation between the sets, where the diagonal entries are the Fisher matrices of each set. Hence, it is imediat to calculate the determinant of $\mathbf{F}_{\rm comb}$ for models 1 and 2. We assumed the same procedure described above for the combined prior matrix $\mathbf{P}_{\rm comb}$, since the minimum value λ_0 changes according to the set.

By having B_{12}, the probability $\mathcal{P}_{12}$ that the right model is 1 rather than 2 is

$$\mathcal{P}_{12} = \frac{B_{12}}{1 + B_{12}} \, . \tag{7.41}$$

As a complement, we computed the Bayesian Information Criterion (BIC), which is a Gaussian approximation to the evidence when the sample size is large. The expression for BIC is given by [161]

$$\mathrm{BIC} = -2 \ln \mathcal{L}_{\rm max} + 2k \ln N \, , \tag{7.42}$$

where k is the number of free parameters and N is the number of data points. The values of k for both models, namely $k_{\rm Y}$ for the Yukawa model and $k_{\rm sg}$ for standard gravity, are displayed in table 9 also with the number of data points N used in each set and in the combined analysis. In our case, the likelihoods are Gaussian and hence we have again $-2 \ln \mathcal{L}_{\rm max} = \chi^2_{\rm min}$. The relative BIC ($\Delta$BIC) is defined as

$$\Delta\mathrm{BIC} \equiv \mathrm{BIC}|_{\beta=0} - \mathrm{BIC}|_{\beta\neq 0} \, . \tag{7.43}$$

The ΔBIC and the confidence level (CL) associated to $\mathcal{P}_{12}$ values for each set and for the combined analysis are reported in Table 9. Expectedly, the BIC gives a rough approximation to the Gaussian evidence. Both prefer the $\beta \neq 0$ model to an extremely high significance, more than 8σ for the combined set.

Table 10 – The maximum likelihood estimation for the $\Upsilon_{*\mathrm{D}}$,$\Upsilon_{*\mathrm{B}}$ and M_{200} parameters, and the goodness of fit χ^2_{red} for each galaxy, for the Yukawa model.

Set	Galaxy	Best-fit values			χ^2_{red}
		$\Upsilon_{*\mathrm{D}}$	$\Upsilon_{*\mathrm{B}}$	$M_{200}(10^{11}M_{\odot})$	
A	F568V1	$0.60^{+0.20}_{-0.10}$	-	$1.31^{+0.26}_{-0.38}$	0.35
A	NGC0024	$0.79^{+0.01}_{-0.01}$	-	$0.73^{+0.10}_{-0.13}$	1.68
A	NGC2683	$0.64^{+0.04}_{-0.04}$	$0.52^{+0.15}_{-0.21}$	$1.71^{+0.29}_{-0.37}$	1.37
A	NGC2915	$0.32^{+0.01}_{-0.02}$	-	$0.34^{+0.05}_{-0.06}$	0.98
A	NGC3198	$0.40^{+0.04}_{-0.05}$	-	$1.94^{+0.13}_{-0.12}$	1.31
A	NGC3521	$0.49^{+0.01}_{-0.02}$	-	$5.40^{+1.00}_{-1.26}$	0.37
A	NGC3769	$0.33^{+0.02}_{-0.03}$	-	$0.86^{+0.11}_{-0.14}$	0.75
A	NGC3893	$0.46^{+0.04}_{-0.04}$	-	$3.89^{+1.16}_{-1.00}$	1.26
A	NGC3949	$0.36^{+0.03}_{-0.05}$	-	$3.99^{+2.09}_{-2.78}$	0.45
A	NGC3953	$0.62^{+0.07}_{-0.07}$	-	$1.53^{+0.74}_{-1.27}$	0.73
B	NGC3992	$0.74^{+0.05}_{-0.03}$	-	$6.52^{+0.92}_{-1.52}$	0.88
B	NGC4051	$0.40^{+0.05}_{-0.10}$	-	$1.04^{+0.50}_{-0.79}$	1.27
B	NGC4088	$0.31^{+0.01}_{-0.01}$	-	$1.63^{+0.30}_{-0.33}$	1.09
B	NGC4100	$0.67^{+0.03}_{-0.03}$	-	$2.12^{+0.34}_{-0.37}$	1.20
B	NGC4138	$0.69^{+0.09}_{-0.05}$	$0.53^{+0.10}_{-0.21}$	$1.43^{+0.45}_{-0.65}$	2.67
B	NGC4157	$0.35^{+0.02}_{-0.03}$	$0.45^{+0.09}_{-0.15}$	$3.35^{+0.59}_{-0.58}$	0.76
B	NGC4183	$0.49^{+0.09}_{-0.14}$	-	$0.59^{+0.10}_{-0.11}$	0.19
B	NGC4559	$0.31^{+0.01}_{-0.01}$	-	$0.83^{+0.10}_{-0.10}$	0.43
B	NGC5005	$0.43^{+0.06}_{-0.11}$	$0.50^{+0.07}_{-0.08}$	$23.83^{+14.77}_{-22.32}$	0.08
B	NGC6503	$0.45^{+0.02}_{-0.03}$	-	$0.90^{+0.09}_{-0.09}$	1.91
C	UGC06983	$0.51^{+0.11}_{-0.16}$	-	$0.75^{+0.13}_{-0.16}$	0.69
C	UGC07261	$0.53^{+0.12}_{-0.21}$	-	$0.18^{+0.05}_{-0.06}$	0.17
C	UGC07690	$0.68^{+0.11}_{-0.06}$	-	$0.06^{+0.02}_{-0.02}$	0.89
C	UGC07866	$0.38^{+0.06}_{-0.08}$	-	$0.01^{+0.03}_{-0.01}$	2.52
C	UGC08490	$0.78^{+0.02}_{-0.01}$	-	$0.27^{+0.04}_{-0.04}$	0.78
C	UGC08550	$0.49^{+0.08}_{-0.17}$	-	$0.08^{+0.02}_{-0.02}$	1.02
C	UGC08699	$0.71^{+0.05}_{-0.05}$	$0.67^{+0.03}_{-0.05}$	$3.09^{+0.52}_{-0.60}$	0.86
C	UGC09992	$0.43^{+0.10}_{-0.13}$	-	$0.01^{+0.01}_{-0.01}$	1.98
C	UGC10310	$0.53^{+0.10}_{-0.22}$	-	$0.13^{+0.03}_{-0.04}$	1.25
C	UGC12506	$0.78^{+0.02}_{-0.01}$	-	$8.00^{+1.14}_{-1.00}$	1.22
D	NGC7331	$0.32^{+0.01}_{-0.01}$	$0.49^{+0.08}_{-0.18}$	$9.26^{+0.39}_{-0.36}$	0.87
D	NGC7793	$0.41^{+0.05}_{-0.05}$	-	$0.46^{+0.09}_{-0.11}$	0.95
D	NGC7814	$0.76^{+0.04}_{-0.03}$	$0.60^{+0.03}_{-0.03}$	$9.63^{+0.93}_{-0.94}$	0.82
D	UGC02259	$0.72^{+0.08}_{-0.05}$	-	$0.34^{+0.04}_{-0.05}$	2.84
D	UGC03546	$0.55^{+0.04}_{-0.04}$	$0.38^{+0.04}_{-0.04}$	$4.20^{+0.30}_{-0.29}$	1.05
D	UGC06446	$0.50^{+0.09}_{-0.19}$	-	$0.25^{+0.03}_{-0.04}$	0.25
D	UGC06930	$0.40^{+0.06}_{-0.10}$	-	$0.53^{+0.09}_{-0.09}$	0.62
D	UGC06983	$0.40^{+0.05}_{-0.09}$	-	$0.74^{+0.09}_{-0.10}$	0.67
D	UGC07261	$0.49^{+0.09}_{-0.18}$	-	$0.15^{+0.04}_{-0.05}$	0.11
D	UGC07690	$0.66^{+0.13}_{-0.07}$	-	$0.05^{+0.01}_{-0.02}$	0.72

Table 11 – The maximum likelihood estimation for the $\Upsilon_{*\mathrm{D}}$,$\Upsilon_{*\mathrm{B}}$ and M_{200} parameters,and the goodness of fit $\chi^2_{\mathrm{red}}|_{\beta=0}$ for each galaxy in the case of $\beta = 0$.

Set	Galaxy	Best-fit values			$\chi^2_{\mathrm{red}}\|_{\beta=0}$
		$\Upsilon_{*\mathrm{D}}$	$\Upsilon_{*\mathrm{B}}$	$M_{200}(10^{11}M_{\odot})$	
A	F568V1	$0.63^{+0.16}_{-0.10}$	-	$2.44^{+0.45}_{-0.58}$	0.63
A	NGC0024	$0.79^{+0.01}_{-0.01}$	-	$1.24^{+0.10}_{-0.13}$	2.31
A	NGC2683	$0.68^{+0.05}_{-0.04}$	$0.52^{+0.11}_{-0.21}$	$1.97^{+0.33}_{-0.43}$	1.20
A	NGC2915	$0.32^{+0.02}_{-0.02}$	-	$0.59^{+0.05}_{-0.06}$	1.17
A	NGC3198	$0.52^{+0.01}_{-0.01}$	-	$2.09^{+0.04}_{-0.05}$	1.44
A	NGC3521	$0.51^{+0.01}_{-0.01}$	-	$7.95^{+1.62}_{-1.51}$	0.29
A	NGC3769	$0.36^{+0.03}_{-0.06}$	-	$1.20^{+0.14}_{-0.17}$	0.68
A	NGC3893	$0.49^{+0.04}_{-0.03}$	-	$5.42^{+1.24}_{-1.18}$	1.27
A	NGC3949	$0.37^{+0.03}_{-0.06}$	-	$8.55^{+4.75}_{-6.35}$	0.29
A	NGC3953	$0.65^{+0.07}_{-0.07}$	-	$1.66^{+3.36}_{-1.41}$	0.54
B	NGC3992	$0.77^{+0.03}_{-0.02}$	-	$6.88^{+0.61}_{-0.72}$	0.82
B	NGC4051	$0.43^{+0.07}_{-0.10}$	-	$1.23^{+0.63}_{-0.99}$	0.92
B	NGC4088	$0.31^{+0.01}_{-0.01}$	-	$2.08^{+0.30}_{-0.32}$	0.60
B	NGC4100	$0.72^{+0.03}_{-0.03}$	-	$2.33^{+0.26}_{-0.29}$	1.28
B	NGC4138	$0.71^{+0.08}_{-0.04}$	$0.53^{+0.17}_{-0.22}$	$1.82^{+0.56}_{-0.72}$	1.50
B	NGC4157	$0.38^{+0.03}_{-0.03}$	$0.46^{+0.09}_{-0.16}$	$3.70^{+0.49}_{-0.45}$	0.55
B	NGC4183	$0.67^{+0.12}_{-0.06}$	-	$0.65^{+0.07}_{-0.09}$	0.18
B	NGC4559	$0.33^{+0.02}_{-0.03}$	-	$1.05^{+0.07}_{-0.06}$	0.24
B	NGC5005	$0.44^{+0.07}_{-0.09}$	$0.51^{+0.08}_{-0.08}$	$38.22^{+24.20}_{-36.48}$	0.09
B	NGC6503	$0.53^{+0.01}_{-0.01}$	-	$1.06^{+0.02}_{-0.02}$	2.80
C	UGC06983	$0.65^{+0.14}_{-0.07}$	-	$0.97^{+0.11}_{-0.14}$	0.71
C	UGC07261	$0.57^{+0.17}_{-0.15}$	-	$0.29^{+0.07}_{-0.10}$	0.21
C	UGC07690	$0.70^{+0.10}_{-0.06}$	-	$0.10^{+0.03}_{-0.03}$	0.67
C	UGC07866	$0.43^{+0.09}_{-0.13}$	-	$0.01^{+0.02}_{-0.01}$	0.61
C	UGC08490	$0.79^{+0.01}_{-0.01}$	-	$0.39^{+0.02}_{-0.03}$	1.52
C	UGC08550	$0.63^{+0.16}_{-0.08}$	-	$0.12^{+0.01}_{-0.01}$	0.69
C	UGC08699	$0.77^{+0.03}_{-0.02}$	$0.67^{+0.02}_{-0.02}$	$3.70^{+0.26}_{-0.31}$	0.69
C	UGC09992	$0.47^{+0.10}_{-0.17}$	-	$0.01^{+0.01}_{-0.01}$	0.32
C	UGC10310	$0.54^{+0.15}_{-0.23}$	-	$0.19^{+0.04}_{-0.05}$	0.58
C	UGC12506	$0.79^{+0.01}_{-0.01}$	-	$8.90^{+0.76}_{-0.64}$	1.73
D	NGC7331	$0.35^{+0.01}_{-0.01}$	$0.48^{+0.09}_{-0.17}$	$9.38^{+0.33}_{-0.33}$	0.83
D	NGC7793	$0.54^{+0.04}_{-0.04}$	-	$0.60^{+0.12}_{-0.15}$	0.90
D	NGC7814	$0.77^{+0.04}_{-0.02}$	$0.66^{+0.03}_{-0.03}$	$11.40^{+0.79}_{-0.75}$	1.42
D	UGC02259	$0.77^{+0.05}_{-0.02}$	-	$0.63^{+0.04}_{-0.04}$	6.35
D	UGC03546	$0.65^{+0.03}_{-0.03}$	$0.37^{+0.03}_{-0.04}$	$4.12^{+0.28}_{-0.27}$	0.98
D	UGC06446	$0.69^{+0.15}_{-0.08}$	-	$0.44^{+0.04}_{-0.05}$	0.44
D	UGC06930	$0.51^{+0.14}_{-0.16}$	-	$0.69^{+0.12}_{-0.14}$	0.28
D	UGC06983	$0.66^{+0.12}_{-0.09}$	-	$0.96^{+0.10}_{-0.12}$	0.71
D	UGC07261	$0.57^{+0.16}_{-0.15}$	-	$0.28^{+0.07}_{-0.08}$	0.19
D	UGC07690	$0.71^{+0.11}_{-0.07}$	-	$0.09^{+0.03}_{-0.03}$	0.64

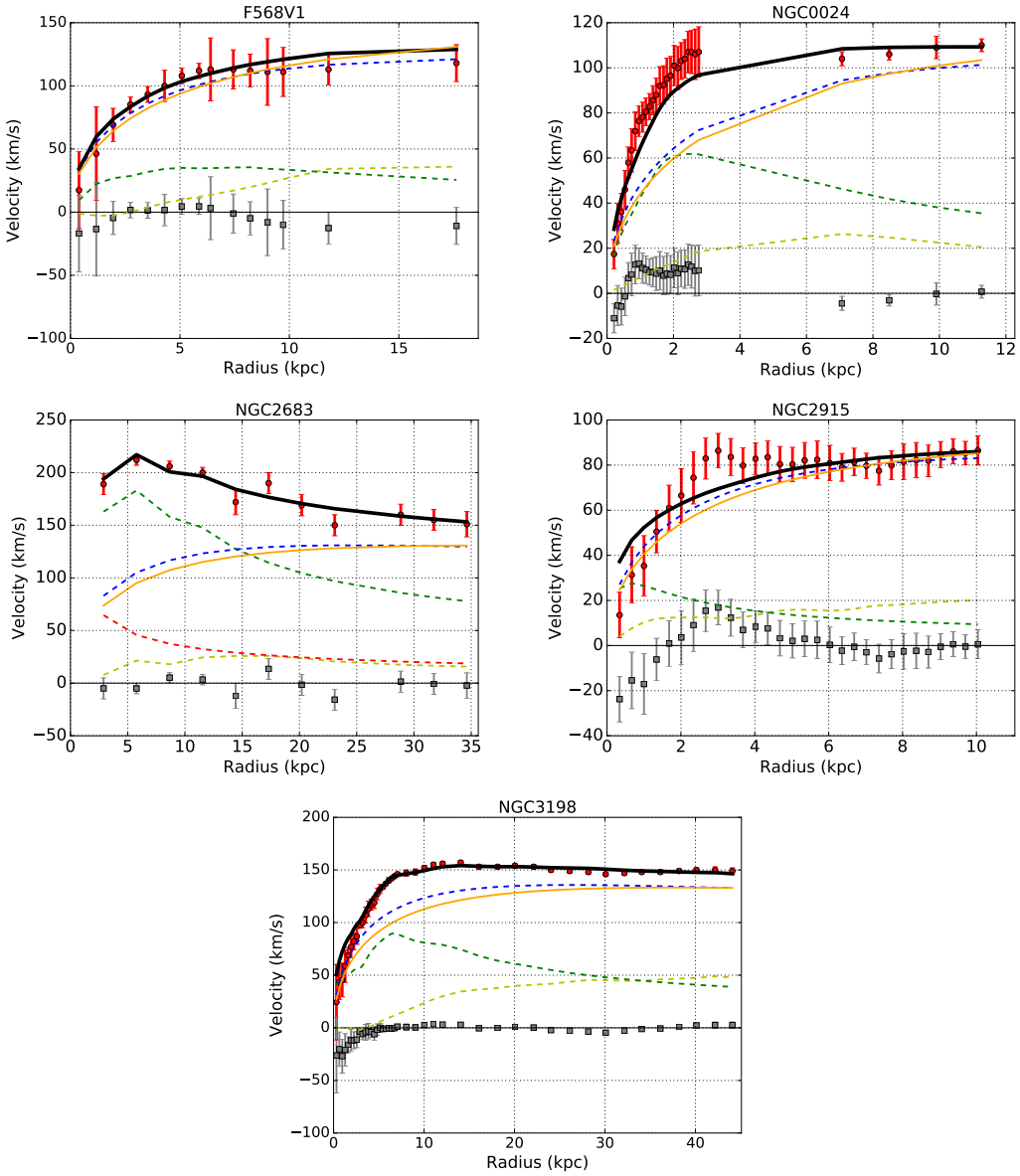

Figure 7 – The rotation curves and their components: gas (dashed yellow line), disk (dashed green line), bulge (dashed red line) and dark matter with Yukawa-like corrections (dashed blue line). The black solid line is the overall best-fit (see equation 7.31) and the values for the parameters are displayed on Tables 10 and 9, the orange solid line is the dark matter component for $\beta = 0$. The red dots with error bars are the observational data taken from SPARC catalogue and the grey ones are the residual of the fit. We have plotted the results for the set A.

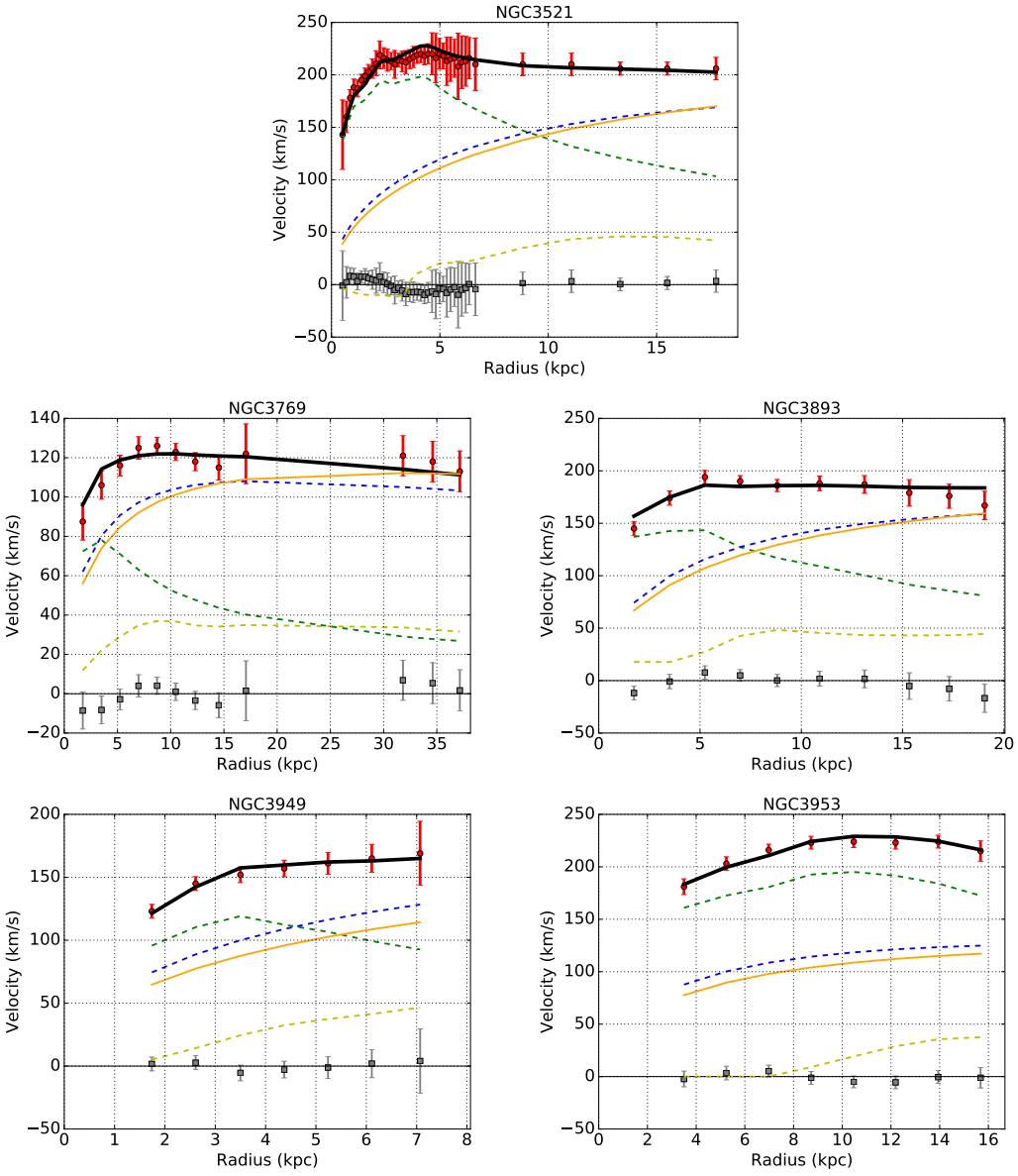

Figure 8 – continued

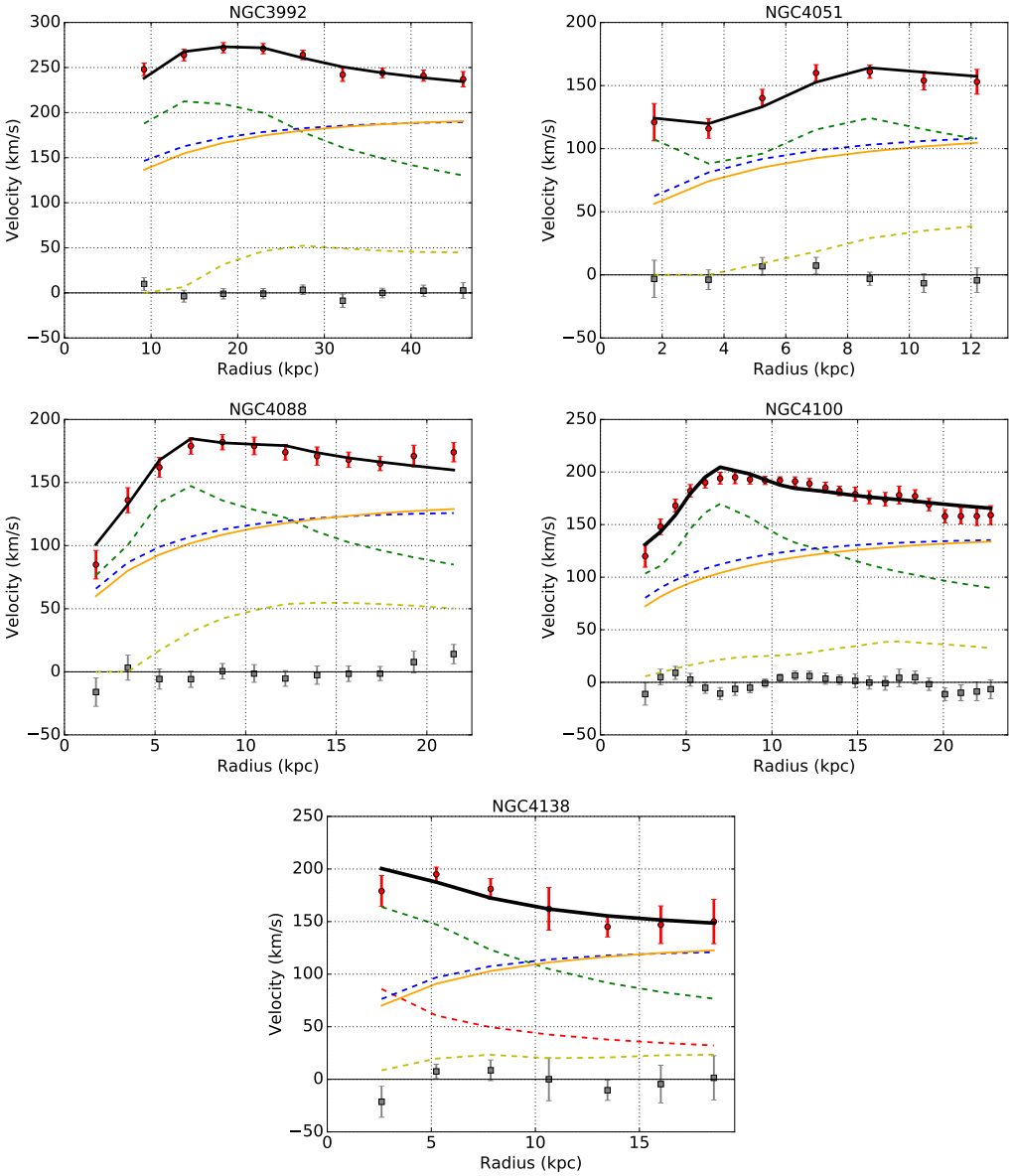

Figure 9 – Same as Figure 7, but for set B.

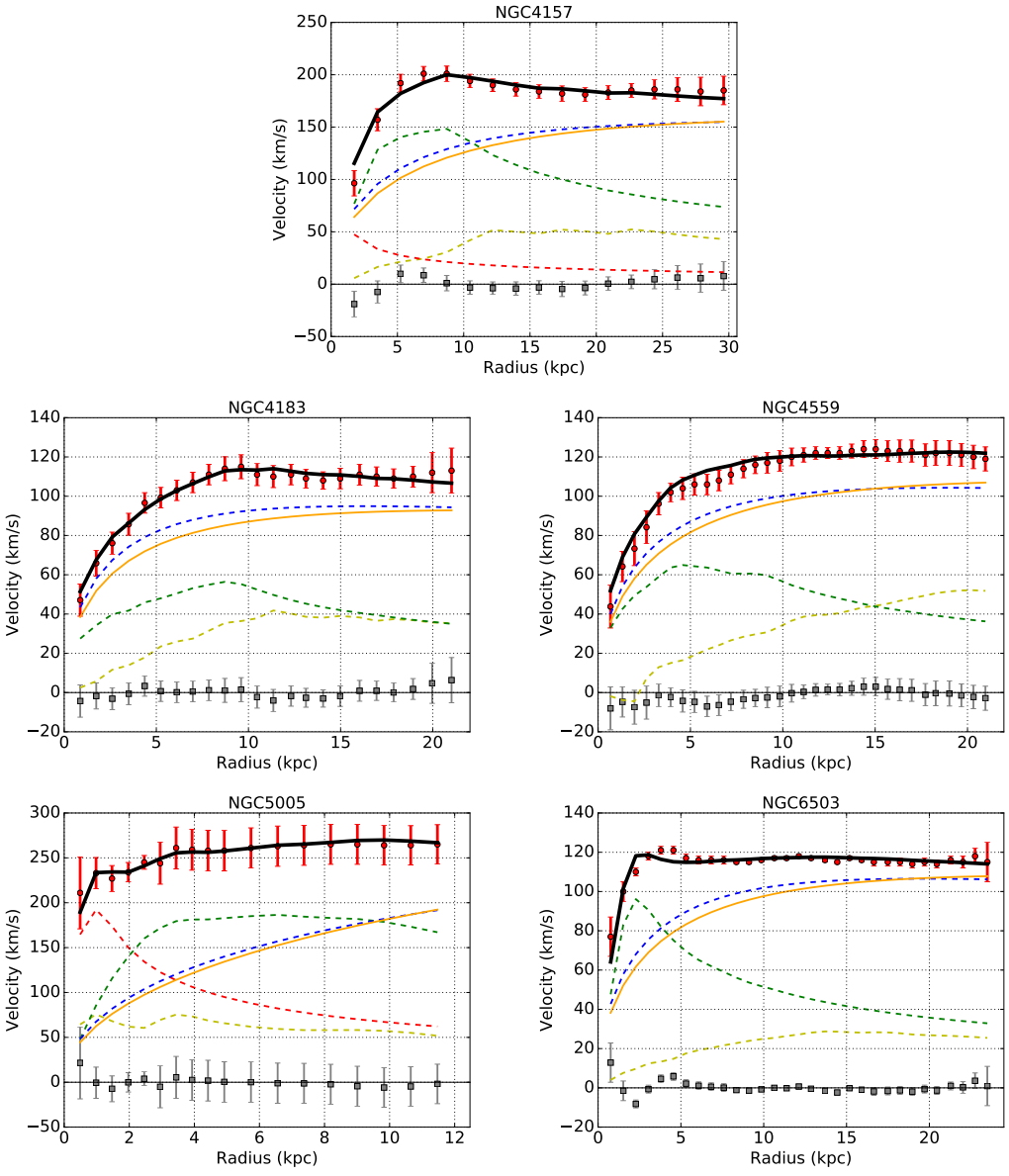

Figure 10 – continued.

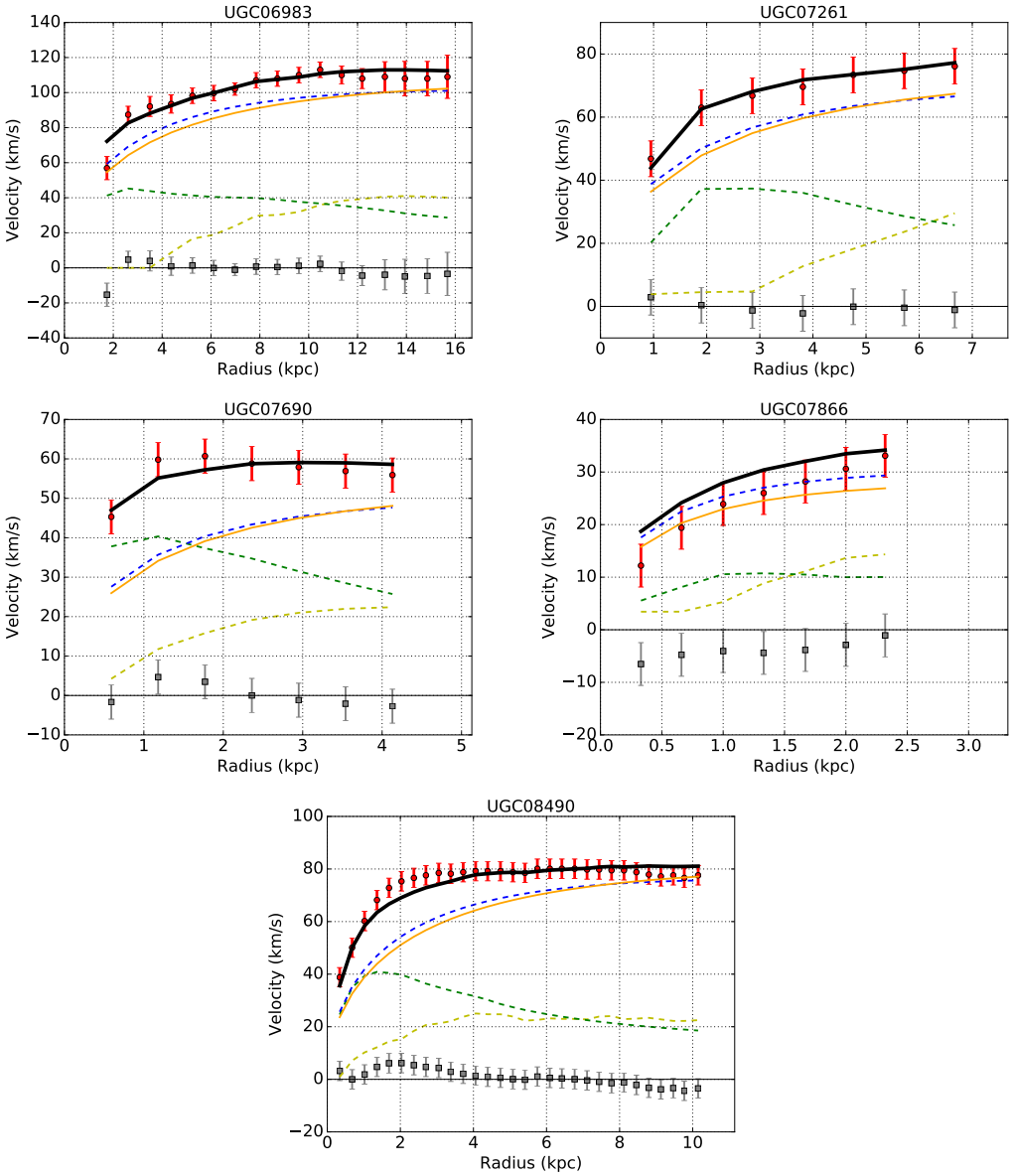

Figure 11 – Same as Figure 7, but for set C.

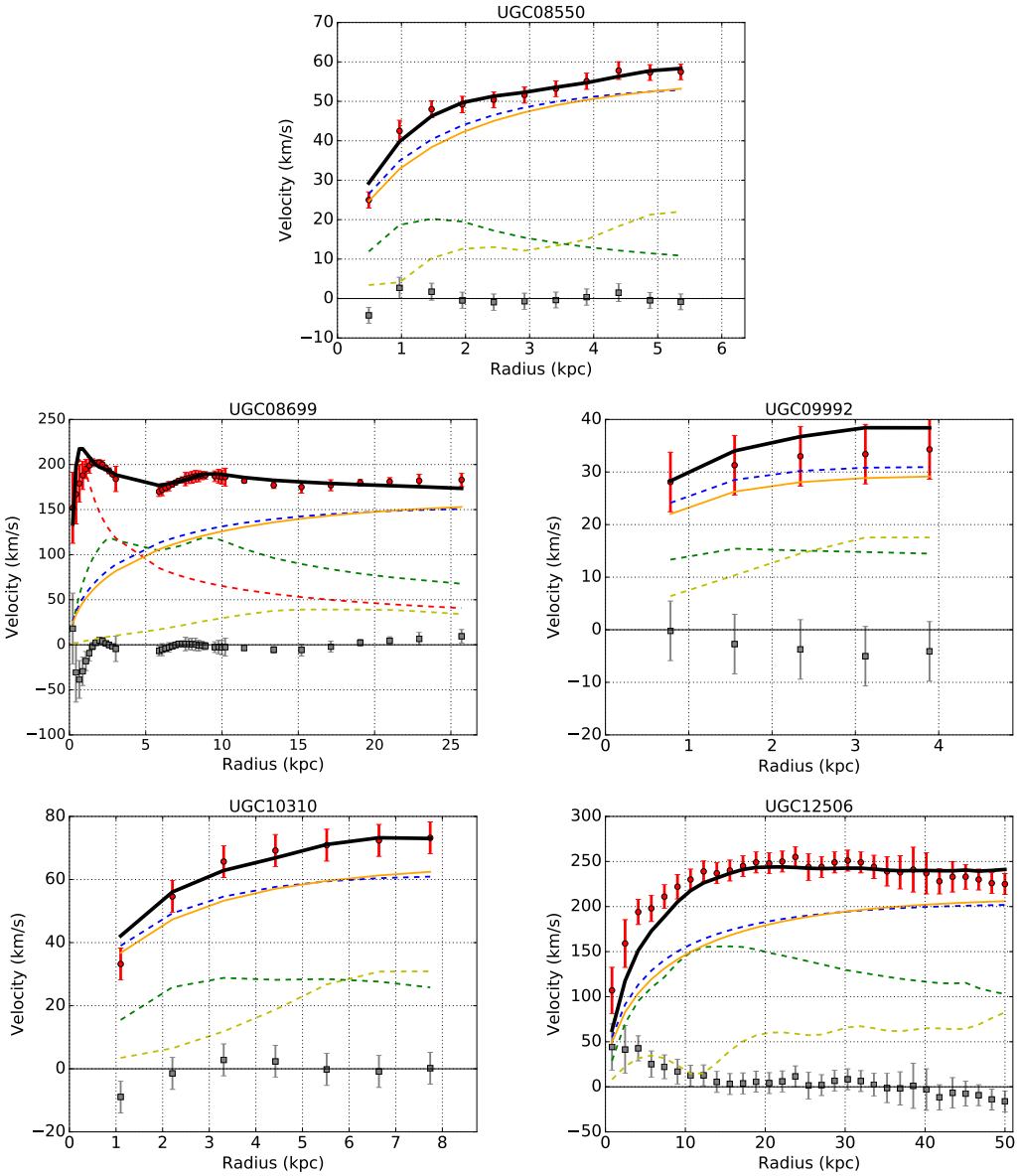

Figure 12 – continued.

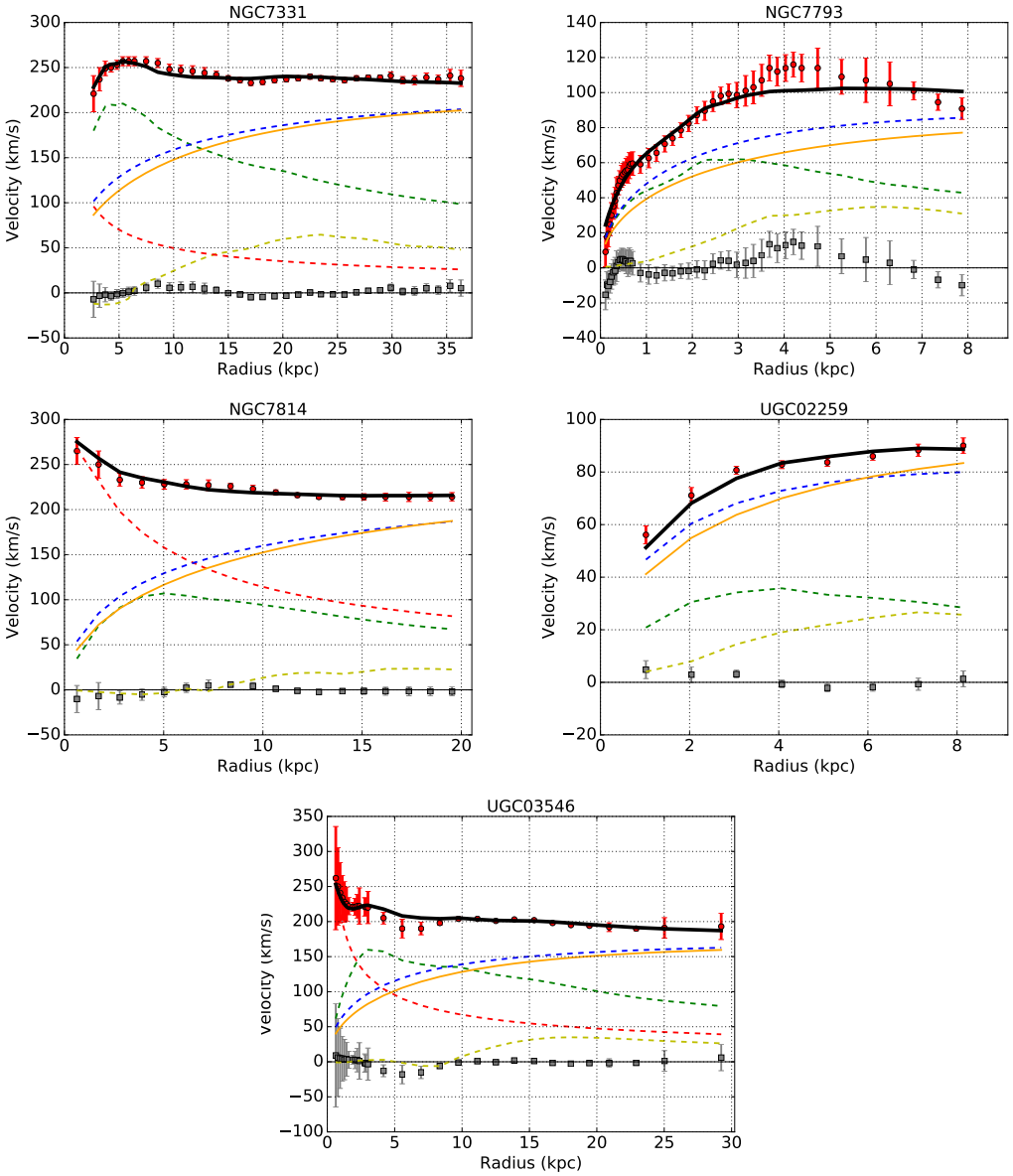

Figure 13 – Same as Figure 7, but for set D.

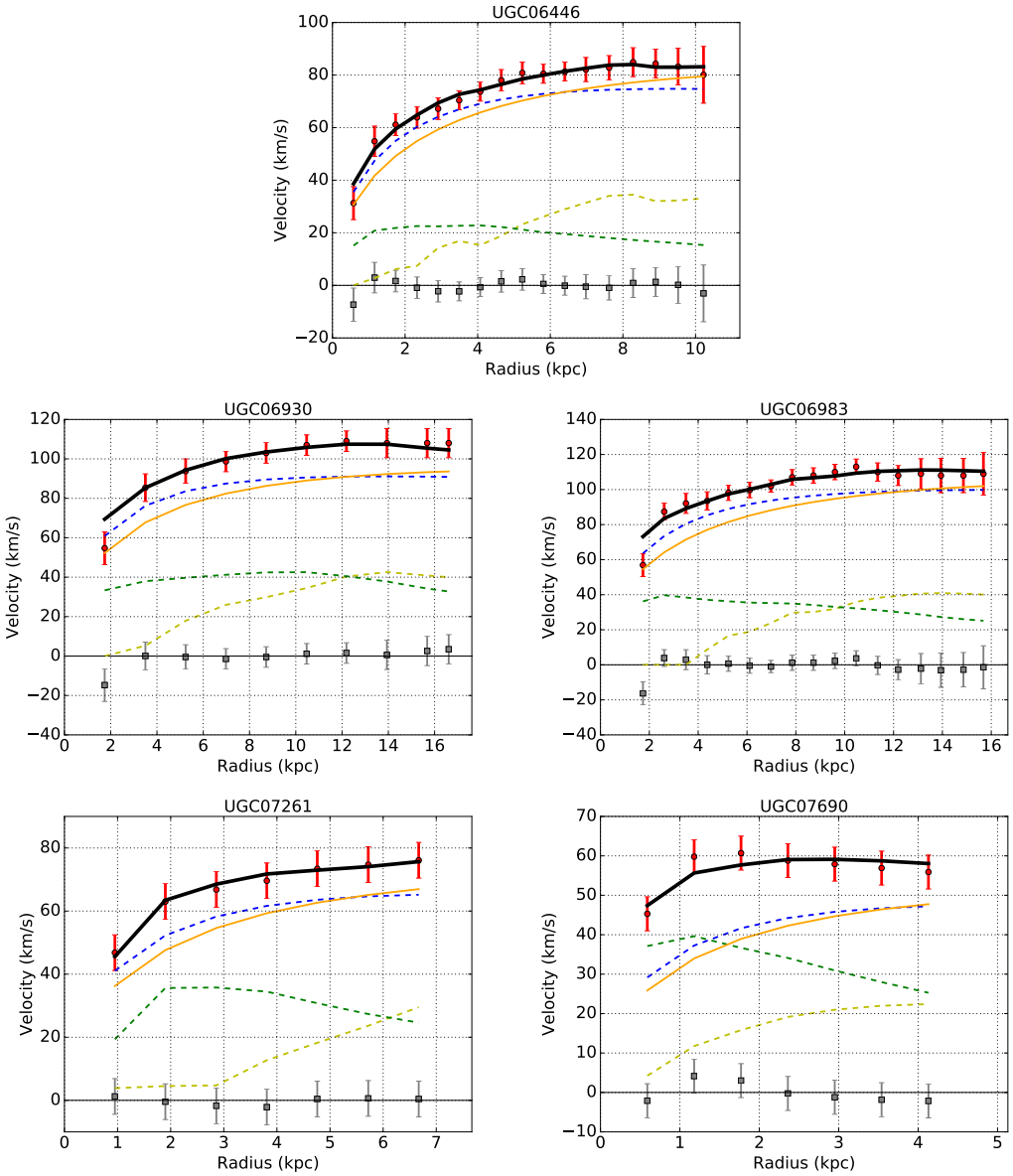

Figure 14 – continued.

8 CONCLUSIONS

In this thesis we consider the effects of modified gravity in the context of galaxies and the Solar System. The latter system has no dark matter that is relevant for its internal dynamics, but it constitutes one of the essential and hardest tests for any theory for gravity. This presentation emphasises the published works [28, 29, 30, 31].

Here we consider three different approaches to standard and modified gravity that have implications to dark matter: i) the nontrivial geometry approach, within GR, of CT and BG (in Chapter 7, Section 7.1); ii) the Renormalization Group extended General Relativity, which considers gravitational effects from infrared RG corrections (in Chapter 3); iii) and the Yukawa correction approach, whose explicit form is chosen such that it is able to describe diverse gravitational models in their weak field limit (in Chapter 7, Section 7.2).

The development and application of the effective Newtonian rotation curve method has shown that both the approaches (BG and CT) have strong problems fitting galaxy rotation curves without dark matter (the selected sample favours the BG approach over the CT one). The method also indicates that if dark matter is considered, the BG approach cannot improve its results significantly, but the CT approach can. Beyond the two GR approaches tested here, we expect that the evaluation of other models could benefit from the method that was introduced in [28] and in this thesis. Also in galaxies context, we investigated the possibility of coexistence of dark matter and modified gravity on the description of rotation curves assuming that the fifth force couples weakly to baryons but with unrestricted strength to dark matter. Contrary to some previous works, our aim is not to replace dark matter with modified gravity but to see how much modified gravity can improve the rotation curve fit. Since baryons are assumed to be weakly coupled, we do not need to invoke a screening mechanism, and the Yukawa term is left free with β and λ as universal parameters for all galaxies. We considered four different sets of 10 galaxies each and we found the region in the parameter space for λ and β that are allowed by the data. To the best of our knowledge, this is the largest set ever analysed in the context of modified gravity theories which predict Yukawa correction. We notice that the β value is remarkably close to $\beta = 1/3$, the value predicted by one of the simplest modified gravity model, the $f(R)$ theory. However, as mentioned in subsection 7.2.1, we should interpret β as the product of a small baryon coupling times a large dark matter coupling, neither of which would be close to the $f(R)$ prediction. So the underlying model can be identified with a scalar-tensor theory with non-universal coupling, rather than the specific form $f(R)$. It is clear that we cannot conclude that standard gravity is ruled out. Rather, we found that a model of the baryon components (gas, disk and bulge), plus a NFW profile for the

dark matter, plus an attractive Yukawa term, fits much better the rotation curves of our sample than a similar model but without the Yukawa correction. Whether this results holds assuming different modelling for the baryon or the dark matter component, remains to be seen.

In the Solar System context, we evaluate a particular realisation named RGGR [9, 10] that is based and extends the approaches of [67, 68]. Considering the external potential effect, we found that $|\bar{\nu}_\odot| \lesssim 10^{-16}$ from the PPN formalism. However, this effect alone cannot fully explain the difference between the effective $\bar{\nu}$ in the Solar System from that in a galaxy, in case RGGR does have a significant impact on galaxy dark matter. The change of $\bar{\nu}$ from system to system may follow a linear correlation to the system mass, as argued in [9, 3], and also be compatible with the bounds here derived for the Solar System. The appendices develop further on the effective changes of $\bar{\nu}$ from system to system, but the precise mechanism that may allow for a variation of $\bar{\nu}$ of about eight to ten orders of magnitude from the Solar System to a galaxy, if there is one, it is still unclear. We extended the Solar System analysis considering a fluid description of Solar System, that is, with the Will-Nordtvedt formalism or usually called as PPN formalism. We find a slightly stronger bound for RGGR, $|\bar{\nu}_\odot| \lesssim 10^{-17}$ (both of these bounds consider the Solar System as part of the Milky Way). Moreover, it also address bounds for a more general class of theories, whose relation between G and the Newtonian potential is given by the expansion 4.13. The bounds for such class are stated in Table 3.

Finally, with respect to the perspectives and future works we could emphasize the impact on particle dark matter search within a modified gravity scenario. The local dark matter density, ρ_0, in our galaxy can be obtained from fitting the rotation curve assuming for dark matter distribution a NFW halo. In a modified gravity scenario which predicts the Yukawa correction to the Newtonian potential, in principle, this quantity can assume a different value compared to the standard case (without Yukawa correction). The value of ρ_0 is important for experiments of dark matter detection, e.g. the Large Underground Xenon (LUX) [13]. Those experiments assumes that the dark matter is made of WIMP [162](Weakly Interacting Particle) and they were designed to measure the interaction between dark matter particle and xenon atom. The local matter density is important to infer the event rates and the cross-section of this interaction. Hence, in a scenario which is allowed a fifth force interaction between baryons and dark matter, the local dark matter density can assume a diferent value with respect to the standard case and, consequently, one can infer the impact of modified gravity in experiments of dark matter detection.

BIBLIOGRAPHY

1 Foreman-Mackey, D. et al. emcee: The MCMC Hammer. *PASP*, v. 125, p. 306, mar. 2013. 4 citations on pages 8, 67, 87, and 88.

2 WILL, C. M. The Confrontation between General Relativity and Experiment. *Living Rev.Rel.*, v. 17, p. 4, 2014. 5 citations on pages 10, 38, 44, 47, and 48.

3 RODRIGUES, D. C. et al. Modified gravity models and the central cusp of dark matter halos in galaxies. *Mon. Not. Roy. Astron. Soc*, v. 445, p. 3823–3838, 2014. 8 citations on pages 10, 29, 45, 76, 78, 79, 104, and 116.

4 GENTILE, G. et al. The cored distribution of dark matter in spiral galaxies. *Mon. Not. Roy. Astron. Soc*, v. 351, p. 903, 2004. 4 citations on pages 10, 62, 72, and 79.

5 de Blok, W. J. G. et al. High-Resolution Rotation Curves and Galaxy Mass Models from THINGS. *Astron. J.*, v. 136, p. 2648–2719, dez. 2008. 3 citations on pages 10, 72, and 79.

6 FARAONI, V.; CAPOZZIELLO, S. *Beyond Einstein Gravity*. Dordrecht: Springer, 2011. v. 170. 170. (Fundamental Theories of Physics, v. 170. 170). ISBN 9789400701649, 9789400701656. Disponível em: <http://www.springerlink.com/content/hl1805/#section=801705&page=1>. One citation on page 15.

7 CAPOZZIELLO, S.; LAURENTIS, M. D. Extended Theories of Gravity. *Phys. Rept.*, v. 509, p. 167–321, 2011. 2 citations on pages 15 and 22.

8 CLIFTON, T. et al. Modified Gravity and Cosmology. *Phys.Rept.*, v. 513, p. 1–189, 2012. 2 citations on pages 15 and 22.

9 RODRIGUES, D. C.; LETELIER, P. S.; SHAPIRO, I. L. Galaxy rotation curves from General Relativity with Renormalization Group corrections. *JCAP*, v. 1004, p. 020, 2010. 6 citations on pages 15, 29, 32, 45, 47, and 104.

10 RODRIGUES, D. C.; CHAUVINEAU, B.; PIATTELLA, O. F. Scalar-Tensor gravity with system-dependent potential and its relation with Renormalization Group extended General Relativity. *JCAP*, v. 1509, n. 09, p. 009, 2015. 8 citations on pages 15, 27, 28, 32, 54, 55, 104, and 115.

11 Zwicky, F. Die Rotverschiebung von extragalaktischen Nebeln. *Helvetica Physica Acta*, v. 6, p. 110–127, 1933. One citation on page 15.

12 RUBIN, V. C.; JR, W. K. F. Rotation of the andromeda nebula from a spectroscopic survey of emission regions. *The Astrophysical Journal*, v. 159, p. 379, 1970. One citation on page 15.

13 AKERIB, D. et al. The large underground xenon (lux) experiment. *Nuclear Instruments and Methods in Physics Research Section A: Accelerators, Spectrometers, Detectors and Associated Equipment*, Elsevier, v. 704, p. 111–126, 2013. 2 citations on pages 15 and 104.

14 APRILE, E. et al. First Dark Matter Search Results from the XENON1T Experiment. *Phys. Rev. Lett.*, v. 119, n. 18, p. 181301, 2017. One citation on page 15.

15 Papastergis, E.; Adams, E. A. K.; van der Hulst, J. M. An accurate measurement of the baryonic Tully-Fisher relation with heavily gas-dominated ALFALFA galaxies. *Astron. Astrophys.*, v. 593, p. A39, set. 2016. One citation on page 15.

16 YEGOROVA, I. A.; SALUCCI, P. The Radial Tully-Fisher relation for spiral galaxies. 1. *Mon. Not. Roy. Astron. Soc*, v. 377, p. 507–515, 2007. One citation on page 15.

17 McGaugh, S. S. The Baryonic Tully-Fisher Relation of Gas-rich Galaxies as a Test of ΛCDM and MOND. *Astron. J.*, v. 143, p. 40, fev. 2012. One citation on page 15.

18 MILGROM, M. MOND impact on and of the recently updated mass-discrepancy-acceleration relation. *ArXiv: 1609.06642 [astro-ph.GA]*, 2016. One citation on page 16.

19 Milgrom, M. A modification of the Newtonian dynamics as a possible alternative to the hidden mass hypothesis. *Astrophys. J.*, v. 270, p. 365–370, jul. 1983. One citation on page 16.

20 MILGROM, M. Mond as modified inertia. *EAS Publications Series*, EDP Sciences, v. 20, p. 217–224, 2006. 2 citations on pages 16 and 81.

21 RODRIGUES, D. C. et al. Absence of a fundamental acceleration scale in galaxies. *Nat. Astron.*, v. 2, p. 668–672, 2018. One citation on page 16.

22 COOPERSTOCK, F. I.; TIEU, S. Galactic Dynamics via General Relativity: A Compilation and New Developments. *Int. J. Mod. Phys.*, A22, p. 2293–2325, 2007. 4 citations on pages 16, 69, 70, and 75.

23 COOPERSTOCK, F.; TIEU, S. Galactic dynamics via general relativity and the exotic dark matter enigma. *Mod.Phys.Lett.*, A21, p. 2133–2142, 2006. 3 citations on pages 16, 69, and 75.

24 COOPERSTOCK, F. I.; TIEU, S. General relativistic velocity: the alternative to dark matter. *Mod. Phys. Lett.*, A23, p. 1745–1755, 2008. 2 citations on pages 16 and 69.

25 CARRICK, J.; COOPERSTOCK, F. General relativistic dynamics applied to the rotation curves of galaxies. *Astrophys.Space Sci.*, v. 337, p. 321–329, 2012. 4 citations on pages 16, 69, 70, and 71.

26 Magalhaes, N. S.; Cooperstock, F. I. Galactic mapping with general relativity and the observed rotation curves. *ArXiv e-prints*, ago. 2015. 3 citations on pages 16, 69, and 75.

27 BALASIN, H.; GRUMILLER, D. Non-Newtonian behavior in weak field general relativity for extended rotating sources. *Int.J.Mod.Phys.*, D17, p. 475–488, 2008. 5 citations on pages 16, 69, 70, 71, and 72.

28 ALMEIDA, Á. O. F. de; PIATTELLA, O. F.; RODRIGUES, D. C. A method for evaluating models that use galaxy rotation curves to derive the density profiles. *Mon. Not. Roy. Astron. Soc*, v. 462, p. 2706, 2016. 4 citations on pages 16, 69, 72, and 103.

29 RODRIGUES, D. C.; MAURO, S.; ALMEIDA, Á. O. F. de. Solar System constraints on Renormalization Group extended General Relativity: The PPN and Laplace-Runge-Lenz analyses with the external potential effect. *Phys. Rev.*, D94, n. 8, p. 084036, 2016. 4 citations on pages 16, 48, 55, and 103.

30 TONIATO, J. D. et al. Will-Nordtvedt PPN formalism applied to renormalization group extensions of general relativity. *Phys. Rev.*, D96, n. 6, p. 064034, 2017. 2 citations on pages 16 and 103.

31 ALMEIDA, A. O. F. de; AMENDOLA, L.; NIRO, V. Galaxy rotation curves in modified gravity models. *JCAP*, v. 1808, n. 08, p. 012, 2018. 9 citations on pages 16, 60, 69, 82, 84, 85, 86, 87, and 103.

32 HOBSON, M. P.; EFSTATHIOU, G. P.; LASENBY, A. N. *General relativity: an introduction for physicists*. [S.l.]: Cambridge University Press, 2006. 2 citations on pages 18 and 20.

33 PLEBANSKI, J.; KRASINSKI, A. *An introduction to general relativity and cosmology*. [S.l.]: Cambridge University Press, 2006. One citation on page 18.

34 WILL, C. *Theory and experiment in gravitational physics*. [S.l.]: Cambridge University Press, 1993. 4 citations on pages 18, 38, 43, and 54.

35 ABBOTT, B. P. et al. Observation of Gravitational Waves from a Binary Black Hole Merger. *Phys. Rev. Lett.*, v. 116, n. 6, p. 061102, 2016. One citation on page 18.

36 MISNER, C. W. et al. Wh freeman and company. *New York, New York, USA,"Gravitation*, 1973. One citation on page 18.

37 AMENDOLA, L.; TSUJIKAWA, S. *Dark energy: theory and observations*. [S.l.]: Cambridge University Press, 2010. 4 citations on pages 19, 22, 25, and 64.

38 LOVELOCK, D. The einstein tensor and its generalizations. *Journal of Mathematical Physics*, AIP, v. 12, n. 3, p. 498–501, 1971. One citation on page 22.

39 LOVELOCK, D. The four-dimensionality of space and the einstein tensor. *Journal of Mathematical Physics*, AIP, v. 13, n. 6, p. 874–876, 1972. One citation on page 22.

40 OLMO, G. J. Post-Newtonian constraints on f(R) cosmologies in metric and Palatini formalism. *Phys. Rev.*, D72, p. 083505, 2005. One citation on page 23.

41 NAVARRO, I.; ACOLEYEN, K. V. f(R) actions, cosmic acceleration and local tests of gravity. *JCAP*, v. 0702, p. 022, 2007. 2 citations on pages 23 and 24.

42 BRANS, C.; DICKE, R. H. Mach's principle and a relativistic theory of gravitation. *Physical review*, APS, v. 124, n. 3, p. 925, 1961. One citation on page 24.

43 TSUJIKAWA, S. et al. Constraints on scalar-tensor models of dark energy from observational and local gravity tests. *Physical Review D*, APS, v. 77, n. 10, p. 103009, 2008. One citation on page 25.

44 JULVE, J.; TONIN, M. Quantum Gravity with Higher Derivative Terms. *Nuovo Cim.*, B46, p. 137–152, 1978. One citation on page 27.

45 SALAM, A.; STRATHDEE, J. Remarks on High-energy Stability and Renormalizability of Gravity Theory. *Phys.Rev.*, D18, p. 4480, 1978. One citation on page 27.

46 FRADKIN, E.; TSEYTLIN, A. A. Renormalizable asymptotically free quantum theory of gravity. *Nucl.Phys.*, B201, p. 469–491, 1982. 2 citations on pages 27 and 28.

47 NELSON, B.; PANANGADEN, P. Scaling behaviour of interacting quantum fields in curved space-time. *Phys.Rev.*, D25, p. 1019–1027, 1982. 2 citations on pages 27 and 28.

48 GOLDMAN, J. T. et al. The Dark matter problem and quantum gravity. *Phys. Lett.*, B281, p. 219–224, 1992. One citation on page 27.

49 SHAPIRO, I. L.; SOLà, J. On the scaling behavior of the cosmological constant and the possible existence of new forces and new light degrees of freedom. *Phys.Lett.*, B475, p. 236–246, 2000. One citation on page 27.

50 BONANNO, A.; REUTER, M. Renormalization group improved black hole space-times. *Phys.Rev.*, D62, p. 043008, 2000. One citation on page 27.

51 BONANNO, A.; REUTER, M. Cosmology with selfadjusting vacuum energy density from a renormalization group fixed point. *Phys.Lett.*, B527, p. 9–17, 2002. One citation on page 27.

52 REUTER, M.; SAUERESSIG, F. Renormalization group flow of quantum gravity in the Einstein-Hilbert truncation. *Phys. Rev.*, D65, p. 065016, 2002. One citation on page 27.

53 BONANNO, A.; REUTER, M. Cosmology of the Planck era from a renormalization group for quantum gravity. *Phys. Rev.*, D65, p. 043508, 2002. One citation on page 27.

54 BENTIVEGNA, E.; BONANNO, A.; REUTER, M. Confronting the IR fixed point cosmology with high redshift supernova data. *JCAP*, v. 0401, p. 001, 2004. One citation on page 27.

55 REUTER, M.; WEYER, H. Quantum gravity at astrophysical distances? *JCAP*, v. 0412, p. 001, 2004. One citation on page 27.

56 BONANNO, A.; ESPOSITO, G.; RUBANO, C. Arnowitt-Deser-Misner gravity with variable G and Lambda and fixed point cosmologies from the renormalization group. *Class.Quant.Grav.*, v. 21, p. 5005–5016, 2004. One citation on page 27.

57 NIEDERMAIER, M.; REUTER, M. The Asymptotic Safety Scenario in Quantum Gravity. *Living Rev. Rel.*, v. 9, p. 5, 2006. One citation on page 27.

58 SHAPIRO, I. L.; SOLà, J. On the possible running of the cosmological 'constant'. *Phys.Lett.*, B682, p. 105–113, 2009. One citation on page 27.

59 WEINBERG, S. Asymptotically Safe Inflation. *Phys.Rev.*, D81, p. 083535, 2010. One citation on page 27.

60 BONANNO, A. An effective action for asymptotically safe gravity. *Phys. Rev.*, D85, p. 081503, 2012. One citation on page 27.

61 SOLà, J. Cosmological constant and vacuum energy: old and new ideas. *J.Phys.Conf.Ser.*, v. 453, p. 012015, 2013. One citation on page 27.

62 SHAPIRO, I. L. Effective Action of Vacuum: Semiclassical Approach. *Class.Quant.Grav.*, v. 25, p. 103001, 2008. One citation on page 27.

63 PERCACCI, R. Approaches to quantum gravity. In: _____. [S.l.]: Cambridge University Press, 2007. cap. Asymptotic Safety, p. 111–128. One citation on page 27.

64 REUTER, M.; SAUERESSIG, F. Quantum Einstein Gravity. *New J. Phys.*, v. 14, p. 055022, 2012. One citation on page 27.

65 APPELQUIST, T.; CARAZZONE, J. Infrared Singularities and Massive Fields. *Phys. Rev.*, D11, p. 2856, 1975. One citation on page 27.

66 GORBAR, E. V.; SHAPIRO, I. L. Renormalization group and decoupling in curved space. *JHEP*, v. 02, p. 021, 2003. One citation on page 27.

67 REUTER, M.; WEYER, H. Renormalization group improved gravitational actions: A Brans-Dicke approach. *Phys.Rev.*, D69, p. 104022, 2004. 2 citations on pages 28 and 104.

68 SHAPIRO, I. L.; SOLà, J.; STEFANCIC, H. Running G and Lambda at low energies from physics at M(X): Possible cosmological and astrophysical implications. *JCAP*, v. 0501, p. 012, 2005. 2 citations on pages 28 and 104.

69 BAUER, F. The Running of the cosmological and the Newton constant controlled by the cosmological event horizon. *Class.Quant.Grav.*, v. 22, p. 3533–3548, 2005. One citation on page 28.

70 KOCH, B.; RAMIREZ, I. Exact renormalization group with optimal scale and its application to cosmology. *Class.Quant.Grav.*, v. 28, p. 055008, 2011. One citation on page 28.

71 RODRIGUES, D. C. Elliptical galaxies kinematics within general relativity with renormalization group effects. *JCAP*, v. 1209, p. 031, 2012. 4 citations on pages 28, 29, 45, and 116.

72 RODRIGUES, D. C.; LETELIER, P. S.; SHAPIRO, I. L. Galaxy Rotation Curves from General Relativity with Infrared Renormalization Group Effects. *Proc. of the Int. Conf. on Two Cosmological Models, ed.: Plaza y Valdés, S.A. de C.V.*, p. 151–159, 2012. One citation on page 29.

73 FABRIS, J. C. et al. Quantum corrections to gravity and their implications for cosmology and astrophysics. *Int.J.Mod.Phys.*, A27, p. 1260006, 2012. One citation on page 29.

74 RODRIGUES, D. C. et al. Disk and elliptical galaxies within renormalization group improved gravity. *AIP Conf.Proc.*, v. 1471, p. 98–102, 2012. One citation on page 29.

75 OLIVEIRA, P. de; PACHECO, J. de F.; REINISCH, G. Testing two alternatives theories to dark matter with the Milky Way dynamics. *Gen.Rel.Grav.*, v. 47, p. 12, 2015. One citation on page 29.

76 FARINA, C. et al. Dynamics of the Laplace-Runge-Lenz vector in the quantum-corrected Newton gravity. *Phys.Rev.*, D83, p. 124037, 2011. 3 citations on pages 29, 45, and 48.

77 ZHAO, S.-S.; XIE, Y. Solar System and stellar tests of a quantum-corrected gravity. *Phys. Rev.*, D92, n. 6, p. 064033, 2015. 4 citations on pages 29, 45, 48, and 117.

78 MOFFAT, J. W. Scalar–tensor–vector gravity theory. *Journal of Cosmology and Astroparticle Physics*, IOP Publishing, v. 2006, n. 03, p. 004, 2006. 3 citations on pages 33, 34, and 35.

79 Moffat, J. W.; Rahvar, S. The MOG weak field approximation and observational test of galaxy rotation curves. *Mon. Not. Roy. Astron. Soc*, v. 436, p. 1439–1451, dez. 2013. 4 citations on pages 33, 35, 81, and 82.

80 FUJII, Y.; MAEDA, K. *The scalar-tensor theory of gravitation*. [S.l.]: Cambridge, USA: Univ. Pr., 2003. One citation on page 43.

81 SCHIFF, L. I. Motion of a gyroscope according to einstein's theory of gravitation. *Proceedings of the National Academy of Sciences*, National Acad Sciences, v. 46, n. 6, p. 871–882, 1960. One citation on page 43.

82 BAIERLEIN, R. Testing general relativity with laser ranging to the moon. *Physical Review*, APS, v. 162, n. 5, p. 1275, 1967. One citation on page 43.

83 JR, K. N. Equivalence principle for massive bodies. ii. theory. *Physical Review*, APS, v. 169, n. 5, p. 1017, 1968. One citation on page 43.

84 WILL, C. M. Theoretical frameworks for testing relativistic gravity. ii. parametrized post-newtonian hydrodynamics, and the nordtvedt effect. *The Astrophysical Journal*, v. 163, p. 611, 1971. One citation on page 43.

85 WILL, C. M. Relativistic gravity tn the solar system. 111. experimental disproof of a class of linear theories of gravitation. *The Astrophysical Journal*, v. 185, p. 31–42, 1973. One citation on page 43.

86 IOCCO, F.; PATO, M.; BERTONE, G. Evidence for dark matter in the inner Milky Way. *Nature Phys.*, v. 11, p. 245–248, 2015. One citation on page 45.

87 PATO, M.; IOCCO, F. The Dark Matter Profile of the Milky Way: a Non-parametric Reconstruction. *Astrophys. J.*, v. 803, n. 1, p. L3, 2015. One citation on page 45.

88 NASA space science data coordinated archive. <http://nssdc.gsfc.nasa.gov/planetary/>. 2016. Disponível em: <http://nssdc.gsfc.nasa.gov/planetary/>. One citation on page 45.

89 SERENO, M.; JETZER, P. Solar and stellar system tests of the cosmological constant. *Phys. Rev.*, D73, p. 063004, 2006. One citation on page 54.

90 CLIFTON, T. The Parameterised Post-Newtonian Limit of Fourth-Order Theories of Gravity. *Phys. Rev.*, D77, p. 024041, 2008. One citation on page 56.

91 BITTENCOURT, E. et al. More about scalar gravity. *Phys. Rev.*, D93, n. 12, p. 124023, 2016. One citation on page 56.

92 MO, H.; BOSCH, F. Van den; WHITE, S. *Galaxy formation and evolution*. [S.l.]: Cambridge University Press, 2010. 2 citations on pages 57 and 84.

93 BINNEY, J.; TREMAINE, S. *Galactic dynamics*. [S.l.]: Princeton university press, 2011. 2 citations on pages 57 and 72.

94 COURTEAU, S. et al. Galaxy Masses. *Rev. Mod. Phys.*, v. 86, p. 47–119, 2014. One citation on page 57.

95 BELL, E. F.; JONG, R. S. de. Stellar mass-to-light ratios and the tully-fisher relation. *The Astrophysical Journal*, IOP Publishing, v. 550, n. 1, p. 212, 2001. One citation on page 58.

96 MACARTHUR, L. A.; COURTEAU, S.; HOLTZMAN, J. A. Structure of disk-dominated galaxies. i. bulge/disk parameters, simulations, and secular evolution. *The Astrophysical Journal*, IOP Publishing, v. 582, n. 2, p. 689, 2003. One citation on page 58.

97 SERSIC, J. L. Atlas de galaxias australes. *Cordoba, Argentina: Observatorio Astronomico, 1968*, 1968. One citation on page 58.

98 de Jong, R. S. B, V, R, I, H and K images of 86 face-on spiral galaxies. *Journal of Astronomical Data*, v. 2, 1996. One citation on page 58.

99 BLOK, W. D. et al. High-resolution rotation curves and galaxy mass models from things. *The Astronomical Journal*, IOP Publishing, v. 136, n. 6, p. 2648, 2008. 3 citations on pages 58, 61, and 62.

100 de Almeida, Á. O. F.; Piattella, O. F.; Rodrigues, D. C. A method for evaluating models that use galaxy rotation curves to derive the density profiles. *Mon. Not. Roy. Astron. Soc*, v. 462, p. 2706–2714, nov. 2016. One citation on page 60.

101 Walter, F. et al. THINGS: The H I Nearby Galaxy Survey. *Astron. J.*, v. 136, p. 2563–2647, dez. 2008. 2 citations on pages 60 and 61.

102 BEGEMAN, K.; BROEILS, A.; SANDERS, R. Extended rotation curves of spiral galaxies: Dark haloes and modified dynamics. *Monthly Notices of the Royal Astronomical Society*, The Royal Astronomical Society, v. 249, n. 3, p. 523–537, 1991. 2 citations on pages 61 and 62.

103 JARRETT, T. et al. The 2mass large galaxy atlas. *The Astronomical Journal*, IOP Publishing, v. 125, n. 2, p. 525, 2003. One citation on page 61.

104 OH, S.-H. et al. High-resolution dark matter density profiles of things dwarf galaxies: correcting for noncircular motions. *The Astronomical Journal*, IOP Publishing, v. 136, n. 6, p. 2761, 2008. One citation on page 61.

105 PERSIC, M.; SALUCCI, P. Rotation curves of 967 spiral galaxies. *Astrophys. J. Suppl.*, v. 99, p. 501, 1995. One citation on page 62.

106 MATHEWSON, D.; FORD, V.; BUCHHORN, M. A southern sky survey of the peculiar velocities of 1355 spiral galaxies. *The Astrophysical Journal Supplement Series*, v. 81, p. 413–659, 1992. One citation on page 62.

107 Lelli, F.; McGaugh, S. S.; Schombert, J. M. SPARC: Mass Models for 175 Disk Galaxies with Spitzer Photometry and Accurate Rotation Curves. *Astron. J.*, v. 152, p. 157, dez. 2016. 2 citations on pages 62 and 85.

108 BLOK, W. D. et al. Mass density profiles of low surface brightness galaxies. *The Astrophysical Journal Letters*, IOP Publishing, v. 552, n. 1, p. L23, 2001. One citation on page 62.

109 SWATERS, R. et al. The rotation curves shapes of late-type dwarf galaxies. *Astronomy & Astrophysics*, EDP Sciences, v. 493, n. 3, p. 871–892, 2009. One citation on page 63.

110 BERSHADY, M. A. et al. The diskmass survey. ii. error budget. *The Astrophysical Journal*, IOP Publishing, v. 716, n. 1, p. 234, 2010. One citation on page 63.

111 GREGORY, P. C. *Bayesian logical data analysis for the physical sciences : a comparative approach with Mathematica support*. Cambridge New York: Cambridge University Press, 2010. ISBN 0521150124. One citation on page 64.

112 IVEZIĆ, Ž. et al. *Statistics, Data Mining, and Machine Learning in Astronomy: A Practical Python Guide for the Analysis of Survey Data*. [S.l.]: Princeton University Press, 2014. One citation on page 64.

113 METROPOLIS, N.; ULAM, S. The monte carlo method. *Journal of the American statistical association*, Taylor & Francis, v. 44, n. 247, p. 335–341, 1949. One citation on page 65.

114 METROPOLIS, N. et al. Equation of state calculations by fast computing machines. *The journal of chemical physics*, AIP, v. 21, n. 6, p. 1087–1092, 1953. 2 citations on pages 66 and 87.

115 HAARIO, H. et al. An adaptive metropolis algorithm. *Bernoulli*, Bernoulli Society for Mathematical Statistics and Probability, v. 7, n. 2, p. 223–242, 2001. One citation on page 66.

116 GILKS, W. R.; ROBERTS, G. O.; GEORGE, E. I. Adaptive direction sampling. *The statistician*, JSTOR, p. 179–189, 1994. One citation on page 67.

117 GOODMAN, J.; WEARE, J. Ensemble samplers with affine invariance. *Communications in applied mathematics and computational science*, Mathematical Sciences Publishers, v. 5, n. 1, p. 65–80, 2010. 2 citations on pages 67 and 87.

118 COWLES, M. K.; CARLIN, B. P. Markov chain monte carlo convergence diagnostics: a comparative review. *Journal of the American Statistical Association*, Taylor & Francis, v. 91, n. 434, p. 883–904, 1996. One citation on page 67.

119 SOKAL, A. Monte carlo methods in statistical mechanics: foundations and new algorithms. In: *Functional integration*. [S.l.]: Springer, 1997. p. 131–192. 2 citations on pages 68 and 87.

120 RAMOS-CARO, J.; AGON, C.; PEDRAZA, J. Kinetic Theory of Collisionless Self-Gravitating Gases: II. Relativistic Corrections in Galactic Dynamics. *Phys.Rev.*, D86, p. 043008, 2012. One citation on page 69.

121 WALD, R. M. *General Relativity*. [S.l.]: Chicago, USA: Univ. Pr., 1984. One citation on page 70.

122 FUCHS, B.; PHLEPS, S. Comment on 'General Relativity Resolves Galactic Rotation Without Exotic Dark Matter' by F.I. Cooperstock and S. Tieu. *New Astron.*, v. 11, p. 608–610, 2006. 2 citations on pages 70 and 71.

123 VOGT, D.; LETELIER, P. S. Presence of exotic matter in the Cooperstock and Tieu galaxy model. astro-ph/0510750. *ArXiv e-prints*, 2005. One citation on page 71.

124 Freeman, K. C. On the Disks of Spiral and so Galaxies. *Astrophys. J.*, v. 160, p. 811, jun. 1970. One citation on page 75.

125 BELL, E. F.; JONG, R. S. de. Stellar mass-to-light ratios and the Tully-Fisher relation. *Astrophys. J.*, v. 550, p. 212–229, 2001. One citation on page 79.

126 MEIDT, S. E. et al. Reconstructing the stellar mass distributions of galaxies using S^4G IRAC 3.6 and 4.5 μm images: II. The conversion from light to mass. *Astrophys. J.*, v. 788, p. 144, 2014. One citation on page 79.

127 Finzi, A. On the validity of Newton's law at a long distance. *Mon. Not. Roy. Astron. Soc*, v. 127, p. 21, 1963. One citation on page 81.

128 Milgrom, M. A modification of the Newtonian dynamics - Implications for galaxies. *Astrophys. J.*, v. 270, p. 371–389, jul. 1983. One citation on page 81.

129 de Blok, W. J. G.; McGaugh, S. S. Testing Modified Newtonian Dynamics with Low Surface Brightness Galaxies: Rotation Curve FITS. *Astrophys. J.*, v. 508, p. 132–140, nov. 1998. One citation on page 81.

130 SANDERS, R. H.; MCGAUGH, S. S. Modified Newtonian dynamics as an alternative to dark matter. *Ann. Rev. Astron. Astrophys.*, v. 40, p. 263–317, 2002. One citation on page 81.

131 Moffat, J. W. Scalar tensor vector gravity theory. *JCAP*, v. 3, p. 004, mar. 2006. One citation on page 81.

132 RODRIGUES, D. C.; LETELIER, P. S.; SHAPIRO, I. L. Galaxy rotation curves from general relativity with renormalization group corrections. *Journal of Cosmology and Astroparticle Physics*, IOP Publishing, v. 2010, n. 04, p. 020, 2010. One citation on page 81.

133 Brownstein, J. R.; Moffat, J. W. Galaxy Rotation Curves without Nonbaryonic Dark Matter. *Astrophys. J.*, v. 636, p. 721–741, jan. 2006. One citation on page 81.

134 Capozziello, S.; Cardone, V. F.; Troisi, A. Low surface brightness galaxy rotation curves in the low energy limit of R^n gravity: no need for dark matter? *Mon. Not. Roy. Astron. Soc*, v. 375, p. 1423–1440, mar. 2007. One citation on page 81.

135 Frigerio Martins, C.; Salucci, P. Analysis of rotation curves in the framework of R^n gravity. *Mon. Not. Roy. Astron. Soc*, v. 381, p. 1103–1108, nov. 2007. One citation on page 81.

136 BANADOS, M. Eddington-Born-Infeld action for dark matter and dark energy. *Phys. Rev.*, D77, p. 123534, 2008. One citation on page 81.

137 MANNHEIM, P. D.; O'BRIEN, J. G. Fitting galactic rotation curves with conformal gravity and a global quadratic potential. *Phys. Rev.*, D85, p. 124020, 2012. One citation on page 81.

138 Sanders, R. H. Anti-gravity and galaxy rotation curves. *Astron. Astrophys.*, v. 136, p. L21–L23, jul. 1984. 2 citations on pages 81 and 82.

139 Scherk, J. Antigravity: A crazy idea? *Physics Letters B*, v. 88, p. 265–267, dez. 1979. One citation on page 81.

140 DRUMMOND, I. T. Bimetric gravity and [dark matter]. *Phys. Rev.*, D63, p. 043503, 2001. 2 citations on pages 81 and 82.

141 Cervantes-Cota, J. L.; Rodríguez-Meza, M. A.; Nuñez, D. Flat rotation curves using scalar-tensor theories. In: *Journal of Physics Conference Series*. [S.l.: s.n.], 2007. (Journal of Physics Conference Series, v. 91), p. 012007. One citation on page 81.

142 CLIFTON, T. The Parameterised Post-Newtonian Limit of Fourth-Order Theories of Gravity. *Phys. Rev.*, D77, p. 024041, 2008. One citation on page 81.

143 Clifton, T.; Bañados, M.; Skordis, C. The parameterized post-Newtonian limit of bimetric theories of gravity. *Classical and Quantum Gravity*, v. 27, n. 23, p. 235020, dez. 2010. One citation on page 81.

144 Cardone, V. F.; Capozziello, S. Systematic biases on galaxy haloes parameters from Yukawa-like gravitational potentials. *Mon. Not. Roy. Astron. Soc*, v. 414, p. 1301–1313, jun. 2011. 2 citations on pages 81 and 82.

145 STABILE, A.; SCELZA, G. Rotation Curves of Galaxies by Fourth Order Gravity. *Phys. Rev.*, D84, p. 124023, 2011. 2 citations on pages 81 and 82.

146 STABILE, A.; CAPOZZIELLO, S. Galaxy rotation curves in $f(R, \phi)$ gravity. *Phys. Rev.*, D87, n. 6, p. 064002, 2013. 2 citations on pages 81 and 82.

147 RAHVAR, S.; MASHHOON, B. Observational Tests of Nonlocal Gravity: Galaxy Rotation Curves and Clusters of Galaxies. *Phys. Rev.*, D89, p. 104011, 2014. One citation on page 82.

148 MOTA, D. F.; SALZANO, V.; CAPOZZIELLO, S. Testing feasibility of scalar-tensor gravity by scale dependent mass and coupling to matter. *Phys. Rev.*, D83, p. 084038, 2011. One citation on page 82.

149 CAPOZZIELLO, S.; FILIPPIS, E. D.; SALZANO, V. Modelling clusters of galaxies by f(R)-gravity. *Mon. Not. Roy. Astron. Soc.*, v. 394, p. 947–959, 2009. One citation on page 82.

150 Piazza, F.; Marinoni, C. Model for Gravitational Interaction between Dark Matter and Baryons. *Physical Review Letters*, v. 91, n. 14, p. 141301, out. 2003. 2 citations on pages 82 and 83.

151 Damour, T.; Esposito-Farese, G. Tensor-multi-scalar theories of gravitation. *Classical and Quantum Gravity*, v. 9, p. 2093–2176, set. 1992. One citation on page 83.

152 AMENDOLA, L. Linear and non-linear perturbations in dark energy models. *Phys. Rev.*, D69, p. 103524, 2004. One citation on page 83.

153 Will, C. M. The Confrontation between General Relativity and Experiment. *Living Reviews in Relativity*, v. 4, p. 4, maio 2001. One citation on page 83.

154 Patrignani, C.; Particle Data Group. Review of Particle Physics. *Chinese Physics C*, v. 40, n. 10, p. 100001, out. 2016. One citation on page 83.

155 DUTTON, A. A.; MACCIò, A. V. Cold dark matter haloes in the Planck era: evolution of structural parameters for Einasto and NFW profiles. *Mon. Not. Roy. Astron. Soc.*, v. 441, n. 4, p. 3359–3374, 2014. One citation on page 84.

156 MACCIÓ, A. V.; DUTTON, A. A.; BOSCH, F. C. v. d. Concentration, Spin and Shape of Dark Matter Haloes as a Function of the Cosmological Model: WMAP1, WMAP3 and WMAP5 results. *Mon. Not. Roy. Astron. Soc*, v. 391, p. 1940–1954, 2008. One citation on page 84.

157 Planck Collaboration et al. Planck 2015 results. XIII. Cosmological parameters. *Astron. Astrophys.*, v. 594, p. A13, set. 2016. One citation on page 85.

158 PIZZUTI, L. et al. CLASH-VLT: constraints on $f(R)$ gravity models with galaxy clusters using lensing and kinematic analyses. *JCAP*, v. 1707, n. 07, p. 023, 2017. One citation on page 85.

159 Meidt, S. E. et al. Reconstructing the Stellar Mass Distributions of Galaxies Using S^4G IRAC 3.6 and 4.5 μm Images. II. The Conversion from Light to Mass. *Astrophys. J.*, v. 788, p. 144, jun. 2014. One citation on page 87.

160 Schombert, J.; McGaugh, S. Stellar Populations and the Star Formation Histories of LSB Galaxies: III. Stellar Population Models. *PASA*, v. 31, p. e036, set. 2014. One citation on page 87.

161 SCHWARZ, G. et al. Estimating the dimension of a model. *The annals of statistics*, Institute of Mathematical Statistics, v. 6, n. 2, p. 461–464, 1978. One citation on page 92.

162 PROFUMO, S. *An introduction to particle dark matter*. [S.l.]: World Scientific, 2017. One citation on page 104.

APPENDIX A – A SPECIFIC COVARIANT SCALE SETTING

Consider the following simple realization of the covariant setting (2.32),

$$\mu = f(U^\alpha U^\beta h_{\alpha\beta}) = A + B\, U^\alpha U^\beta h_{\alpha\beta}, \tag{A.1}$$

where A and B are constants. This simple covariant scale setting was introduced in [10], and it will be shown in detail in this and the next Appendix that, under certain reasonable limits, it is as a covariant extension of the scale setting (2.37).

Adopting a comoving coordinate system ($U^i = 0$), the scalar $U^\alpha U^\beta h_{\alpha\beta}$ can be expressed as, with $\gamma_{\alpha\beta} = \eta_{\alpha\beta}$,

$$\begin{aligned} U^\alpha U^\beta h_{\alpha\beta} &= U^0 U^0 h_{00} \\ &= -\frac{h_{00}}{g_{00}} \\ &= -\left(1 + \frac{1}{G\bar{g}_{00}}\right) \\ &= -1 + \frac{G^{-1}}{1 - \bar{h}_{00}}. \end{aligned} \tag{A.2}$$

In the above, it was used $\bar{g}_{00} \equiv G^{-1} g_{00}$. The above expression fixes a relation between μ and $\bar{h}_{00}$. For a Minkowski background, following subsection 2.3.3, the relation between $\bar{h}_{00}$ and the Newtonian potential Φ, reads

$$\bar{h}_{00} = -2\Phi + O(2,2), \tag{A.3}$$

where it was used that the metric that solves the Einstein equation $\tilde{G}_{\alpha\beta} = 8\pi \tilde{T}_{\alpha\beta}$ is $\tilde{g}_{\alpha\beta}$, whose time-time component satisfies $\tilde{g}_{00} = -1 - 2\Phi + O(2)$, and that $\tilde{g}_{00} = G^{-1} g_{00} + O(2,2) = \bar{g}_{00} + O(2,2)$.

The function $\mu(\bar{h}_{00})$, or $\mu(\Phi)$, will not be an analytical function in general. Indeed, considering the $G(\mu)$ expression as given in eq. (2.31), the equation (A.2) is a transcendental one for μ.

Far away from any mass, $h_{\alpha\beta}$ should become zero (i.e., the metric $g_{\alpha\beta}$ should coincide with the background), hence in this limit $\mu = A$, which in turn implies that $G^{-1} = 1 + 2\nu \ln A$. Using unities such that $G|_{h_{\alpha\beta}=0} = G_0 = 1$, one finds

$$A = 1. \tag{A.4}$$

To avoid any singularity in G for any $\mu \in [1, \infty)$, ν needs to be positive, and this is always assumed henceforth.

Combining the previous equations,

$$\begin{aligned} \mu &= 1 + B\left(-1 + \frac{G^{-1}}{1-\bar{h}_{00}}\right) \\ &= 1 + B\left(-1 + \frac{1+2\nu\ln\mu}{1+2\Phi} + O(2,2)\right). \end{aligned} \tag{A.5}$$

This is a transcendental equation for μ, but it can be solved for Φ,

$$\Phi = \frac{1}{2}\left(\frac{1+2\nu\ln(1+\delta\mu)}{1+\frac{\delta\mu}{B}} - 1\right) + O(\nu^2). \tag{A.6}$$

In the above, we introduced $\delta\mu \equiv \mu - 1 > 0$. As expected, from the above one finds $\lim_{\delta\mu\to 0}\Phi = 0$.

Up to this point, B is simply any real number, but from the previous results, and two considerations, its value can be found. For sufficiently small $\delta\mu$, Φ reads

$$\Phi|_{\substack{\delta\mu \ll |B| \\ \delta\mu \ll 1}} \approx \frac{1}{2}\left(2\nu\delta\mu - \frac{\delta\mu}{B}\right) = \frac{1}{2}\delta\mu(2\nu - B^{-1}). \tag{A.7}$$

The first consideration is that the inequality $\Phi \leq 0$ must be satisfied, hence, since $\nu > 0$,

$$0 < B \leq \frac{1}{2\nu}. \tag{A.8}$$

The second consideration is that when $\delta\mu \to 0$ or equivalently when $h_{\alpha\beta} \to 0$, Φ should smoothly go to zero, implying that

$$\lim_{\delta\mu\to 0} \partial_{\delta\mu}\Phi = 0. \tag{A.9}$$

Therefore,

$$B = \frac{1}{2\nu}. \tag{A.10}$$

With the above, equation (A.6) can now be simply written as

$$\Phi = \nu\ln(1+\delta\mu) - \nu\delta\mu + O(\nu^2). \tag{A.11}$$

To clarify the meaning of the above equation, it is stating a correlation between $\delta\mu$ and Φ, and this correlation, naturally, only exists if $\nu \neq 0$. This correlation is the one that comes from the covariant scale setting, and should be compared with the noncovariant one (2.37). The above equation cannot be solved analytically to express either $\delta\mu$ or μ as a function of Φ, hence equation (2.37) should be seen as a local analytical approximation for the function $\mu(\Phi)$.

Figure 15 shows a parametric plot on the evolution of δG as a function of Φ for different values of ν. The highest value of ν used in that figure corresponds to the value used in galaxies without dark matter [71, 3], and the smallest one is close to the Solar System

bound derived in [77]. It can be seen that changes of many orders of magnitude on Φ translate into a much smaller variation in δG. The range of Φ includes values corresponding the surface of a neutron star ($\sim 10^{-1}$), and down to 10^{-10}, which is about the Newtonian potential generated by the baryonic matter of dwarf galaxies at their farthest observed rotation curve radius.

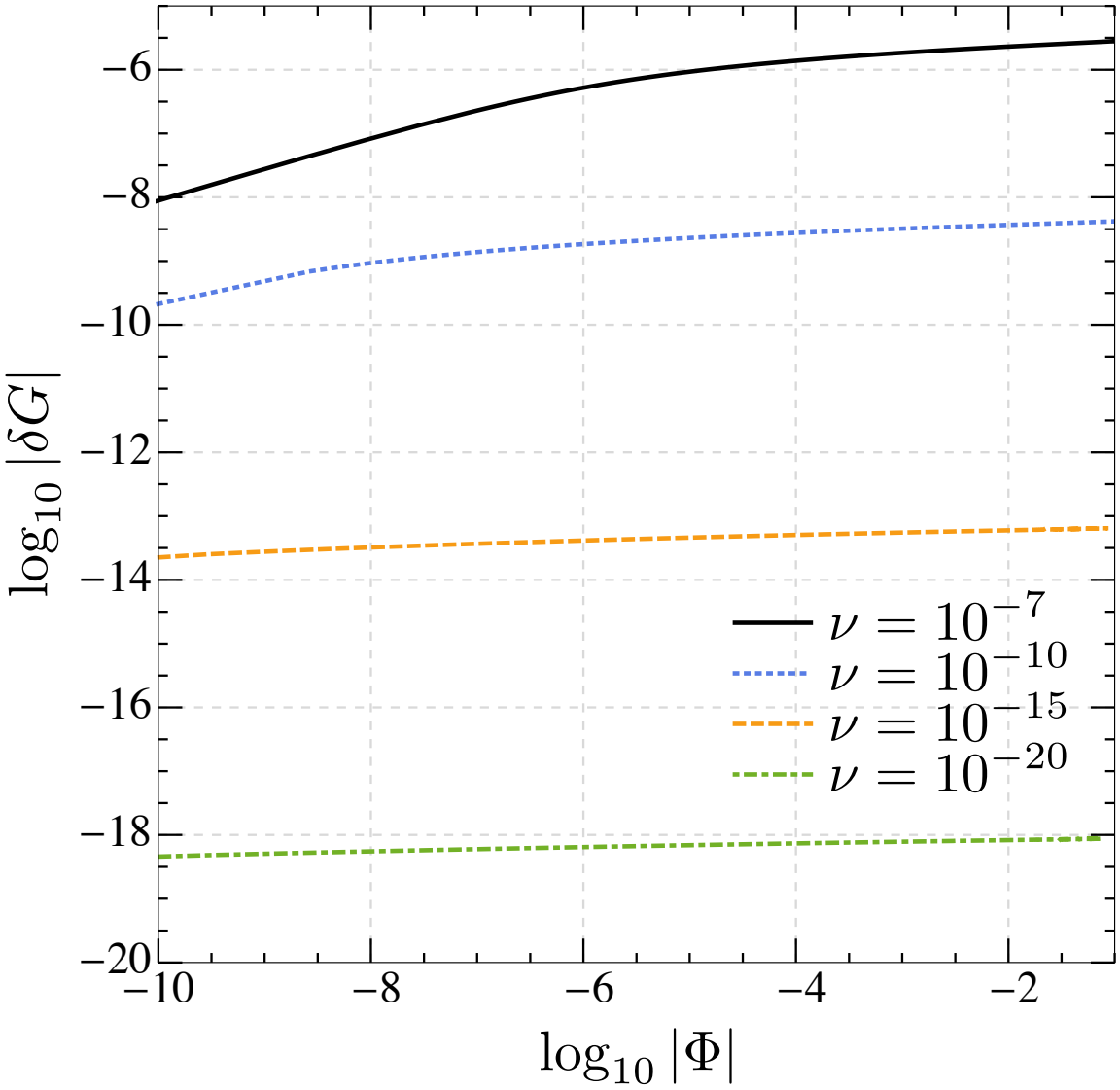

Figure 15 – The relation between $|\delta G| = |G - 1| \approx 2\nu \ln \mu$ (from equation 2.31) and $|\Phi|$ (from equation A.6) for four different values of ν.

APPENDIX B – THE NONCOVARIANT SCALE SETTING AS AN APPROXIMATION TO THE COVARIANT ONE

Equation (2.37) implies that

$$\alpha = \frac{1}{\mu\,\partial_\mu \ln(-\Phi)}, \tag{B.1}$$

where ∂_μ is the derivative with respect to μ. In equation (2.37), α appears as a constant, but from the perspective of the covariant scale setting, α should in general be a function of μ, as given by the above equation. If, for a given system, α is close to a constant, then for that system the noncovariant scale setting may work as a good approximation. The relation between α and Φ can be seen in Figure 16, which indeed shows that α changes slowly even if Φ changes by some orders of magnitude.

By using the noncovariant approach, one is using an approximation to derive the PPN parameters of the covariant approach. This approximation must be sufficiently precise. One way to evaluate this error is to consider, from a given value of Φ, the relative error between the two μ's inferred from the eqs. (2.37, A.11). Since it is possible to analytically express $\Phi(\mu)$, it is more convenient to adopt the inverse route, that is, from a given μ, to find the relative error between the potentials inferred by eqs. (2.37, A.11), which we call here Φ and Φ_A respectively. If the maximum relative error between Φ and Φ_A, along the Mercury's orbit, is $\varepsilon_\nu^{\max}$, then the PPN parameter γ, and consequently β, acquires an additional uncertainty of $\pm\gamma\varepsilon_\nu^{\max}$ when inferred from the other approach. In particular, if $\varepsilon_\nu^{\max} \sim 10$, it is no longer possible to use one approach (the noncovariant scale setting) to state precisely the order of magnitude of either γ or β of the other approach (the covariant scale setting case).

In order to show that both the approaches lead to compatible bounds for Mercury's orbit, we compare the Newtonian potential from equation (A.11), $\Phi(\mu)$, to an approximated potential given by equation (2.37), namely

$$\Phi_A(\mu, \mu_0) \equiv \mu^{1/\alpha(\mu_0)}\Phi_0(\mu_0), \tag{B.2}$$

where $\alpha(\mu)$ is given by equation (B.1), and $\Phi_0(\mu_0)$ is such that $\Phi_A(\mu_0, \mu_0) = \Phi(\mu_0)$. In the plot of Figure 16, the above approximation corresponds to a straight line approximation

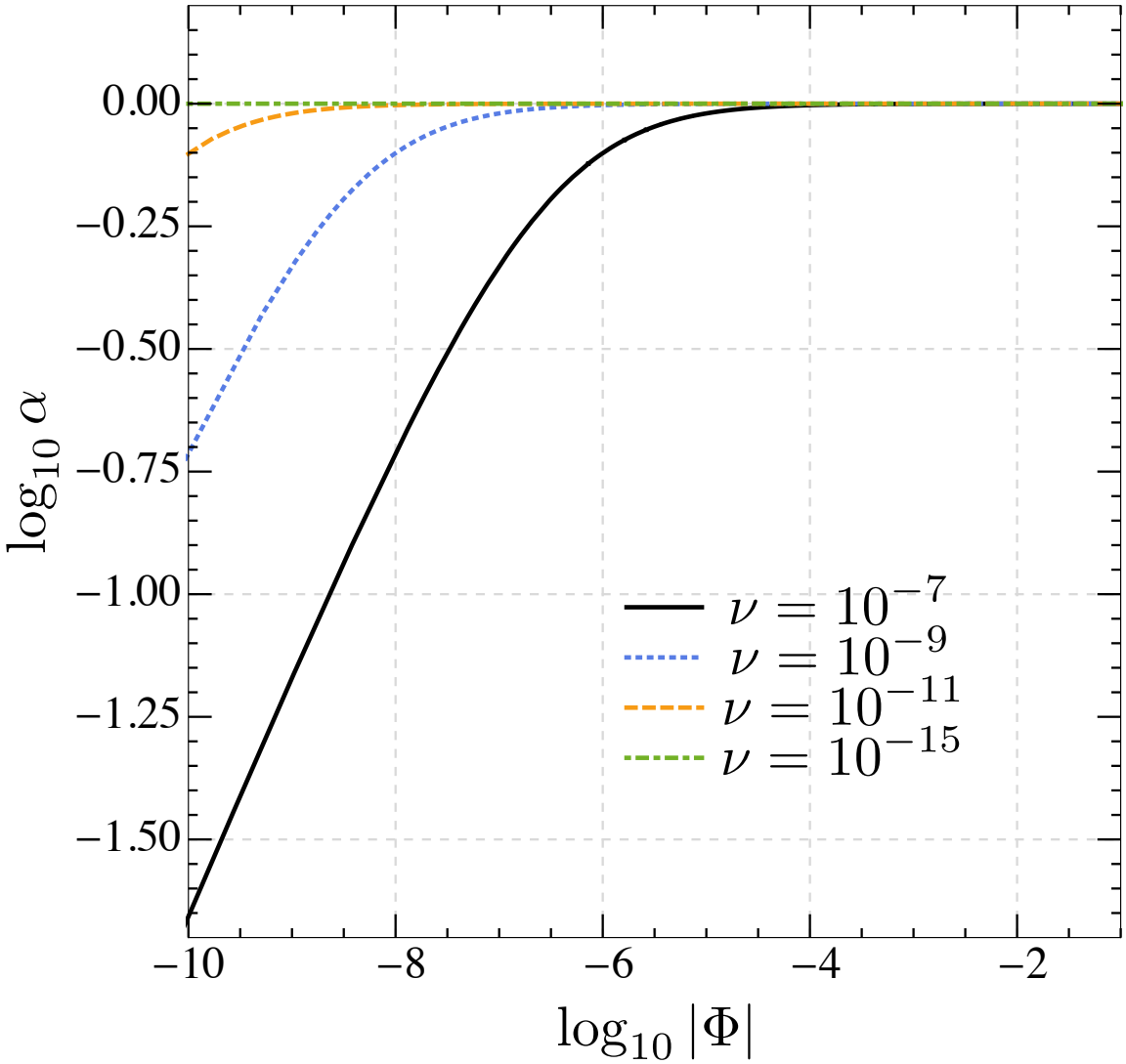

Figure 16 – The relation between α and Φ for different values of ν. It shows that the noncovariant approximation, where α is a constant, can be a good approximation for many systems, since large changes of Φ lead to much smaller changes on α.

at μ_0 to the $\alpha(\mu)$ curve. To quantify the approximation, we use the relative error that is given by

$$\varepsilon_\nu(\mu, \mu_0) \equiv \left| 1 - \frac{\Phi(\mu)}{\Phi_A(\mu, \mu_0)} \right| . \tag{B.3}$$

Without considering the external potential effect, the range of Φ values of relevance is from -3.2×10^{-8} to -2.1×10^{-8}. The contribution of the Milky Way to the local potential depends on whether dark matter is being considered or not, but for both cases it is about $\phi_{\rm MW}(r_\odot) \sim 10^{-6}$ at the Solar System position. This means that the range of variation of the Newtonian potential along the orbit of Mercury is $[-(K_{\rm MW} + 0.032) \times 10^{-6}, -(K_{\rm MW} + 0.021) \times 10^{-6}]$, where $K_{\rm MW}$ is a number about the unity whose precise value depends on the amount of dark matter in the Milky Way.

Figure 17 shows that the relative error introduced by the approximation (2.37) is small enough to allow for a PPN evaluation for the planet Mercury for all the relevant values of ν. For the case without external potential effect, one can draw a similar plot as that of Figure 17, with higher values of the relative errors, but no higher than 10^{-2}.

Since the main focus here is on order of magnitude evaluations of the Solar System bounds, the above shows that there exists a value for α such that equation (2.37) can work as a satisfactory approximation to the covariant scale setting (A.1), considering the post-Newtonian analysis of Mercury's orbit.

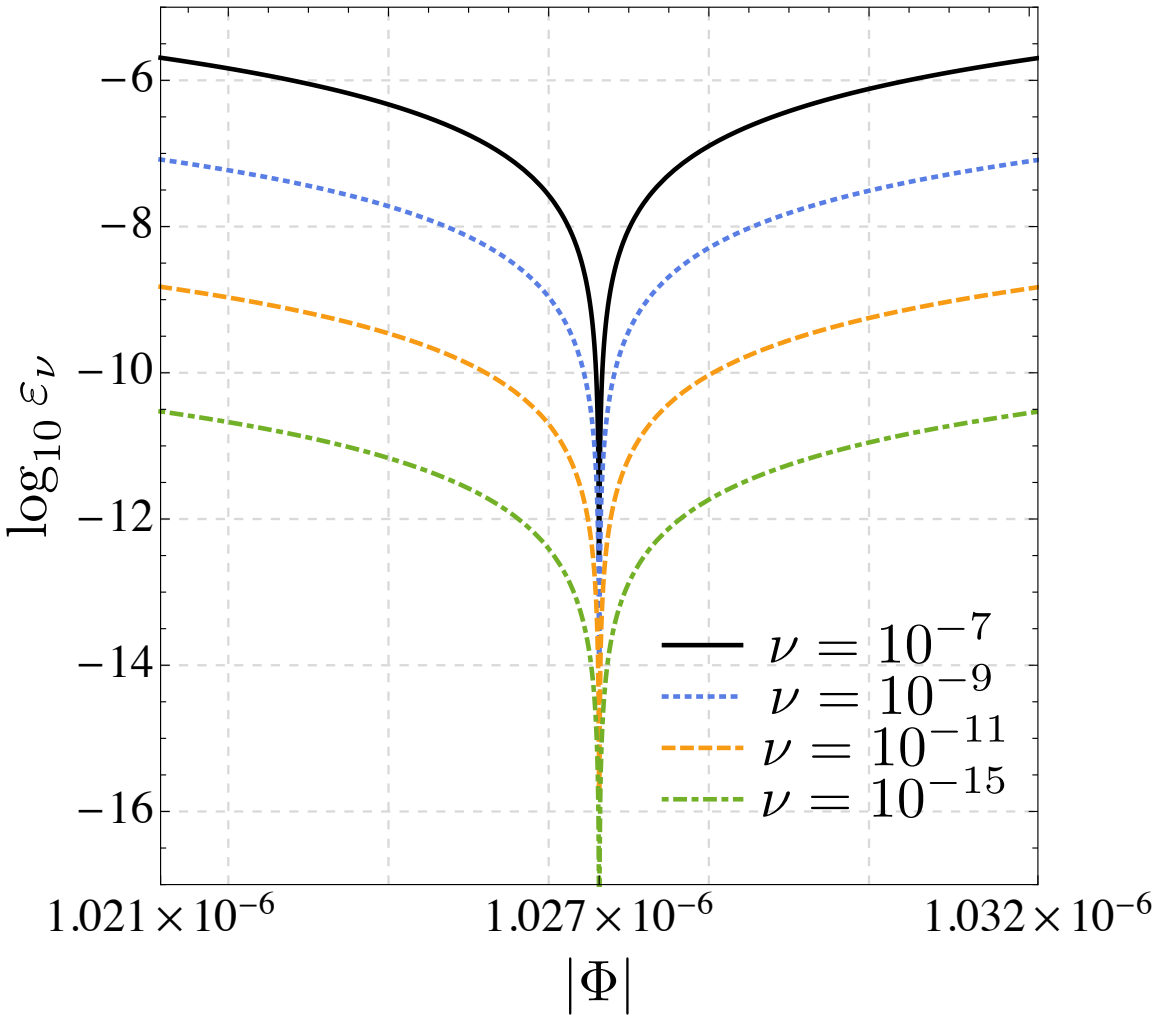

Figure 17 – The relative errors (B.3) introduced by the use of the approximation (2.37), in the context of Mercury's orbit with the external potential of the Galaxy. The range of Φ in this plot spans the variation of the Newtonian potential through the planet orbit added by 10^{-6}. Dividing or multiplying the latter value by 5, does not change the value of $\log_{10}\varepsilon$ significantly. The plot indicates that the noncovariant scale setting works as a good approximation for the covariant one, in the context of Mercury's orbit.